1949

Optimization and Applications of the Functional Renormalization Group

Thesis for the Degree of Doctor of Philosophy (PhD)

István Gábor Márián

Supervisor: Dr. István Nándori

University of Debrecen
Doctoral Council of Natural Sciences and Information Technology
Doctoral School of Physics
Debrecen, 2020

Hereby I declare that I prepared this thesis within the Doctoral Council of Natural Sciences and Information Technology, Doctoral School of Physics, University of Debrecen in order to obtain a PhD Degree in Natural Sciences at Debrecen University.

The results published in the thesis are not reported in any other PhD theses.

Debrecen, 2020

.....

István Gábor Márián
candidate

Hereby I confirm that István Márián Gábor candidate conducted his studies with my supervision within the Particle Physics Doctoral Program of the Doctoral School of Physics between 2016 and 2020. The independent studies and research work of the candidate significantly contributed to the results published in the thesis.
I also declare that the results published in the thesis are not reported in any other theses.
I support the acceptance of the thesis.

Debrecen, 2020

.....

Dr. István Nándori
supervisor

Optimization and Applications of the Functional Renormalization Group

Dissertation submitted in partial fulfilment of the requirements for the doctoral (PhD) degree in Physics

Written by István Gábor Márián certified Physicist

Prepared in the framework of the Doctoral School of Physics of the University of Debrecen
(Particle Physics programme)

Dissertation advisor: Dr. István Nándori

The official opponents of the dissertation:

Dr. .....

Dr. .....

The evaluation committee:

chairperson: Dr. .....

members: Dr. .....

Dr. .....

Dr. .....

Dr. .....

The date of the dissertation defence: .....

Contents

Introduction

Two of the greatest achievements in theoretical physics are the theory of special relativity and quantum mechanics. A fundamental theory of physics must unite these areas and be both relativistic and quantized. This is how quantum field theory was formed describing the fundamental forces of nature as interactions between elementary particles, which are excitations of the more fundamental objects, the quantum fields. One of the consequences of unifying the theory of special relativity and quantum mechanics is that the physical quantities such as the charge or mass of a particle measured in vacuum become scale-dependent due to quantum fluctuations. This means that even the strength of an interaction depends on the energy or momentum scale of the interaction. A powerful tool to describe this scale-dependence is the functional renormalization group (FRG) method which takes into account the fluctuations of a system at different scales by integrating out the modes of fluctuations successively. It can be used to study critical phenomena, phase diagrams, phase transitions of a large number of models providing a deep insight into their universal properties.

The FRG equation is an exact one, however, in most cases approximations are needed to obtain a solution. When approximations are used the results could depend on the so called regulator function. The question arises, which regulator function gives the most accurate predictions for physical quantities such as critical exponents at a certain level of approximation?

Approximate results may also suggest unphysical properties of a system, like the presence of a fixed point indicating a spurious phase transition. Thus, it is crucial to know what is a sufficient approximation that produces reliable results when different models are investigated.

Another interesting question is whether it is possible to view the time evolution of the Universe going through different temperatures and energy scales as a renormalization group (RG) flow. A consequence of this connection is the possibility to constrain the parameters of a candidate Higgs-inflationary model at the scale of inflation by astrophysical observations, and then calculate its RG running down to the electroweak scale by the RG method, where it should recover the measured parameters of the Standard model Higgs potential.

Furthermore, the RG approach could be applied not only in the post-inflationary, but also in the pre-inflationary period up to very high energies around the Planck scale. Thus the inflationary potential can have an RG evolution in this

period. Is it possible to use this mechanism to induce inflation?
My thesis is centered around these questions presenting the results of my research which provide some of the answers.

The structure of my thesis is the following. In Part I. I introduce the theoretical framework used during my analysis. First, the basic concepts of statistical physics are described, then the renormalization group approach is explained via the blocking construction technique. In the third chapter the statistical description is translated to the language of quantum field theory while the fourth chapter is dedicated to the functional renormalization group approach starting with the derivation of the Wetterich equation and giving special focus to the optimization of the regulator function. In the fifth chapter the most studied models of my thesis are introduced, namely the $O(N)$ and sine-Gordon type models, while in the final chapter of this part a brief introduction is given to inflationary cosmology.

The findings of my research are presented in Part II.
First, my study of the compactly supported smooth (CSS) regulator is discussed based on the optimization method called the principle of minimal sensitivity [1]. This principle is applied in the framework of the $O(N)$ and the massive sine-Gordon models. Then, the parameters of the CSS regulator is also optimized based on the requirement of the absence of spontaneous symmetry breaking in the one-dimensional sine-Gordon model beyond LPA [2].

In the following chapter I examined the reliability of the FRG method on $O(N)$ models paying special attention to its truncated Taylor expanded potential and the local potential approximation discussing what is sufficient to recover the Mermin-Wagner theorem [3, 4].

In the next two chapters I have applied the FRG technique in the context of cosmology. I have proposed a new Higgs-inflationary model the massive sine-Gordon theory, constrained its parameters at the scale of inflation using the observed data of the cosmic microwave background radiation. Then, by applying the FRG method I have calculated the parameters of the model at the electroweak scale [5].

I have also applied the FRG method to the pre-inflationary period, and proposed a new mechanism to induce inflation based on the convexification of the inflationary potential over its RG evolution [6].

In the Summary the results are concluded by stating my thesis points.

Finally let me note, that some technical issues of the FRG method, such as the graphical representation of the RG flow and its fixed point analysis can receive important application in the study of differential equations which is at the heart of almost every physical systems. As an example I would like to mention a rather unusual topic, the dynamics of magnetic nanoparticles, in particular their application in tumor therapy which is the so called magnetic hyperthremia, where I participated in a theoretical research [7].

Part I

Theoretical Framework

Chapter 1

Statistical mechanics

In this chapter I will introduce the reader briefly to the basics of statistical mechanics following mainly Refs. [8–10]. Statistical mechanics describes how the fundamental microscopic interactions generate the macroscopic properties and laws of large systems in equilibrium, therefore it is the first step to understand many-particle systems.

Let us start with introducing the concept of information and entropy. Suppose that we have n elementary events with equal probabilities. Then the probability of each event is $p = 1/n$ and the information one obtains by observing which event actually occurred is $\log_2 n$ bits. Now consider grouping these n equally probable events into the disjunct sets A_i that can happen by k_i equally probable events. Then an A_i event has a probability of $p(A_i) = p_i = k_i/n$ and contains an information I_i. Now assuming the additive property of independent informations one can write the following

$$\log_2 n = I_i + \log_2 k_i \,. \tag{1.1}$$

This means that the information of an elementary event can be obtained by first observing which A_i event occurred, then how this A_i happened, by which of the k_i possibilites. Rearranging the above equation, the information obtained by measuring A_i is

$$I_i = -\log_2 \frac{k_i}{n} = -\log_2 p_i \,. \tag{1.2}$$

Instead of measuring the information in bits, let us measure it in a different unit, in units of the Boltzmann constant k, and also let us use the natural log. This way the expectation value of the received information during the measurement of A_i is

$$S = -k \sum_i p_i \log p_i \,. \tag{1.3}$$

This formula is a cornerstone of statistical physics and called the Shannon entropy formula.

One of the key principles of statistical mechanics is the principle of maximal entropy. It states that the p_i probability distribution of the microscopic states of

the system gives maximal entropy. Suppose a many-particle system with a large number of particles. In this case, it is basically impossible to know the microscopic (quantum) state of every particle, there are too many degrees of freedom. Therefore one can only measure averages, macroscopic properties. By requiring the entropy to be maximal one makes as few assumptions about the system as possible, or in other words one assumes that a measurement will give maximal information.

Another key principle of statistical mechanics is the assumption that one can divide the system into a large number of smaller, homogeneous, weakly-interacting parts. Thus, the central limit theorem can be used, since homogeneity assures that the random variables have the same distribution, while neglecting the interactions between the parts means that these random variables are independent. Using the central limit theorem one can take the thermodynamic limit of a system by increasing the number of particles and volume of the system while keeping their ratio fixed.

$$N \to \infty \qquad V \to \infty \qquad \frac{N}{V} = \text{const}\,. \tag{1.4}$$

Let us see what are the implications of these principles. Consider a closed system with fixed macroscopic properties, fixed internal energy, volume, and number of particles (U, V, N). The mathematical formulation of maximal entropy states that the derivative of the entropy is zero. Imposing the condition that the sum of all probabilities are one and using the Lagrange multiplier $k\lambda$, one gets

$$\frac{\partial}{\partial p_j}\left(S - k\lambda \sum_i p_i\right) = -k \log p_j - k - k\lambda = 0\,, \tag{1.5}$$

which yields

$$p_j = e^{-1-\lambda}\,. \tag{1.6}$$

The consequence of this formula is that the probabilities are equal, thus each microscopic configuration is considered by equal weight, which seems a reasonable thing to do. Therefore, if the number of microscopic configurations is W, then $p_i = 1/W$ and the entropy for the so called microcanonical ensemble writes

$$S = k \log W\,, \tag{1.7}$$

as it stands famously on the grave of Boltzmann, one of the great pioneers of statistical physics.

For the derivation of Boltzmann's formula the only condition imposed was the necessity of the sum of all probabilities to be one, but the situation is different if there are other constraints, for example if the system is in a heat bath with the temperature $\beta = 1/(kT)$. By definition temperature is the inverse of the derivative of the entropy with respect to the energy

$$\frac{\partial S}{\partial U} = \frac{1}{T}\,. \tag{1.8}$$

This means that the system is not closed like in the microcanonical ensemble, therefore the total energy is not fixed, it can fluctuate around the average U. This

is another condition: the expectation value of the energy should be $\sum_i p_i E_i = U$. With this extra condition the derivative of the entropy is

$$\frac{\partial}{\partial p_j}\left(S - k\lambda\sum_i p_i - k\beta\sum_i p_i E_i\right) = \\ -k\log p_j - k - k\lambda - k\beta E_j = 0\,, \tag{1.9}$$

therefore the probabilities are proportional to the Boltzmann factor, i.e., the negative exponential of the energy

$$p_j = e^{-1-\lambda}\, e^{-\beta E_j}\,. \tag{1.10}$$

The obtained ensemble is called the canonical ensemble. It is very useful to define the function

$$Z(\beta, V, N) = \sum_i e^{-\beta E_i}\,, \tag{1.11}$$

which is called the canonical partition function. From the first condition this fixes the first Lagrange multiplier

$$\sum_i p_i = e^{-1-\lambda}\sum_i e^{-\beta E_i} = 1 \quad\Longrightarrow\quad e^{-1-\lambda} = \frac{1}{Z}\,, \tag{1.12}$$

and one can write the probabilities in a nice way

$$p_i = \frac{1}{Z}\, e^{-\beta E_i}\,. \tag{1.13}$$

The partition function is also useful since physical quantities can be extracted from it like the average energy

$$-\frac{\partial \log Z}{\partial \beta} = \frac{1}{Z}\sum_i E_i e^{-\beta E_i} = \sum_i E_i p_i = U\,, \tag{1.14}$$

or the variance of the energy

$$-\frac{\partial^2 \log Z}{\partial \beta^2} = \left\langle E^2\right\rangle - \left\langle E\right\rangle^2\,. \tag{1.15}$$

Finally the entropy writes as

$$S = -k\sum_i p_i \log p_i = -k\sum_i \frac{e^{-\beta E_i}}{Z}\log\frac{e^{-\beta E_i}}{Z} = \\ k\sum_i \beta E_i p_i + k\log Z = k\beta U + k\log Z\,. \tag{1.16}$$

Let us allow the change in the number of particles as well, not just the fluctuation of the energy. This way even more microstates will have non-zero probability,

thus this ensemble is called the grand canonical ensemble. The extra condition for the average number of particles is $\sum_i p_i N_i = N$, and the derivative of the entropy writes as

$$\frac{\partial}{\partial p_j}\left(S - k\lambda\sum_i p_i - k\beta\sum_i p_i E_i - k\lambda_N\sum_i p_i N_i\right) = \\ -k\log p_j - k - k\lambda - k\beta E_j - k\lambda_N N_j = 0\,, \tag{1.17}$$

hence the probabilities

$$p_j = e^{-1-\lambda}\, e^{-\beta E_j - \lambda_N N_j}\,. \tag{1.18}$$

Just like for the canonical ensemble, here the grand canonical partition function is introduced

$$\mathcal{Z}(\beta, V, \lambda_N) = \sum_i e^{-\beta E_j - \lambda_N N_j}\,. \tag{1.19}$$

Then physical quantities can be extracted from this function

$$-\frac{\partial \log \mathcal{Z}}{\partial \beta} = U \qquad -\frac{\partial \log \mathcal{Z}}{\partial \lambda_N} = N\,, \tag{1.20}$$

and the probabilities can be written as

$$p_i = \frac{1}{\mathcal{Z}}\, e^{-\beta E_j - \lambda_N N_j}\,, \tag{1.21}$$

while the entropy becomes

$$S = -k\sum_i p_i \log p_i = k\beta U + k\lambda_N N + k\log\mathcal{Z}\,. \tag{1.22}$$

The three ensembles, the microcanonical, the canonical and the grand canonical ensembles are equivalent in the thermodynamic limit.

It is generally true that the entropy and its derivatives contains all information about a thermodynamic system. Such functions are called thermodynamic potentials. Entropy is not the only function with this property, the internal energy is also a thermodynamic potential and other functions can be derived via Legendre transformations. The logarithms of the partition functions are also thermodynamic potentials, since they are the Legendre transformations of the entropy. The logarithm of the canonical partition function is the Legendre transformation of the entropy with respect to the internal energy

$$k\log Z(\beta, V, N) = S - \frac{\partial S}{\partial U}U = S - k\beta U\,, \tag{1.23}$$

while the logarithm of the grand canonical partition function is the Legendre transformation of the entropy with respect to the internal energy and the number of particles

$$k\log\mathcal{Z}(\beta, V, \lambda_N) = S - \frac{\partial S}{\partial U}U - \frac{\partial S}{\partial N}N = S - k\beta U - k\lambda_N N\,. \tag{1.24}$$

These equations are the rearrangements of (1.16) and (1.22) which is not surprising since when there are constraints, due to these conditions the full entropy cannot be maximal. Instead, one has to look for the extremum of the corresponding thermodynamic potential.

From the Legendre transformation of the internal energy, further thermodynamic potentials can be obtained. To mention a few, here is the Helmholtz free energy

$$F(T,V,N) = U - \frac{\partial U}{\partial S} S = U - TS = -kT \log Z(T,V,N)\,, \tag{1.25}$$

and the Landau potential

$$\Omega(T,V,\mu) = U - TS - \mu N = -kT \log \mathcal{Z}(T,V,\mu)\,, \tag{1.26}$$

where $\mu = -kT\lambda_N$.

In the thermodynamic limit physical results will be the same no matter which potential is used, since it does not matter if one fixes the macroscopic properties or allow fluctuations, because the relative fluctuations tend to zero in this limit. However there are situations where the assumptions for the central limit theorem are not justified. If the system is not homogeneous, then it is not in the state of equilibrium, because the inhomogeneities will give rise to currents that want to eliminate these inhomogeneities. In this instance non-equilibrium thermodynamics must be used. The most important case for this thesis is when the interactions cannot be neglected as a long-range correlation forms between the degrees of freedom in the system. This is what happens at phase transitions. The corresponding thermodynamic potential does not have a sharp peak, but a spread out extremum, therefore even small fluctuations can drastically change the system. Thus a better method is needed to analyze phase transitions, so let us turn our attention to the renoramlization group.

Chapter 2

Renormalization group

As we discussed in the previous chapter, there are cases when the central limit theorem cannot be used. This is the situation in case of phase transitions since one cannot divide the system into smaller parts where the correlation between the parts are negligible. Another tool is necessary to analyze the system. In this chapter the renormalization group (RG) is discussed, which is a more appropriate method to study the scale dependence of a model and its critical properties around phase transitions [11].

Before going straight to the topic let us discuss the $O(N)$ model which we will use as a "toy model" to better understand the effect of the renormalization group transformations.

2.1 The $O(N)$ model

We have to choose a model that is easy to solve and demonstrates the effects of our method well, by showing a nice intuitive picture. The $O(N)$ models, especially the $O(1)$ or the Ising model, prove to be a good choice.

The $O(N)$ spin models as their name suggests have an N dimensional orthogonal rotational symmetry. Their Hamiltonian can be written as

$$H_{\mathrm{ON}} = -J \sum_{\langle i,j \rangle} S_i S_j - \sum_i h_i S_i \,, \tag{2.1}$$

where S_i are N dimensional spin vectors placed on a d dimensional grid, h_i is an external magnetic field at site i, and $\langle i,j \rangle$ denotes that the sum goes over the pairs of adjacent spins, therefore it contains only nearest neighbor interactions. For further calculations periodic boundary conditions are assumed in the spin-lattice. The partition function of this model writes as

$$Z = \mathrm{Tr}\, e^{-\beta H_{\mathrm{ON}}} \,. \tag{2.2}$$

where the trace is a summation over all possible spin configurations. By differentiating the logarithm of the partition function with respect to the external field, one gets the expectation value of the spin

$$\frac{1}{\beta}\frac{\partial \log Z}{\partial h_i} = \langle S_i \rangle = \frac{1}{Z} \operatorname{Tr} S_i e^{-\beta H_{\mathrm{ON}}} , \tag{2.3}$$

while differentiating twice gives the second momentum of the spin, also called the correlation function, since it describes the correlation between two spins

$$G_{ij} = \langle S_i S_j \rangle - \langle S_i \rangle \langle S_j \rangle . \tag{2.4}$$

Depending on what d dimension and what N parameter we choose, we can obtain models with different properties. If we use $N = 1$, we get the Ising model. The $N = 2$ case is referred to as XY, the $N = 3$ case is referred to as the Heisenberg model, whereas if $N \to \infty$ it is called the spherical model. These models are well known in statistical physics as they describe the statistics of an interacting spin system (magnetic moments) placed on a d dimensional grid see Fig. 2.1. If

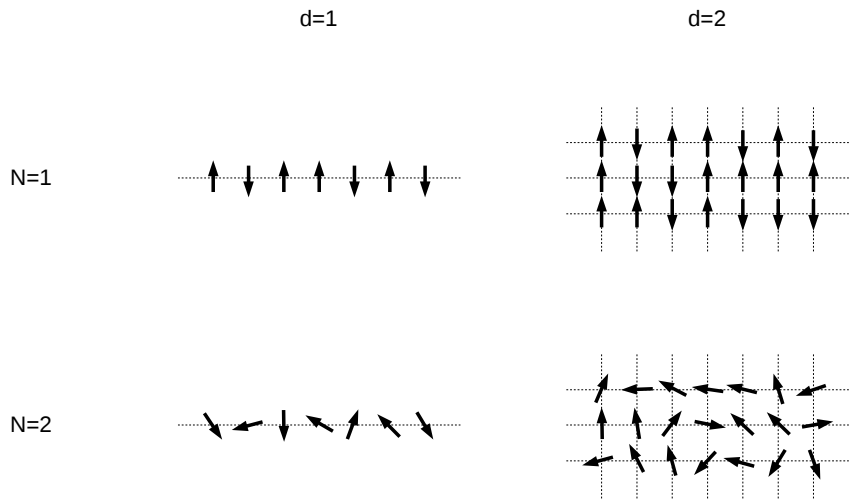

Figure 2.1: The $O(N)$ spin models in $d = 1, 2$ dimensions with $N = 1, 2$. While d determines the dimension of the grid, N defines the dimension of the interior space, i.e., the dimension of the spins (arrows situated on the grid points).

J is positive the interaction is ferromagnetic and the lowest energy state of two adjacent spins is when they are parallel. Then, in the $T \to 0$ limit, when the fluctuations can be neglected, all spins point in the same direction in the lowest energy state. This breaks the rotational symmetry. The phenomenon when the

symmetry is broken not by a term in the Hamiltonian but by the ground state is called spontaneous symmetry breaking.

In the next sections we will examine one of the simplest examples, the $O(1)$, i.e., the Ising model with a positive coupling J. When $N = 1$ the spins have only two states and the Hamiltonian has a discrete Z_2 symmetry. In $d = 1$ and $d = 2$ dimensions this model is solved exactly, which means it is possible to write down the partition function of the model in a closed compact form. For example in $d = 1$ dimension when there is no external field $h = 0$ the Hamiltonian is simply

$$H_{\text{Ising}} = -J \sum_{\langle i,j \rangle} S_i S_j \,. \tag{2.5}$$

Therefore the partition function is

$$Z = \operatorname{Tr} e^{-\beta H_{\text{Ising}}} \,, \tag{2.6}$$

where the Boltzmann factor can be written as

$$e^{-\beta S_i S_j} = \cosh \beta + S_i S_j \sinh \beta \,, \tag{2.7}$$

where β was redefined to include the strength of the interaction $\beta = J/(kT)$. Then the partition function takes the compact form

$$Z = 2^n \left[\cosh^n \beta + \sinh^n \beta \right] \,, \tag{2.8}$$

where n is the number of particles. When there is no external field the expectation value of the spins are zero $\langle S_i \rangle = 0$. It is also straightforward to calculate the correlation function $G(r)$ and correlation length ξ

$$G(r) = \langle S_i S_{i+r} \rangle - \langle S_i \rangle \langle S_{i+r} \rangle \propto e^{-\frac{r}{\xi}} \,. \tag{2.9}$$

In the thermodynamic limit

$$\xi = \frac{-1}{\log \tanh \beta} \,. \tag{2.10}$$

Knowing the exact solution and the above formulas will help to better understand the renormalization group, which is discussed in the next section.

2.2 Blocking construction

One way to perform the renormalization group transformation on a spin system is called the Wilson-Kadanoff blocking construction [12, 13]. The main step of this method is to block or group together a fixed number of degrees of freedom, spins S, and create new, blocked degrees of freedom, new spin variables S'. To do this blocking one has to integrate out some degrees of freedom of the original partition function thus creating the new blocked spins. These new blocked spins will be basically averages of the original spins. A recommended step in this process is to

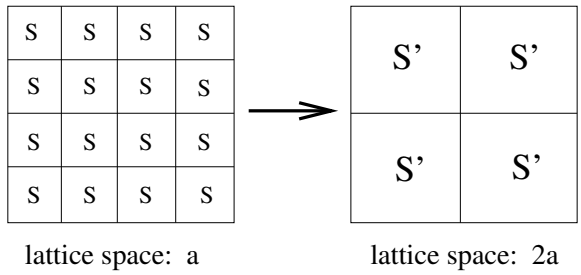

Figure 2.2: Blocking spins by rescaling the lattice space $a \to 2a$.

change the scale of observation by rescaling the lattice spacing $a \to a' = ba$ or in reciprocal space to decrease the running momentum cut-off, $k \sim 1/a$, see Fig. 2.2

During this transformation new interaction terms could be generated therefore the idea is to start with a general ansatz that already include all possible interaction terms. If one includes all interaction terms generated by the transformation, then the functional form of the partition function is preserved and only the parameters i.e., the couplings might change.

Generally the blocking can be achieved by a block transformation function

$$T([S'],[S]) = \begin{cases} 1 \text{ if one gets } [S'] \text{ by blocking } [S] \\ 0 \text{ othervise} \end{cases} . \tag{2.11}$$

Therefore the new Boltzmann factor is

$$e^{-\beta' H'[S']} \propto \sum_{[S]} T([S'],[S]) e^{-\beta H[S]} , \tag{2.12}$$

which is the RG transformation that maps a Hamiltonian onto another effective Hamiltonian that still contains all the long range information of the system. In other words the RG transformation can be summarized as an operation R_b on the couplings g_i of a Hamiltonian. This operation creates RG trajectories in the space of the couplings moving from small lattice spacings (large momentum) to large ones (small momentum).

From this simple fact a large number of very interesting phenomenon can be explained [14].

Universality. If the RG trajectories tend to go in one direction for example to a single fixed point then it means that it does not matter what is the microscopic physics of the system, the long-range behavior is always the same. This phenomenon is called universality and it is present in a large number of system. Even different models, different microscopic laws often produce the same long distance physics.

Wilson-Fisher fixed points. If the RG trajectories run in two different directions, then there must be two phases and a phase separating critical surface between them.

If a trajectory starts with the right couplings which are on this critical surface then this trajectory cannot leave the surface and often tends into a critical fixed point. This critical fixed point is attractive towards the critical surface and repulsive perpendicular to the surface like a saddle point. This means that a saddle point is not only a good indication of a phase transition, but a critical system is also in a saddle or the so called Wilson-Fisher (WF) fixed point after the RG transformation. Therefore the properties of the WF fixed point describes the critical properties of the model. A trivial property of a fixed point is scale invariance, which means that a critical system is also scale invariant, i.e., invariant under the RG transformation. This is only possible if the correlation length is infinite $\xi = \infty$, or zero, since otherwise the correlation length would decrease during the scale transformation.

Relevance. Those couplings which survive the RG evolution are called relevant while those that tend to zero are called irrelevant couplings. There is a strong connection between relevancy and dimensionality. It is easy to see why. The RG transformation changes the scale of the system, in real space $a \to \infty$ while in momentum space $k \to 0$. Therefore if a coupling has a dimension d_g, then it has a trivial scaling which is proportional to its dimension $g \propto k^{d_g}$. For this reason it is often useful to introduce dimensionless couplings $\tilde{g} = gk^{-d_g}$ so that one can observe only the non-trivial scaling of the couplings.

Power-law scaling around the fixed points. Let us see the effect of the RG operator R_b on the couplings $\{g_1, g_2, \dots\} = g$

$$g \to g' = R_b(g)\,. \tag{2.13}$$

If it is applied on a fixed point g^* then due to scale-invariance the couplings do not change

$$R_b(g^*) = g^*\,. \tag{2.14}$$

Suppose that g^* is a stable fixed point on the critical surface and consider the linearization of the RG around this fixed point

$$g_i' - g_i^* = \sum_j T_{ij}(g_j - g_j^*) + \mathcal{O}((g_j - g_j^*)^2)\,, \tag{2.15}$$

where

$$T_{ij} = \left.\frac{\partial R_b^i}{\partial g_j}\right|_{g^*}\,. \tag{2.16}$$

For this linearized RG operator one can write the following eigenvalue equation

$$u'_i = \lambda_i u_i\,. \tag{2.17}$$

Applying the blocking by changing the lattice spacing by a factor of b then by a factor of c is the same as applying only one blocking with the blocking parameter bc. If $b = 1$, the RG should be the identity operator therefore the following relations are true for the eigenvalues

$$\lambda(bc) = \lambda(b)\lambda(c), \qquad \lambda(1) = 1\,. \tag{2.18}$$

These properties of λ guarantees that it is a power-law function of b thus one obtains

$$\lambda(b) = b^y = e^{y \log b}\,, \tag{2.19}$$

therefore the RG evolution of the couplings around the fixed point is also a power-law function

$$u_i' = b^{y_i} u_i\,. \tag{2.20}$$

The value of y_i determines the behavior in the i direction.

- $\mathrm{Re}\, y_i > 0 \implies$ u_i increases, mowing away from the fixed point, relevant coupling
- $\mathrm{Re}\, y_i < 0 \implies$ u_i decreases, moving towards the fixed point, irrelevant coupling
- $\mathrm{Re}\, y_i = 0 \implies$ the linearized approximation is not enough, marginal coupling

Homogeneity of the thermodynamic potential. Suppose that there are two relevant couplings in the eigendirections t and h. (The generalization for an arbitrary number of couplings is trivial and not mentioned here.) The irrelevant couplings can be neglected therefore the thermodynamic potential density $f(t,h)$ can be considered as a function of only t and h. The thermodynamic potential is an extensive quantity which means that it has an additive property. Thus by blocking together degrees of freedom it will increase by a factor of b^d

$$f(t',h') = b^d f(t,h)\,. \tag{2.21}$$

Using the power-law scaling of the couplings

$$t' = b^{y_t} t, \qquad h' = b^{y_h} h\,, \tag{2.22}$$

one can rewrite the thermodynamic potential showing its homogeneous property

$$f(t',h') = f(b^{y_t}t, b^{y_h}h) = f(\lambda^{a_t}t, \lambda^{a_h}h) = \lambda f(t,h)\,, \tag{2.23}$$

where $a_t = y_t/d$, $a_h = y_h/d$ and $\lambda = b^d$.

Relations between the critical exponents. From the homogeneity of the thermodynamic potential it is easy to show that all the critical exponents can be expressed in terms of the powers a_t and a_h, since the physical quantities can be generated from the thermodynamic potential and its derivatives. For example differentiating the specific free energy of the Ising model with respect to the homogeneous external field h yields

$$\frac{\partial f(\lambda^{a_t}t, \lambda^{a_h}h)}{\partial h} = \lambda^{a_h}\Delta(\lambda^{a_t}t, \lambda^{a_h}h) = \lambda\Delta(t,h)\,, \tag{2.24}$$

where $\Delta(t,h) = \partial f(t,h)/\partial h$ is the order parameter of the phase transition and t in this case is the reduced temperature $t = (T - T_c)/T_c$. After substituting $t = 0$ and $\lambda = h^{-1/a_h}$ one gets

$$\Delta(0,1)h^{(1-a_h)/a_h} = \Delta(0,h)\,, \tag{2.25}$$

where $\Delta(0,1)$ is only a constant. Therefore, the critical exponent of the order parameter with respect to the external field is $\delta = a_h/(1-a_h)$, where we used the definition of δ which is $\Delta(0,h) \propto h^{1/\delta}$. Similarly, in the $T < T_c$ region one obtains the following expression by substituting $h = 0$ and $\lambda = (-t)^{-1/a_t}$ into Eq. (2.24)

$$(-t)^{(1-a_h)/a_t}\Delta(-1,0) = \Delta(t,0)\,. \tag{2.26}$$

Thus, the critical exponent of the order parameter with respect to the reduced temperature is $\beta = (1-a_h)/a_t$, since the definition of β is $\Delta(t,0) \propto (-t)^{\beta}$.

The models that have the same critical exponents are in the same universality class.

As a simple example let us perform the RG transformation for the 1d Ising model as promised. The partition function of the Ising model is

$$Z = \sum_{S_1=-1}^{1} \sum_{S_2=-1}^{1} \dots e^{\beta S_1 S_2} e^{\beta S_2 S_3} \dots\,. \tag{2.27}$$

It is easy to do the summation for every even spin. For example for the second spin

$$\sum_{S_2=-1}^{1} (\cosh\beta + S_1 S_2 \sinh\beta)(\cosh\beta + S_2 S_3 \sinh\beta) = (\cosh^2\beta + S_1 S_3 \sinh^2\beta). \tag{2.28}$$

Therefore the following equality arises between the partition function of the blocked spins, which are denoted by odd indexes, and the original partition function, where we did the summation for every second spin

$$\begin{aligned} Z &= \mathcal{N} \sum_{S_1=-1}^{1} \sum_{S_3=-1}^{1} \dots \cosh\beta(1 + S_1 S_3 \tanh\beta)\cosh\beta(1 + S_3 S_5 \tanh\beta)\dots \\ &= \sum_{S_1=-1}^{1} \sum_{S_3=-1}^{1} \dots \cosh^2\beta(1 + S_1 S_3 \tanh^2\beta)\cosh^2\beta(1 + S_3 S_5 \tanh^2\beta)\dots\,. \end{aligned} \tag{2.29}$$

It is clear that only the norm of the partition function changed and the coupling

$$\tanh\beta' = \tanh^2\beta\,, \tag{2.30}$$

while we blocked two adjacent spins together and increased the lattice spacing by $a \to 2a$. More generally if the blocking is done over b spins, increasing the lattice spacing by a factor of b, then the above formula takes the general form

$$x' = x^b, \qquad x = \tanh\beta\,. \tag{2.31}$$

By performing the blocking several times one can obtain the long-range behavior of the system. For the 1d Ising model remembering that $\beta = J/(kT)$ there are two limiting cases

$$T \to \infty \quad \text{or} \quad J \to 0 \quad \Longrightarrow \quad x \to 0\,, \tag{2.32}$$

$$T \to 0 \quad \text{or} \quad J \to \infty \quad \Longrightarrow \quad x \to 1\,. \tag{2.33}$$

If $x < 1$ then during the blocking x tends to zero which is the first case. If $x = 1$ then it stays one, which is the second case. These are the two fixed points, but the second one corresponds to zero temperature. For any positive temperature only the other phase is present, which means that the critical temperature is $T_c = 0$ and the model has only one phase.

Now doing the linearization around the $x = 1$ fixed point by introducing the coupling $u = 1 - x$ yields

$$u' = 1 - x' = 1 - x^b = 1 - (1-u)^b \approx 1 - [1 - bu + \mathcal{O}(u^2)] = bu\,. \tag{2.34}$$

Therefore the power of b is one, which means that in this case $y = 1$. From this, one can obtain the critical exponent of the correlation length. Increasing the lattice results in the decrease in the correlation length by the same factor $\xi' = \xi/b$. By expressing b from (2.34) one can write ξ' as a function of u'

$$\xi' = \frac{1}{b}\xi = \frac{u}{u'}\xi \propto {u'}^{-1}\,. \tag{2.35}$$

From this relation the power of u' is by definition the critical exponent of the correlation length which is negative one. From the exact formula one can also obtain the scaling and critical exponent of the correlation length

$$\xi = -\frac{1}{\log\tanh\beta} = -\frac{1}{\log(1-u)} \approx -\frac{1}{-u} = u^{-1}\,, \tag{2.36}$$

which confirms our result using the RG method. However while the exact solution is known for a very small number of models, the RG method can be widely used in many cases, giving a powerful tool to analyze the phases and critical properties of many models.

Chapter 3

Quantum field theory

Now let us turn our attention to one of the most advanced and fundamental areas of physics, that gives the most accurate predictions for particle physics, quantum field theory [15, 16]. Quantum field theory describes the particles as excitation of fields. For every elementary particle there is a more fundamental object, the field. The fermions are described by fermion fields, the force carrier bosons are described by gauge fields and the scalar particles such as the Higgs boson, are a described by scalar fields. Quantum field theory models are constructed at high energies using symmetries. For example the current best model in particle physics, the standard model is derived by requiring three local symmetries $SU(3)_C \times SU(2)_Y \times U(1)_\gamma$.

Fortunately there are a lot of analogies and parallels that can be drawn between statistical physics and quantum field theories. In quantum field theory there is a functional called generating functional Z, which is defined by the path integral, i.e., the integral over all field configurations of the negative exponential of the bare action S

$$Z = \int \mathcal{D}\phi \, e^{-S} \,, \tag{3.1}$$

where the natural units ($c = \hbar = 1$) are used and imaginary time ($t \to it$) is introduced by performing a Wick rotation, thus the metric is changed from Minkowski to Euclidean. One can immediately see the parallels to the partition function. This functional also contains all the information about the model described by the action, just like a partition function, and from its functional derivatives physical quantities can be derived such as correlation functions, transition amplitudes, cross-sections. Here the weight given to one field configuration is proportional to the negative exponential of the action, therefore the expectation value of a physical quantity A can be calculated by the integral

$$\langle A \rangle = \frac{1}{Z} \int \mathcal{D}\phi \, A \, e^{-S} \,. \tag{3.2}$$

It is very useful to generalize this functional by adding a source J to the action

$$Z[J] = \int \mathcal{D}\phi \, e^{-S + \int J\phi} \,. \tag{3.3}$$

This way the expectation values, and moments of the field can be generated by the functional derivatives of the generating functional with respect to the source

$$\langle \phi_1 \dots \phi_2 \rangle = \frac{1}{Z^n} \frac{\delta^n Z[J]}{\delta J_1 \dots \delta J_2} \bigg|_{J=0}, \tag{3.4}$$

where the notations $\phi_i = \phi(x_i)$ and $J_i = J(x_i)$ are used. These are the so called n-point functions. Using perturbation theory these functions can be represented by Feynman diagrams, which provide an elegant way to compute them using graphs.

However the goal is to obtain correlation functions. For this reason we define the generating functional of the connected Feynman graphs as

$$W[J] = \log Z[J]\,. \tag{3.5}$$

Differentiating the above functional with respect to J gives the expectation value of the field

$$\frac{\delta W[J]}{\delta J(x)} = \frac{1}{Z} \frac{\delta Z}{\delta J(x)} = \langle \phi \rangle_J = \varphi_J\,, \tag{3.6}$$

the same way as the expectation value of the spin is obtained by differentiating the logarithm of the partition function of the $O(N)$ model with respect to the external field. The second derivative gives the two point correlation function of the field, also called the propagator

$$\frac{\delta^2 W[J]}{\delta J_1 \delta J_2} = \frac{1}{Z} \frac{\delta^2 Z}{\delta J_1 \delta J_2} - \frac{1}{Z} \frac{\delta Z}{\delta J_1} \frac{1}{Z} \frac{\delta Z}{\delta J_2} = \langle \phi_1 \phi_2 \rangle - \varphi_1 \varphi_2 = \langle \phi_1 \phi_2 \rangle_c\,. \tag{3.7}$$

Since the disconnected averages are subtracted, the derivatives of $W[J]$ generates only the connected n-point functions. Therefore the correlation functions after substituting $J = 0$ write as

$$\langle \phi_1 \dots \phi_n \rangle_c = \frac{\delta^n W}{\delta J_1 \dots \delta J_2} \bigg|_{J=0}. \tag{3.8}$$

However this is still not the functional we are looking for, because it depends on the source J, which is basically only a mathematical tool to generate the n-point functions. We want something more physical, for example the expectation value of the field. Therefore let us do a Legendre transformation, like we did for the thermodynamic potentials, and define a functional that depends on φ instead of J

$$\Gamma[\varphi] = -W[J_\varphi] + \int J_\varphi \varphi\,. \tag{3.9}$$

This functional is called the effective action or the generating functional of the one particle irreducible graphs, the graphs that do not become disjoint after a line is cut. Differentiating the effective action with respect to φ gives the source

$$\frac{\delta \Gamma[\varphi]}{\delta \varphi} = -\frac{\delta W}{\delta \varphi} + \int \varphi \frac{\delta J_\varphi}{\delta \varphi} + J_\varphi = -\int \frac{\delta W}{\delta J_\varphi} \frac{\delta J_\varphi}{\delta \varphi} + \int \varphi \frac{\delta J_\varphi}{\delta \varphi} + J_\varphi = J_\varphi\,. \tag{3.10}$$

For on-shell particles, when the source is zero, the derivative of the effective action is $\delta\Gamma[\varphi_*]/\delta\varphi = 0$, where the field φ_* that satisfies this equation gives the vacuum state. Differentiating $\Gamma[\varphi]$ with respect to both φ and J and using the chain rule gives

$$\frac{\delta^2\Gamma[\varphi(z)]}{\delta\varphi(x)\delta J(y)} = \int_v \frac{\delta^2\Gamma[\varphi(z)]}{\delta\varphi(x)\delta\varphi(w)}\frac{\delta^2 W[J(u)]}{\delta J(v)\delta J(y)} = \frac{\delta J(x)}{\delta J(y)} = \delta(x-y)\,, \tag{3.11}$$

therefore the second derivative of effective action is the inverse of the connected propagator

$$\frac{\delta^2\Gamma[\varphi]}{\delta\varphi\delta\varphi} = \left(\frac{\delta^2 W[J]}{\delta J\delta J}\right)^{-1}. \tag{3.12}$$

By approximating the field and the source in the spacetime volume Ω as constants ($\varphi(x) = \phi_0$, $J(x) = J_0$), the effective action can be reduced to the effective potential as follows

$$\Gamma[\phi] = \Omega\, V_{\text{eff}}(\phi_0)\,, \quad W[J] = \Omega w(J_0)\,, \tag{3.13}$$

while (3.12) can be written as

$$\left(\frac{\delta^2 V_{\text{eff}}}{\delta\phi_0\delta\phi_0}\right)\left(\frac{\delta^2 w}{\delta J_0\delta J_0}\right) = 1\,. \tag{3.14}$$

In the above expression the second term, i.e., the second derivative of the generating functional of the connected Green functions is the connected correlation function which takes only positive values. Therefore, the effective potential must be convex [17]

$$\left(\frac{\delta^2 V_{\text{eff}}}{\delta\phi_0\delta\phi_0}\right) \geq 0\,. \tag{3.15}$$

In the next chapter after giving a definition for a scale-dependent effective action $\Gamma_k[\varphi]$, a renormalization group equation for its scale-dependence is derived which also entails a renormalization group equation for the scale-dependent potential.

The strong connection between quantum field theory and statistical physics is not that surprising. Both deals with many particle systems where fluctuations are present. In statistical physics the temperature gives rise to these fluctuations while in quantum field theories the quantum fluctuations are in the nature of the fields since the Heisenberg uncertainty principle is present. In fact a $d = D + 1$ dimensional generating functional of quantum field theory can be mapped onto a d dimensional partition function of a statistical mechanical system. For example the XY spin model ($N = 2$) can be mapped to the $O(2)$ scalar field theory (see Sect. 5.1) via the Hubbard-Stratonovich transformation. In this case, the generating functional of the XY model can be written as

$$Z = \int \mathcal{D}S \;\; \exp\left[\beta J\sum_{\langle ij\rangle} S_i S_j + 2\beta\mu\sum_i S_i^2\right] \;\; \prod_j \delta(S_j^2 - 1) \tag{3.16}$$

$$= \int \mathcal{D}\phi \;\; \exp\left[-\frac{1}{2}\sum_q \phi_q \varepsilon(q)\phi_{-q} - \sum_r U(\phi_r)\right], \tag{3.17}$$

where

$$\varepsilon(q) = 2(Jd+\mu)\frac{d-\varepsilon_0(q)}{J\varepsilon_0(q)+\mu}, \qquad \varepsilon_0(q) = \sum_{\nu}^{d}\cos(q_\nu a)\,, \tag{3.18}$$

$$U(\phi) = -U_0\left(2\sqrt{\frac{\beta}{J}}(Jd+\mu)|\phi|\right) + \frac{Jd+\mu}{J}|\phi|^2, \qquad U_0(\phi) = \log(\pi I_0(|\phi|))\,, \tag{3.19}$$

where I_0 is the modified Bessel function of the first kind [18]. Without violating the symmetries of the model, one can Taylor expand the potential obtaining the Taylor expansion of an $O(2)$ symmetric potential of a field theory. Therefore from an RG point of view, the only differences between the XY spin model and the $O(2)$ field theory are the initial conditions.

In quantum field theory there is also a very strong energy scale dependence. In fact quantum field theories heavily rely on renormalization. At the early development of quantum field theory the naive approach to the momentum loop integrals gave infinities. A solution is to introduce a regularization, for example a momentum cut-off scale Λ. This cut-off parameter can be eliminated by fixing a physical measurable at the energy scale μ. Now, if there are no singularities preventing it, one can take the limit $\Lambda \to \infty$ eliminating the regularization in high energies while preserving the value of the measurable quantities at low energies, i.e., at the scale of measurement. This means that we are fixing a low-energy point in RG space and by taking the $\Lambda \to \infty$ limit we are tracing back an RG trajectory that starts from a Gaussian fixed point, i.e., from a free field theory, where the scale dependence on this cut-off can be eliminated. This technique was developed in the framework of perturbation theory, approximating this renormalization flow around the Gaussian fixed point. But perturbation theory has its drawbacks. One of these drawbacks is that irrelevant interactions cannot be considered consistently, because towards high energies the coupling constants could increase, and divert the RG trajectory from the Gaussian fixed point. Therefore for each order of the perturbative expansion new type of diagrams has to be introduced in order to control the divergent tendency of the irrelevant interactions and to be able to eliminate the cut-off parameter. Fortunately irrelevant couplings are decreasing towards low energies and became, as their name suggests, irrelevant. Thus they are usually not included in the action when doing perturbative calculations. However, if there is another fixed point in the theory the classification of the coupling may change, and can become relevant at low energies. The other drawback is that perturbation theory requires the couplings to be small in order to do the perturbative expansion. This means that it works well only around the Gaussian fixed point.

For these reasons a non-perturbative method is necessary to analyze the full phase diagram of a model, therefore the next chapter is dedicated to the functional renormalization group method, that takes into account irrelevant couplings as well.

Chapter 4

Functional renormalization group

In this chapter the functional renormalization group (FRG) method is discussed. FRG is a powerful method to obtain the phase diagram of models, describe their scale dependence and critical properties. Unlike the perturbative method it can consider irrelevant interactions and remain accurate far from the Gaussian fixed point.

4.1 Derivation

In this section I am going to derive a differential equation for the scale-dependent effective action $\Gamma_k[\varphi]$, the so called Wetterich or FRG equation following mainly the derivations discussed in Refs. [19, 20]. It is presented for a single scalar field, but it can be generalized for multiple fields. First let us write ϕ as an average field φ plus a fluctuation term χ around the average

$$\phi = \varphi + \chi \,. \tag{4.1}$$

This way one can rewrite the generating functional as the integral of the fluctuating field only

$$Z[J] = e^{W[J]} = e^{-\Gamma[\varphi]+\int J\varphi} = \int \mathcal{D}\phi \, e^{-S[\phi]+\int J\phi} = \int \mathcal{D}\chi \, e^{-S[\varphi+\chi]+\int J(\varphi+\chi)} \,. \tag{4.2}$$

After simplifying with the term $e^{\int J\varphi}$ and using that the source is $J = \frac{\delta\Gamma[\varphi]}{\delta\varphi}$, one gets an equation for $\Gamma[\varphi]$ as follows

$$e^{-\Gamma[\varphi]} = \int \mathcal{D}\chi \, e^{-S[\varphi+\chi]+\int \chi \frac{\delta\Gamma[\varphi]}{\delta\varphi}} \,. \tag{4.3}$$

From this the on-shell ($J = \frac{\delta\Gamma[\varphi_*]}{\delta\varphi} = 0$) ground state can be calculated

$$e^{-\Gamma[\varphi_*]} = \int \mathcal{D}\chi \, e^{-S[\varphi_*+\chi]} = Z \quad \Longrightarrow \quad \Gamma[\varphi_*] = -\log Z \,. \tag{4.4}$$

Doing the path integral in (4.3) using the saddle point approximation gives the loop expansion of the effective action

$$\Gamma[\varphi] = S[\varphi] + \frac{1}{2} \operatorname{Tr} \log \frac{\delta^2 S[\varphi]}{\delta\varphi\delta\varphi} + \dots \,. \tag{4.5}$$

To implement the idea of the renormalization group approach one has to introduce a running cut-off scale. Here we consider an infrared (IR) cut-off k by changing the measure of the path integral. This is done by adding another term to the action

$$\mathcal{D}\chi \to \mathcal{D}\chi \, e^{-\Delta S_k[\chi]} \,, \tag{4.6}$$

that guarantees that the modes lower than k are suppressed, and therefore only the modes higher than the cut-off k are integrated out. Implementing this idea the scale-dependent effective action by definition is written as

$$e^{-\Gamma_k[\varphi]} = \int \mathcal{D}\chi \, e^{-S[\varphi+\chi]-\Delta S_k[\chi]+\int \chi \frac{\delta\Gamma_k[\varphi]}{\delta\varphi}} \,. \tag{4.7}$$

The term ΔS_k must suppress the lower modes by not letting them propagate. This can be achieved by a large mass term, thus the cut-off function is

$$\Delta S_k[\phi] = \frac{1}{2} \int \phi R_k(-\partial^2)\phi \,, \tag{4.8}$$

where R_k is called the regulator function, which in momentum space depends on the momentum $R_k(p)$. This function must satisfy the following conditions

$$R_{k\to 0}(p) = 0, \quad R_{k\to\Lambda}(p) = \infty, \quad R_k(p \to 0) > 0 \,. \tag{4.9}$$

The first condition is necessary in order to recover the full effective action in the $k \to 0$ limit. It is trivially true, since in this limit the regulator is zero. From the second condition if $k \to \Lambda$ the regulator function tends to infinity, therefore it does not allow any fluctuation to propagate. Thus Γ_Λ is the bare action, our starting point where the quantum fluctuations are not taken into account yet. From the loop expansion of the scale-dependent effective action

$$\Gamma_k = S_\Lambda + \frac{1}{2} \int \frac{d^d p}{(2\pi)^d} \ln \left[R_k + S^{(2)}_\Lambda \right] + \dots \,, \tag{4.10}$$

it is also clear that if the regulator is infinitely large, then all the terms containing it become field independent and can be excluded. The only term that survives is the first one, S_Λ, the bare action. Therefore the scale-dependent effective action is interpolating between the classical bare action and the full effective action.

$$\Gamma_{k\to 0} = \Gamma_{\text{eff}}, \qquad \Gamma_{k\to\Lambda} = \Gamma_\Lambda = S_\Lambda \,. \tag{4.11}$$

The third condition of the regulator is necessary for the IR regularization. To see this, consider a typical massless propagator $G(p) = 1/p^2$, that is divergent in the $p \to 0$ limit. The regulator changes this propagator as follows

$$G(p) = \frac{1}{p^2} \quad \to \quad \frac{1}{p^2 + R_k} \,. \tag{4.12}$$

Since the regulator stays positive in the $p \to 0$ limit, $R_k(p \to 0) > 0$, the denominator does not tend to zero and the propagator does not become divergent in this limit, see Fig. 4.1. A few typical choices for the regulator functions are listed here to see their properties. They are discussed in detail in Sect. 4.2.2.

$$R_k^{\rm opt}(p^2) = (k^2 - p^2)\theta(k^2 - p^2) \tag{4.13}$$

$$R_k^{\rm exp}(p^2) = \frac{p^2}{e^{p^2/k^2} - 1} \tag{4.14}$$

$$R_k^{\rm pow}(p^2) = \left(\frac{k^2}{p^2}\right)^b \tag{4.15}$$

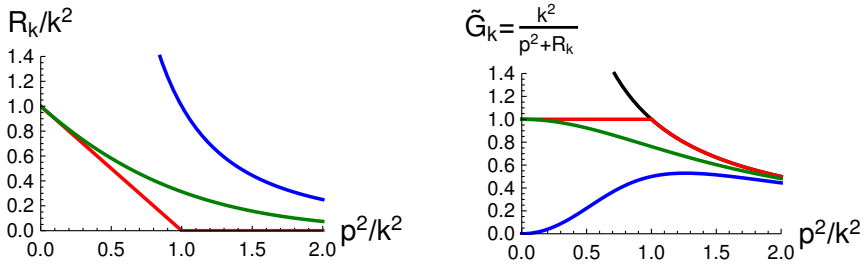

Figure 4.1: On the left the typical regulator functions are shown. Different colors represent different regulators. The red corresponds to the optimized, the blue to the exponential while the green to the power-law regulator. On the right the effect of these regulators is shown to a massless propagator while the black curve is the propagator without a regulator.

Now we turn our attention back to the scale-dependent effective action. The definition of the scale-dependent generating functional of the connected diagrams writes as

$$e^{W_k[J]} = \int \mathcal{D}\phi \, e^{-S[\phi] - \Delta S_k[\phi] + \int J\phi} \,. \tag{4.16}$$

Is $\Gamma_k[\varphi]$ the Legendre transformation of this functional, $W_k[J]$? The answer is no, to obtain the correct Legendre transform of the scale-dependent $W_k[J]$ one also has to add the cut-off function.

$$\Gamma_k[\varphi] + \Delta S_k[\varphi] = -W_k[J] + \int \varphi J \,. \tag{4.17}$$

Therefore the relations (3.10) and (3.12) also change accordingly

$$\frac{\delta(\Gamma_k[\varphi]+\Delta S_k[\varphi])}{\delta\varphi}=J_\varphi\,,\qquad \frac{\delta^2(\Gamma_k[\varphi]+\Delta S_k[\varphi])}{\delta\varphi\delta\varphi}=\left(\frac{\delta^2 W_k[J]}{\delta J\delta J}\right)^{-1}. \tag{4.18}$$

To see why, let us use the following property of the cut-off function

$$\begin{aligned}\Delta S_k[\varphi+\chi]=&\frac{1}{2}\int(\varphi+\chi)R_k(\varphi+\chi) &(4.19)\\ =&\frac{1}{2}\int\varphi R_k\varphi+\int\varphi R_k\chi+\frac{1}{2}\int\chi R_k\chi &(4.20)\\ =&\Delta S_k[\varphi]+\int\frac{\delta\Delta S_k[\varphi]}{\delta\varphi}\chi+\Delta S_k[\chi]\,. &(4.21)\end{aligned}$$

Solving this equation for $\Delta S_k[\chi]$ and substituting into (4.7) one gets

$$\begin{aligned}&e^{-\Gamma_k[\varphi]-\Delta S_k[\varphi]}= &(4.22)\\ &=\int\mathcal{D}\chi\,\exp\left[-S[\varphi+\chi]-\Delta S_k[\varphi+\chi]+\int\chi\frac{\delta(\Gamma_k[\varphi]+\Delta S_k[\varphi])}{\delta\varphi}\right] &(4.23)\\ &=\int\mathcal{D}\phi\,\exp\left[-S[\phi]-\Delta S_k[\phi]+\int(\phi-\varphi)\frac{\delta(\Gamma_k[\varphi]+\Delta S_k[\varphi])}{\delta\varphi}\right]. &(4.24)\end{aligned}$$

From the first relation of (4.18) and using the definition of $W_k[J]$, one obtains

$$e^{-\Gamma_k[\varphi]-\Delta S_k[\varphi]}=e^{W_k[J]-\int\varphi J}\,, \tag{4.25}$$

which is equivalent to (4.17) that we wanted to prove.

Finally we are ready to derive a differential equation for the functional $\Gamma_k[\varphi]$. Therefore the next step is to differentiate (4.17) with respect to the scale, while keeping φ constant. This can be done, however the source will be scale-dependent, since it is the derivative of the scale-depenent Γ_k with respect to the field. Keeping this in mind the derivative becomes

$$\begin{aligned}k\partial_k\Gamma_k[\varphi]=&-k\partial_k W_k[J]-k\partial_k\Delta S_k[\varphi]-\int\frac{\delta W_k[J]}{\delta J}k\partial_k J+\int\varphi k\partial_k J &(4.26)\\ =&\langle k\partial_k\Delta S_k[\phi]\rangle-k\partial_k\Delta S_k[\varphi] &(4.27)\\ =&\frac{1}{2}\int\langle\phi\phi\rangle\,k\partial_k R_k-\frac{1}{2}\int\varphi\varphi k\partial_k R_k &(4.28)\\ =&\frac{1}{2}\int\frac{\delta^2 W_k[J]}{\delta J\delta J}k\partial_k R_k &(4.29)\\ =&\frac{1}{2}\,\mathrm{Tr}\left(\frac{\delta^2\Gamma_k[\varphi]}{\delta\varphi\delta\varphi}+R_k\right)^{-1}k\partial_k R_k &(4.30)\\ =&\frac{1}{2}\,\mathrm{Tr}\,\frac{k\partial_k R_k}{R_k+\Gamma_k^{(2)}[\varphi]}\,. &(4.31)\end{aligned}$$

Therefore the final equation, the so called Wetterich or FRG equation [21,22] writes as

$$\boxed{k\partial_k\Gamma_k[\varphi] = \frac{1}{2}\,\mathrm{Tr}\,\frac{k\partial_k R_k}{R_k + \Gamma_k^{(2)}[\varphi]}} \tag{4.32}$$

To end this section let us note a few important properties of this equation. It is a non-linear integro-differential equation that constitutes functionals. This equation is exact, no approximations were used for its derivation. However approximations are usually necessary to obtain its solutions. Unlike perturbation theory here the approximations are usually not in powers of a small parameter, instead the theory space is restricted by using a gradient or derivative expansion of the scale-dependent effective action. The effect of these approximations are discussed in the next section. The regulator does not only regularize the IR behavior, but the $k\partial_k R_k$ term also makes the equation finite in the large momentum, i.e., in the ultraviolet (UV) limit. For example the θ function of the optimized regulator

$$k\partial_k R_k = 2k^2\theta(k^2-p^2) + (k^2-p^2)\delta(k^2-p^2) = 2k^2\theta(k^2-p^2)\,, \tag{4.33}$$

shows that the upper bound of the momentum integral is k which is a finite value, thus the integral also stays finite. It is generally true that the scale derivative of the regulator tends to zero, regularizing the momentum integral in the UV limit. Because of the UV regularization and because the integral only goes up to k, the higher modes of the fluctuations coming from, for example a mass term m, do not influence the RG running for $k < m$. The path integral does not need to be performed, because the FRG equation describes the relation between two infinitesimally close points in phasespace. Therefore only a loop integral has to be performed, integrating out an infinitesimal range of fluctuations on a momentum shell. Comparing the FRG equation to the scale derivative of the loop expansion (4.10), the only difference is the replacement $S_\Lambda \to \Gamma_k$. For this reason the FRG equation is also called the 1-loop improved RG equation.

4.2 Optimization and regulator functions

In this section further properties of the FRG equation and the regulator functions are discussed relying on Ref. [23]. The exact RG equation provides physical results that are independent of the specific form of the regulator [24, 25], which means that the UV and IR limits of the scale-dependent effective action are well-defined, i.e., $\Gamma_{k\to 0} = \Gamma_{\text{eff}}$ and $\Gamma_{k\to\Lambda} = S_\Lambda$. This is guaranteed by the imposed properties of the regulator function (4.9). The RG flow in the parameter space depends on the actual choice of the regulator but the initial and final value does not, see Fig. 4.2.

The FRG equation is an integro-differential equation for functionals and thus, it is generally not possible to have exact solutions. Therefore, approximations must be used. One of the most often used approximations is the reduction of the theory space by truncating the so called gradient or derivative expansion of the effective

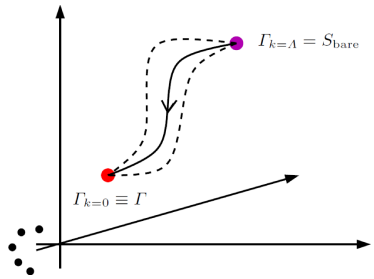

Figure 4.2: Exact RG flow in the parameter space for the effective action which depends on the particular choice of the regulator. The initial and final values of the running effective action are regulator independent.

action,

$$\Gamma_k[\varphi] = \int d^d x \left[V_k(\varphi) + Z_k(\varphi) \frac{1}{2} (\partial_\mu \varphi)^2 + ... \right]. \tag{4.34}$$

The most drastic truncation is called the local potential approximation (LPA) where only the first derivative is kept and the wave-function renormalization is fixed as a scale-independent constant $Z_k \equiv 1$. Within LPA the FRG equation can be simplified and written as an equation for the effective potential

$$k\partial_k V_k(\varphi) = \frac{1}{2} \, \mathrm{Tr} \, \frac{k\partial_k R_k}{R_k + p^2 + V_k''(\varphi)} \, . \tag{4.35}$$

A better approximation is the LPA′, where the wave-function renormalization is also a running coupling but it does not depend on the field $Z_k = Z_k(\not{\varphi})$.

Further approximations are also commonly used such as the Taylor or Fourier expansion of the potential $V_k(\varphi)$

$$V_k(\varphi) = \sum_{n=1}^{N_{\rm cut}} \frac{g_n(k)}{n!} \, \varphi^n, \qquad\qquad V_k(\varphi) = \sum_{n=1}^{N_{\rm cut}} u_n(k) \, \cos(n\beta\varphi), \tag{4.36}$$

where $N_{\rm cut}$ denotes the number of terms kept in the series. The couplings $g_n(k)$ or $u_n(k)$ depend on the running RG scale k encoding the scale-dependence of the potential.

The use of approximations can lead to the scheme-dependence of the RG running, i.e., the obtained physical results may depend on the particular choice of the regulator. Hence, it is important to study which regulator gives the most accurate results for a given approximation.

4.2.1 Optimization

To improve the accuracy of the approximate FRG calculations, it is necessary to optimize the regulator-dependence. One of the most well-known optimization

methods is called the Litim–Pawlowski method [24,25] which is based on the convergence properties of amplitude expansions. This general optimization criterion states that the most regular FRG running is obtained if the gap in the inverse propagator C is maximal

$$\min_{p^2\geq 0}\left(\left.\frac{\delta^2\Gamma_k[\varphi]}{\delta\varphi(p)\delta\varphi(-p)}\right|_{\phi=\phi_0}+R_k(p^2)\right)=Ck^2>0\,. \tag{4.37}$$

For example, the FRG equation in LPA can be written as

$$k\partial_k V_k = -\alpha_d k^d\int_0^\infty \mathrm{d}y\,\frac{dr}{dy}\,\frac{y^{d/2+1}}{P^2+\omega}\,, \tag{4.38}$$

$$P^2 = [1+r(y)]\,y\,,\quad \omega=\frac{V_k''}{k^2}\,, \tag{4.39}$$

where $\alpha_d=\Omega_d/(2(2\pi)^d)$ with $\Omega_d=2\pi^{d/2}/\Gamma(d/2)$ being the d-dimensional solid angle, while $r(y)$ is the dimensionless form of the regulator defined as

$$r(y)=\frac{R_k(p)}{p^2},\quad y=\frac{p^2}{k^2}\,. \tag{4.40}$$

In this case, the amplitude expansion takes the form

$$k\,\partial_k V_k=\sum_{m=1}^{\infty}\frac{2m}{d}\;a_{2m-d}\;(-\omega)^{m-1}\,, \tag{4.41}$$

$$a_n=\int_0^\infty \mathrm{d}y\left(-\frac{d}{2}\frac{r'}{(1+r)^{d/2+1}}\right)P^{-n}\,, \tag{4.42}$$

while the gap in the RG flow after neglecting the momentum-independent terms, or equivalently, the radius of convergence of the series can be given by the expression

$$C=\min_{y\geq 0}P^2(y)\,. \tag{4.43}$$

According to the method, the optimal regulator provides the fastest convergence in this series. Following this general guideline for optimization and choosing a momentum-independent propagator, $P^2=1$, Litim's optimized regulator has been derived from (4.39) and (4.43) [24]. It is a continuous function with compact support, which gives excellent analytic results [26], however it is not differentiable, thus it does not support the derivative expansion [27,28]. The Litim–Pawlowski optimization procedure can also determine the optimal parameters for various types of regulators by searching for the best convergence properties.

Another well-known optimization method is based on the principle of minimal sensitivity (PMS) [29], which as the name suggests, attempts to choose the optimal parameters of a regulator by making the physical quantities as insensitive as possible to any conceivable changes in these parameters. It is not to be confused with the principle of minimal sensitivity in perturbation theory, where the term is used

for the optimization condition that ensures the vanishing of higher loop order contributions to physical quantities [30]. This procedure can be utilized in any order of the gradient expansion, however its disadvantage is that it operates under the implicit assumption that the insensitivity produces the optimal parameters rather than some non-optimal values in parameter space. Another disadvantage of the method is that regulators that have different functional form cannot be compared to each other.

Solution for the above problems of differentiability (in case of the Litim–Pawlowski optimization) and comparability (in case of the PMS method) could be the recently introduced [31] compactly supported smooth (CSS) regulator. It is a smooth, inflinitely differentiable (class C^∞) function with compact support, which can recover all major types of regulator functions proposed in the literature. Thus, using the CSS regulator with the PMS optimization method allows the comparison of different regulators. Additionally, the CSS regulator is an inffinitely differentiable, smooth function with compact support, therefore its "Litim limit" can be considered at any order of the derivative expansion.

4.2.2 Regulator functions

Various functional forms has been proposed in the literature for the regulator function. Here the most common ones are discussed using their dimensionless form, $r(y)$ defined in (4.40). For instance, the regulator can take the simple form

$$r_{\mathrm{sharp}}(y) = \frac{1}{\theta(y-1)} - 1\,, \tag{4.44}$$

where the suppression of certain modes are controlled by the Heaviside step function $\theta(y)$. This regulator is called the sharp-cutoff, and in LPA it allows the momentum integral of (4.35) to be evaluated analytically, obtaining an RG identical to the Wegner-Houghton equation [32] in this approximation. However, due to the Heaviside step function, higher derivatives in the gradient expansion cannot be determined unambiguously.

On the other hand, an exponential regulator [21] such as

$$r_{\mathrm{exp}}(y) = \frac{a}{\exp\left(c_2 y^b\right) - 1}\,, \tag{4.45}$$

is compatible with the gradient expansion. The optimal parameters of this regulator are $a = 1$, $c_2 = \ln(2)$ and $b = 1.44$ determined by the Litim–Pawlowski optimization procedure [24, 25]. The disadvantage of this regulator type is that analytic RG equations cannot be indicated, i.e., it requires the momentum integral to be performed numerically.

Another type of regulator which supports the gradient expansion (if $b \geq 1$) is the power-law regulator [22]

$$r_{\mathrm{pow}}(y) = \frac{a}{y^b}\,. \tag{4.46}$$

Based on the Litim–Pawlowski optimization method the favorable parameter choices are $a = 1$ and $b = 2$ [24,25]. For this regulator it is also possible to perform the momentum integral analytically, but only in LPA. It has the disadvantageous property that it is not UV finite in all dimensions for $b = 1$.

The issue of UV safety can be avoided by the (general) optimized regulator, also called Litim regulator [24], which can be written as

$$r_{\mathrm{opt}}^{\mathrm{gen}}(y) = a\left(\frac{1}{y^b} - 1\right)\Theta(1 - y^b)\,. \tag{4.47}$$

It is a continuous regulator which has a compact support, however it is not differentiable. According to the Litim–Pawlowski method, the optimal parameter choices in LPA are $b = 1$ and $a = 1$ [24,25]. This regulator allows the momentum integral to be performed analytically for all dimensions in LPA, and also when the wave-function renormalization is taken into account if higher derivatives of the gradient expansion are not included. As discussed above, the Litim regulator, as a solution to the Litim–Pawlowski optimization, provides the best convergence properties for the amplitude expansion in LPA. Indeed, it was demonstrated that in LPA it yields the closest results to the accepted ones for the critical exponents of the three-dimensional $O(N)$ model [26]. In LPA, the derived FRG equation using this regulator is equivalent to the Polchinski RG [33]. Nevertheless, the Litim regulator also has the disadvantage that it is not compatible with the gradient expansion beyond second order due to its non-differentiability [27,28]. However, differentiability is argued to be an important condition for optimization.

One of the main goals of this thesis is the optimization of the so called CSS regulator [31] which has the form

$$r_{\mathrm{css}}^{\mathrm{gen}}(y) = \frac{\exp\left[cy_0^b/(f - hy_0^b)\right] - 1}{\exp[cy^b/(f - hy^b)] - 1}\theta(f - hy^b), \tag{4.48}$$

which is an infinitely differentiable function even at the point $f - hy^b = 0$. It must be noted, that this form can be simplified with no loss of generality by substituting $f = 1$,

$$r_{\mathrm{css}}^{\mathrm{modif}}(y) = \frac{\exp\left[cy_0^b/(1 - hy_0^b)\right] - 1}{\exp[cy^b/(1 - hy^b)] - 1}\theta(1 - hy^b). \tag{4.49}$$

Both variations can reproduce all major types of regulator functions, namely Litim's optimized one (4.47), the power-law type (4.46) and the exponential (4.45) regulators,

$$\begin{aligned}
\lim_{c\to 0} r_{\mathrm{css}}^{\mathrm{gen}} &= \lim_{c\to 0, h=1} r_{\mathrm{css}}^{\mathrm{modif}} = \frac{y_0^b\,(y^{-b} - 1)}{1 - y_0^b}\,\theta(1 - y^b),\\
\lim_{f\to\infty} r_{\mathrm{css}}^{\mathrm{gen}} &= \lim_{h\to 0, c\to 0} r_{\mathrm{css}}^{\mathrm{modif}} = \frac{y_0^b}{y^b},\\
\lim_{h\to 0, c=f} r_{\mathrm{css}}^{\mathrm{gen}}(y) &= \lim_{h\to 0, c\to 1} r_{\mathrm{css}}^{\mathrm{modif}} = \frac{\exp\left[y_0^b\right] - 1}{\exp[y^b] - 1}.
\end{aligned} \tag{4.50}$$

In the limit $c \to 0, h \to 1$ it recovers the It is possible to further reduce the number of free parameters by fixing the value of y_0, so that the numerator of the CSS regulator simplifies to a linear function of c.

$$r_{\text{css}}^{\text{norm1}}(y) = \frac{c}{\exp[cy^b/(1-hy^b)]-1}\theta(1-hy^b). \tag{4.51}$$

The critical properties of the $O(1)$ theory was studied using this normalized form of the CSS in [34] to investigate the scheme-dependence of the RG equations obtained for Quantum Einstein Gravity. The linearly normalized CSS regulator (4.51) has the limits,

$$\lim_{c\to 0,h\to 1} r_{\text{css}}^{\text{norm1}} = \left(\frac{1}{y^b}-1\right)\theta(1-y^b), \tag{4.52a}$$

$$\lim_{c\to 0,h\to 0} r_{\text{css}}^{\text{norm1}} = \frac{1}{y^b}, \tag{4.52b}$$

$$\lim_{c\to 1,h\to 0} r_{\text{css}}^{\text{norm1}} = \frac{1}{\exp[y^b]-1}. \tag{4.52c}$$

The norm (4.51) is one of the simplest choices for y_0, and this type of the CSS can reproduce the optimized Litim regulator (with $b = 1$), the optimized power-law regulator (with $b = 2$), yet it cannot recover the optimal parameters for the exponential regulator (4.45) [$c_2 = \ln(2)$].

However it is also possible to choose other types of normalization, for example an exponential one, such as

$$r_{\text{css}}^{\text{norm}}(y) = \frac{\exp[\ln(2)c]-1}{\exp\left[\frac{\ln(2)cy^b}{1-hy^b}\right]-1}\Theta(1-hy^b) = \frac{2^c-1}{2^{\frac{c\,y^b}{1-hy^b}}-1}\Theta(1-hy^b), \tag{4.53}$$

with the limits,

$$\lim_{c\to 0,h\to 1} r_{\text{css}}^{\text{norm}} = \left(\frac{1}{y^b}-1\right)\Theta(1-y^b), \tag{4.54a}$$

$$\lim_{c\to 0,h\to 0} r_{\text{css}}^{\text{norm}} = \frac{1}{y^b}, \tag{4.54b}$$

$$\lim_{c\to 1,h\to 0} r_{\text{css}}^{\text{norm}} = \frac{1}{\exp[\ln(2)y^b]-1}. \tag{4.54c}$$

This norm has the advantage that it can recover all major types of regulators with their optimal parameters, thus using the CSS regulator with the PMS optimization method allows the comparison of different regulators. While the Litim regulator does not support the derivative expansion, the CSS regulator still has a compact support, but it is also smooth and infinitely differentiable, therefore its "Litim limit" (with a small but nonzero c parameter) can be considered at any order of the derivative expansion.

Chapter 5

$O(N)$ and sine-Gordon type models

In my thesis the most studied models are the $O(N)$ and sine-Gordon type models, therefore this section is dedicated to them. Their symmetries, critical properties, phase diagrams and other properties are discussed that will be used in the second part of the thesis.

5.1 $O(N)$ models

In this section let us revisit the $O(N)$ model in the context of quantum field theory and functional renormalization group [14].

The $O(N)$ model as a scalar field must have an action that is symmetric to the $O(N)$ transformations. Thus the Euclidean action of the $O(N)$ model in the local potential approximation, where the higher derivatives of the field are neglected and the wave-function renormalization is set to one, takes the form [14, 26]

$$S_{\mathrm{ON}}[\varphi] = \int \left[\frac{1}{2} (\partial_\mu \varphi)^2 + V_{\mathrm{ON}}(\varphi) \right] , \tag{5.1}$$

where φ is a vector with N components, and the potential can only depend on the magnitude of φ due to the $O(N)$ symmetry. As discussed in Chapt. 3 this scalar field model can be mapped to statistical models using the Hubbard-Stratanovich transformation, therefore the properties discussed below also apply to those.

In these models the fluctuations and the interactions are competing against each other. As we saw for the ferromagnetic spin models it is energetically favorable for the spins to align, but there are cases when the temperature fluctuations win and a spatial long-range order cannot form. The situation is the same in quantum field theory, the quantum fluctuations can prevent the formation of long-range correlations. In this competition the dimensionality, i.e., both the dimension of spacetime and the internal dimension of the field play an important role. It is

easy to understand why, while in lower dimension the fluctuations dominate, by increasing the dimension the number of neighbors and the number of pair interactions also increase for each spin (or field, considering spacetime as a lattice), therefore the interactions will become the dominant factor. This also means that a mean field theory becomes a better approximation as the dimension increases. In fact in $d \geq 4$ the critical behavior of the Ising model can be described entirely by its mean field theory therefore $d = 4$ is called the upper critical dimension of the Ising model [15,35]. In small dimensions the fluctuations dominate and it was shown by Landau that in $d = 1$, it is impossible for any model to have a phase transition. In $d \leq 2$ there is a theorem called Mermin-Wagner theorem stating that if *(i)* there are fluctuations ($T \neq 0$), *(ii)* the interaction has a short range, *(iii)* the system is in its thermodynamic limit, then a continuous symmetry cannot be broken, indicating that there cannot be a second order phase transition between the symmetric and the symmetry-broken phase [36–38]. This however does not exclude all phase transitions in $d \leq 2$. Indeed there are very famous exceptions among the $O(N)$ models. One is the Ising or $O(1)$ model in $d = 2$. Since the Ising model has a only a Z_2 symmetry i.e., a discrete symmetry, the Mermin-Wagner theorem does not apply, and indeed this model has two phases [10]. Another exception is the XY or $O(2)$ model in $d = 2$. This model is restricted by the Mermin-Wagner theorem, however it still has a topological phase transition [18].

These properties can be investigated by the FRG method. Without breaking the $O(N)$ symmetry the potential can be Taylor expanded as a further approximation. Using the dimensionless potential $u_k \equiv k^{-d}V_k$ and dimensionless variables the Taylor expansion of the potential around zero writes as

$$u_k(\varphi) = \sum_{n=1}^{N_{CUT}} \frac{1}{(2n)!} g_n(k)\, \varphi^{2n}. \tag{5.2}$$

For simplicity the tilde notation for dimensionless variables is not used here. A new field variable $\rho = (1/2)\varphi^2$ can be introduced, therefore the Taylor expanded potential takes the form

$$u_k(\rho) = \sum_{n=1}^{N_{CUT}} \frac{1}{n!} \lambda_n(k)\, \rho^n. \tag{5.3}$$

As indicated, the scale-dependence is encoded in the dimensionless couplings which are connected by the relation $g_n(k)/(2n-1)!! = \lambda_n(k)$.

Since φ is an N component vector the FRG equation for the potential in LPA reads [14]

$$k\partial_k V_k = \frac{1}{2}\,\mathrm{Tr}\left[k\partial_k R_k \left(\frac{\partial^2 V_k}{\partial\varphi_i \partial\varphi_j} + (p^2 + R_k)\delta_{ij}\right)^{-1}\right], \tag{5.4}$$

where the trace means not only the integration over p, but also the summation over the N indices of φ. Using the $O(N)$ symmetry we can choose the direction of φ to be aligned with the first axis, thus all the components of φ is zero except the

first one

$$\varphi = (\varphi_1, 0, 0, \dots) \,. \tag{5.5}$$

The second derivative of the potential can be written as

$$\frac{\partial^2 V_k}{\partial\varphi_i \partial\varphi_j} = \frac{\partial V_k}{\partial\rho}\delta_{ij} + \frac{\partial^2 V_k}{\partial\rho^2}\varphi_i\varphi_j = \frac{\partial V_k}{\partial\rho}\delta_{ij} + 2\rho\frac{\partial^2 V_k}{\partial\rho^2}\delta_{1i}\delta_{1j} \,. \tag{5.6}$$

Therefore the right hand side of (5.4) contains a diagonal matrix that can be easily inverted

$$\frac{\partial^2 V_k}{\partial\varphi_i \partial\varphi_j} + (p^2 + R_k)\delta_{ij} = \begin{pmatrix} p^2 + R_k + \frac{\partial V_k}{\partial\rho} + 2\rho\frac{\partial^2 V_k}{\partial\rho^2} & & & \\ & p^2 + R_k + \frac{\partial V_k}{\partial\rho} & & \\ & & \ddots & \\ & & & p^2 + R_k + \frac{\partial V_k}{\partial\rho} \end{pmatrix} . \tag{5.7}$$

After calculating the inverse and the trace of this matrix one obtains

$$k\partial_k V_k = \frac{1}{2}\int_p k\partial_k R_k \left(\frac{1}{p^2 + R_k + V_k' + 2\rho V_k''} + \frac{N-1}{p^2 + R_k + V_k'} \right) , \tag{5.8}$$

where the prime means taking the derivative with respect to ρ. By substituting the Litim regulator ((4.47) with $b = 1$) the integration can be easily evaluated analytically. Using the dimensionless potential $u_k \equiv k^{-d} V_k$ and dimensionless variables we finally obtain the FRG equations in LPA for the $O(N)$ model [14]

$$\begin{aligned} k\partial_k u &= (d-2)\rho u' - du + \frac{(N-1)A_d}{1+u'} + \frac{A_d}{1+u'+2\rho u''}, \\ A_d &= \frac{1}{2^{d+1}}\frac{1}{\pi^{d/2}}\frac{1}{\Gamma(d/2)}\frac{4}{d}, \end{aligned} \tag{5.9}$$

where $u' = \partial_\rho u$ and $\Gamma(x)$ is the gamma function. Let us look at the simplest example one can think of, the Ising model in $d = 2$ dimensions, with the most drastic approximation, i.e., when $N_{CUT} = 2$.

Differentiating the FRG equation for the potential with respect to the field, then substituting zero yields the FRG equations for the couplings,

$$k\partial_k g_1 = -2g_1 - \frac{1}{4\pi}\frac{g_2}{(1+g_1)^2}, \tag{5.10}$$

$$k\partial_k g_2 = -2g_2 + \frac{6}{4\pi}\frac{g_2^2}{(1+g_1)^3}. \tag{5.11}$$

By solving these differential equations one can obtain the phase diagram shown in Fig. 5.1. As the figure shows, the model has two phases, a symmetric and a spontaneous symmetry-broken phase. The critical WF fixed point corresponding to the phase transition is drawn by a green point. In the symmetry-broken phase the RG trajectories run into the IR convexity fixed point indicated by a red point.

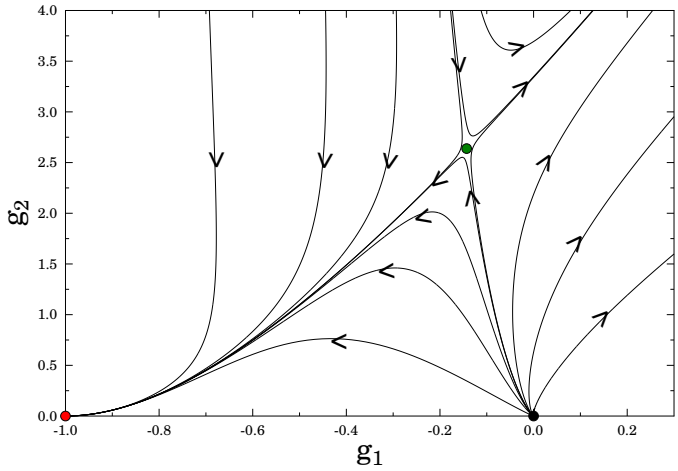

Figure 5.1: Phase diagram of the Ising model in $d = 2$ dimensions.

Here the potential has degenerate minima, therefore by choosing one of the minima, the ground state spontaneously breaks the symmetry of the potential. When all couplings are zero the model is reduced to a free field theory and there is no RG running. This is the Gaussian fixed point shown by the black point on the figure. By increasing the dimension up to $d = 4$ the WF and the Gaussian fixed points merge and the mean field theory appropriately describes the critical behavior of the model [39]. In dimensions smaller than four one obtains similar diagrams using the LPA. However as discussed above, in $d = 1$ the model cannot have a phase transition and therefore cannot have a WF fixed point. Also the symmetry-broken phase cannot exist, since in $d = 1$ the quantum mechanic and the quantum field theory descriptions are equivalent and the quantum mechanical effect of quantum tunneling prevents spontaneous symmetry breaking [15, 40]. This discrepancy can be resolved by using an improved approximation. A question arises, what is the appropriate approximation that is sufficient to restore the Mermin-Wagner theorem? My second thesis point is dedicated to this question.

5.2 Sine-Gordon type models

5.2.1 Sine-Gordon model

Besides the $O(N)$ models one of the most studied models by FRG is the sine-Gordon (SG) model. The SG model is defined by the action [41]

$$S_{\mathrm{SG}} = \int \left[\frac{1}{2} \left(\partial_\mu \varphi \right)^2 + u \cos(\beta \varphi) \right] , \tag{5.12}$$

where the two couplings are the Fourier amplitude u, and the frequency β. Strictly speaking from an FRG viewpoint this is only valid in LPA, otherwise all interaction terms should be included that the RG running can generate. In fact even in LPA substituting this action into the FRG automatically generates the higher modes of a periodic function, therefore a full ansatz for the potential has the form

$$V_{\mathrm{SG}} = \sum_{n=1}^{N_{CUT}} u_n \cos(n\beta\varphi)\,. \tag{5.13}$$

The model has a Z_2 symmetry and it is also periodic. The action is invariant under the following transformations

$$\varphi \to \phi = -\varphi, \tag{5.14}$$

$$\varphi \to \phi = \varphi + \frac{2\pi}{\beta}\,. \tag{5.15}$$

These symmetries play a crucial role shaping the phase diagram of the model, since the RG transformations must preserve them. This also means that the dimensionful frequency, β, does not change under the RG transformation, otherwise the periodicity would be lost. However beyond LPA it is often merged with the wave-function renormalization by rescaling the field allowing to consider a single coupling, the scale-dependent frequency. As it was discussed, the effective potential, i.e., the potential in the IR limit must be convex. The only function that is both periodic and convex is a constant, therefore the dimensionful u_k tends to zero as $k \to 0$.

Although the SG model is not part of the standard model of particle physics, it has been used to describe the topological phase transition of superfluid films, vortex dynamics, and it can be mapped to the Coulomb-gas in arbitrary dimensions. Its possible applications are also studied in axion, Higgs and inflaton physics [42]. In $d = 2$ it is also equivalent to the fermionic Thirring model and to the XY model [15]. One can already know from this equivalency that the SG model must have a topological phase transition in two dimensions. Indeed Fig. 5.2 shows the phase diagram of the SG model in $d = 2$, obtained by solving the FRG equations in LPA$'$, using the single Fourier-mode approximation ($N_{CUT} = 1$) [42]. As the figure shows the SG model has two phases, a symmetric and a symmetry-broken one. For small $\tilde{u} = uk^{-2}$ values the topological phase transition occurs at the critical frequency $\beta_c^2 = 8\pi$; if $\beta^2 > \beta_c^2$, then the RG trajectories tend to the $\tilde{u} \to 0$ axis which is a line of attractive fixed points corresponding to the symmetric phase, while if $\beta^2 < \beta_c^2$, then the trajectories converge to the IR convexity fixed point where spontaneous symmetry breaking occurs. This is not forbidden by the Mermin-Wagner theorem, since both symmetries that are broken, the periodicity and the Z_2 symmetry are discrete symmetries. The saddle point corresponding to the phase transition is at $\beta_c^2 = 8\pi$, $\tilde{u} = 0$.

Interestingly this exact critical frequency can be easily obtained by FRG using simple approximations [41]. First substituting the Litim regulator into the FRG

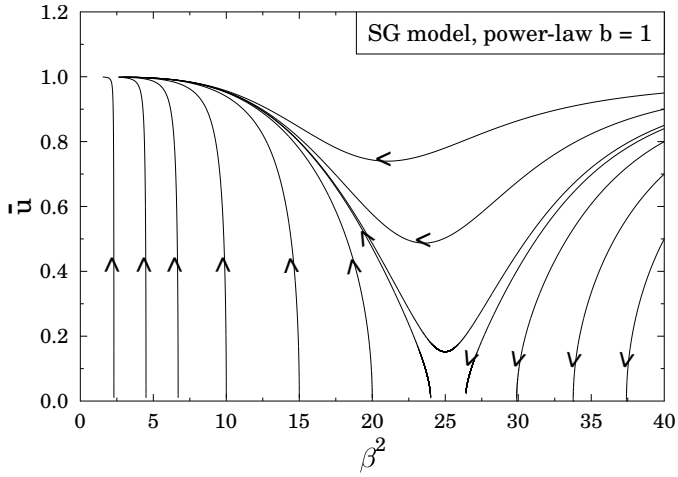

Figure 5.2: Phase diagram of the sine-Gordon model in $d = 2$ dimensions obtained in LPA$'$ using the scale-dependent frequency as a single coupling for both the frequency and the wave-function renormalization.

equation in LPA yields

$$k\partial_k V_k = \frac{1}{4\pi}\frac{k^4}{k^2 + V_k''}\,. \tag{5.16}$$

Then by linearizing the right hand side in terms of V_k'' and throwing out the field-independent term, one obtains

$$k\partial_k V_k = -\frac{1}{4\pi}V_k'' + \mathcal{O}(V_k''^2)\,. \tag{5.17}$$

Substituting the potential and using the single Fourier-mode approximation gives

$$k\partial_k(u_k\cos(\beta\varphi)) = \frac{\beta^2}{4\pi}u_k\cos(\beta\varphi)\,. \tag{5.18}$$

In LPA β does not depend on the RG running scale, k, otherwise the periodicity of the potential would be lost. Therefore the above equation is a simple differential equation for u that has the solution

$$u_k = u_\Lambda\left(\frac{k}{\Lambda}\right)^{\frac{\beta^2}{4\pi}}, \qquad \tilde{u}_k = \tilde{u}_\Lambda\left(\frac{k}{\Lambda}\right)^{\frac{\beta^2}{4\pi}-2}. \tag{5.19}$$

This shows that the tendency of the dimesnionless $\tilde{u}$ changes at $\beta_c^2 = 8\pi$, indicating the correct critical frequency. This value is exact, since in the $\tilde{u} \to 0$ limit the wave-function renormalization does not give contributions and the linearized LPA equation becomes exact. This also means that the critical frequency does not depend on the choice of the regulator and cannot be used for optimization [43].

In higher dimensions the model has only a single phase, the symmetry-broken one, thus all trajectories converge to the IR fixed point [42]. In one dimension, even in LPA′, due to the approximations, the FRG method shows that the two phases are still present, similarly to the Ising model in LPA. However as discussed there, quantum field theory in $d = 1$ is equivalent to a quantum mechanic description, which means that the tunneling effect prevents a spontaneous symmetry breaking. One of the goals of my thesis is to use this phenomenon for optimization.

5.2.2 Massive sine-Gordon model

A possible extension of the sine-Gordon model is the massive sine-Gordon (MSG) model, where an explicit mass term is also added to the periodic self-interaction. Its action has the form [43–45]

$$S_{\mathrm{MSG}} = \int \left[\frac{1}{2}(\partial_\mu \varphi)^2 + \frac{1}{2} M^2 \varphi^2 + u \cos(\beta \varphi) \right] . \tag{5.20}$$

One of the first things to notice is that this mass term breaks the periodicity of the model, while the Z_2 symmetry is intact. This suggests that the MSG model, similarly to the Ising model, has a second-order phase transition, not a topological one, like the SG model in $d = 2$.

One of the advantages of this model in $d = 2$ is that via bosonisation transformations it can be equivalently rewritten as a gauge and fermionic model. As the SG model is equivalent to the fermionic Thirring model, the MSG model is also equivalent to the QED_2 with a massive Dirac fermion, which is also called the massive Schwinger model [46]

$$S_{\mathrm{QED}_2} = \int \left[\bar{\psi} \left(i \gamma^\mu \partial_\mu - m - e \gamma^\mu A_\mu \right) \psi - \frac{1}{4} F_{\mu\nu} F^{\mu\nu} \right] . \tag{5.21}$$

For this equivalency the following relations must be true

$$\beta^2 = 4\pi, \qquad M^2 = e^2/\pi, \qquad u = \frac{e\,m}{2\pi^{3/2}} e^{\gamma}, \qquad \gamma = 0.57721\ldots , \tag{5.22}$$

where γ is the Euler-Mascheroni constant, and the byproduct of the bosonization procedure, i.e., the vacuum angle parameter is chosen to be $\theta = \pm\pi$ for $u > 0$ and $\theta = 0$ for $u < 0$ (see Ref. [44]).

In Fig. 5.3 the phase diagram of the MSG reveals two phases in $d = 2$. The symmetry broken phase, where the RG trajectories merge into a single line, and the symmetric phase where they do not. The phase transition is indeed an Ising-type and it is controlled by the dimensionless ratio u/M^2. This ratio is related to the critical ratio $(m/e)_c$ of QED_2, which separates the half-asymptotic and the confining phases of the fermionic model. The value of this critical ratio has been determined by the density matrix RG approach to be $0.13 < (m/e)_c < 0.33$ [47]. This implies that the critical ratio of the MSG model is around $0.156 < [u/M^2]_c < 0.168$. In the FRG framework in LPA the calculated value is $[u/M^2]_c = 2/(4\pi) \approx$

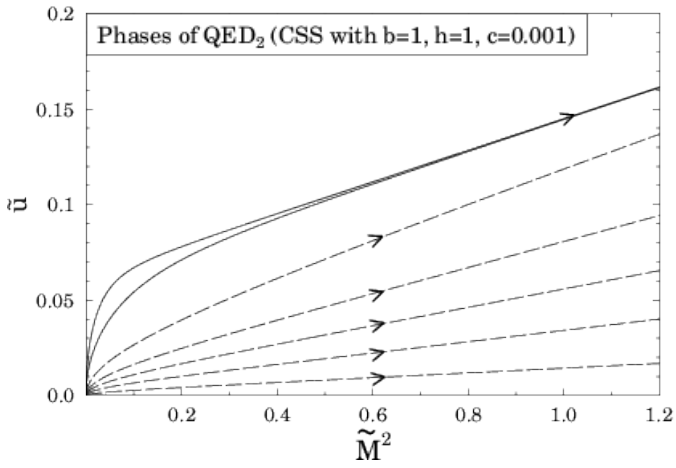

Figure 5.3: Phase diagram of the QED_2 model equvivalent to the MSG model in $d = 2$ with $\beta^2 = 4\pi$ obtained by the CSS regulator in the "Litim limit" ($b = 1, h = 1, c = 0.001$). In the symmetry broken phase the RG trajectories (solid lines) merge into a single line, while the dashed lines correspond to the symmetric phase.

0.15915, that can be derived analytically by considering spinodal instability and the IR behavior of the propagator. Spinodal instability occurs when the FRG equation reaches a singularity, i.e., when the inverse propagator becomes zero. This condition gives the equation

$$\lim_{k\to 0}(k^2 + V_k''(\varphi)) = 0, \tag{5.23}$$

where $V_k(\varphi)$ is the scaling potential which, beside the mass term, should contain all the higher harmonics generated by RG transformations [44]. If all Fourier modes are taken into account, one obtains the mentioned critical ratio $[u/M^2]_c = 2/(4\pi)$. However if the single Fourier-mode approximation is used, i.e., a potential $V_k(\varphi)$ that includes only a single cosine and the mass term, then the analytic considerations based on the IR behavior of the propagator [44, 48] leads to

$$\chi_c = \left[\frac{u}{M^2}\right]_c = \frac{1}{(4\pi)} \approx 0.07957, \tag{5.24}$$

which is half of the result obtained in LPA without further approximations. In this case, the CSS regulator (4.53) with $b = 1$ and $c = 0.01$ gives the ratio $[u/M^2]_c = 0.07964$ close to the analytic prediction. However, other regulator functions such as the power-law type regulator with $b = 1$ run into a singularity, and stop at some finite momentum scale due to the spinodal instability, rendering the determination of the critical ratio [44] impossible. Thus, the scheme dependent convergence properties of the RG equations in the single Fourier mode approximation provides us another tool to optimize the regulator functions.

Chapter 6

Inflationary cosmology

One of the most interesting topics of today's research is inflationary cosmology where particle physics can play a role describing the early stages of the Universe. Recent studies suggest that it is maybe possible to identify the time evolution and the cooling of the Universe as an RG evolution. The consequences of this possibility are studied in the second part of my thesis therefore here I give a very brief introduction to the topic following mostly Ref. [49] and also Refs. [23, 50, 51].

A rapid expansion of the early Universe called inflation explains many issues such as the horizon problem, the flatness of the Universe, and the absence of magnetic monopoles [52]. It is believed that the scale of the Universe got multiplied by a large factor around e^{60}. Let us start with the definition of the so-called Friedmann–Lamaître–Robertson–Walker (FLRW) metric that describes an isotropic, homogeneous expanding Universe, using $(-1,1,1,1)$ signature and $c \equiv 1$

$$g_{\mu\nu} = \begin{pmatrix} -1 & 0 & 0 & 0 \\ 0 & a^2 & 0 & 0 \\ 0 & 0 & a^2 & 0 \\ 0 & 0 & 0 & a^2 \end{pmatrix}, \qquad a = a(t), \qquad g^{\mu\nu} = \begin{pmatrix} -1 & 0 & 0 & 0 \\ 0 & a^{-2} & 0 & 0 \\ 0 & 0 & a^{-2} & 0 \\ 0 & 0 & 0 & a^{-2} \end{pmatrix}, \tag{6.1}$$

$$\begin{aligned} ds^2 =& g_{\mu\nu} dx^\mu dx^\nu = -dt^2 + a^2 \left(dx^2 + dy^2 + dz^2 \right), \\ =& -dt^2 + a^2 \left(dr^2 + r^2 d\theta^2 + r^2 \sin^2\theta \, d\phi^2 \right), \end{aligned} \tag{6.2}$$

which is modified in curved spacetime as

$$ds^2 = -dt^2 + a^2 \left(\frac{dr^2}{1-kr^2} + r^2 d\theta^2 + r^2 \sin^2\theta \, d\phi^2 \right), \tag{6.3}$$

$$ds^2 = a^2 \left(-d\tau^2 + \frac{dr^2}{1-kr^2} + r^2 d\theta^2 + r^2 \sin^2\theta \, d\phi^2 \right), \tag{6.4}$$

where $k = -1, 0, 1$ means open, flat and closed Universes and $d\tau \equiv dt/a$ is the

conformal time. The distance between two particles at $(t,0)$ and (t,r) is

$$d = \int ds = a\int_0^r \frac{dr}{\sqrt{1-kr^2}} = a(t)\begin{cases}\sinh^{-1} r & \text{if } k=-1\\ r & \text{if } k=0\\ \sin^{-1} r & \text{if } k=1\end{cases}, \tag{6.5}$$

and the time derivative of this equation gives the Hubble law

$$\dot{d} = \frac{\dot{a}}{a}d = Hd, \qquad H \equiv \frac{\dot{a}}{a}. \tag{6.6}$$

In order to derive the time-dependence of the scalar factor $a(t)$ one has to use the Einstein equation

$$G_{\mu\nu} = R_{\mu\nu} - \frac{1}{2}Rg_{\mu\nu} = 8\pi G T_{\mu\nu}, \tag{6.7}$$

where R is the scalar curvature and assuming isotropy and homogeneity the stress-energy tensor writes as

$$T^{\mu}_{\nu} = \begin{pmatrix}-\rho & 0 & 0 & 0\\ 0 & p & 0 & 0\\ 0 & 0 & p & 0\\ 0 & 0 & 0 & p\end{pmatrix}, \qquad T_{\mu\nu} = g_{\mu\alpha}T^{\alpha}_{\nu} = \begin{pmatrix}\rho & 0 & 0 & 0\\ 0 & a^2p & 0 & 0\\ 0 & 0 & a^2p & 0\\ 0 & 0 & 0 & a^2p\end{pmatrix}. \tag{6.8}$$

Substituting the FLRW metric and the stress-energy tensor into the Einstein equations gives only two independent equations, the Friedmann and the Raychaudhuri equations

$$H^2 = \left(\frac{\dot{a}}{a}\right)^2 = \frac{8\pi G\rho}{3} - \frac{k}{a^2}, \qquad \text{(Friedmann)} \tag{6.9}$$

$$\frac{\ddot{a}}{a} = -\frac{8\pi G}{6}(\rho + 3p). \qquad \text{(Raychaudhuri)} \tag{6.10}$$

and from the combination of these, one can get a continuity equation (by differentiating the first one and substituting the second)

$$\dot{\rho} + 3H(\rho + p) = 0. \qquad \text{(continuity)} \tag{6.11}$$

Let us note that this can also be interpreted as the consequence of the 1st law of thermodynamics $dU = -pdV \implies d(\rho a^3) = -pd(a^3)$. Now we turn to the discussion of the solutions of the Friedmann equation for $k = 0$, i.e., flat curvature. Let's assume that $\rho \sim a^{-n}$. This is equivalent with an assumption that the equation of state is $p = \omega\rho$. This can be shown using the continuity Eq. (6.11) as follows

$$\frac{d\rho}{\rho} = -3\frac{da}{a}(1+\omega) \implies \rho \sim a^{-3(1+\omega)}, \tag{6.12}$$

therefore

$$\rho \sim a^{-n} \quad \Leftrightarrow n = 3(1+\omega), \quad p = \omega\rho. \tag{6.13}$$

Let us first discuss the case ($p = -\rho$) which results in exponential expansion

$$\begin{aligned} n = 0, \omega = -1 \quad &\Longrightarrow \quad \rho \sim a^0 = \text{const} \implies H^2 = \frac{8\pi G}{3}\rho = \text{const}, \\ &\Longrightarrow \quad \dot{a} = Ha \implies a \sim e^{Ht}. \end{aligned} \tag{6.14}$$

The case of exponential expansion can also be understood as an inclusion of a new term in the Einstein equation

$$\begin{aligned} T^{\mu}_{\nu} = \text{diag}(-\rho, -\rho, -\rho, -\rho), \qquad & G_{\mu\nu} = 8\pi G\, T_{\mu\nu} \\ \Leftrightarrow \qquad \rho = \frac{\Lambda}{8\pi G}, \qquad & G_{\mu\nu} = -\Lambda g_{\mu\nu}, \end{aligned} \tag{6.15}$$

where Λ stands for the cosmological constant (related to dark energy). In other words, the requirement for the equation of states ($p = -\rho$) and the inclusion of Λ in the Einstein equation results in the same exponential expansion. Finally, let us note that the cases $n = 3, 4$ ($\omega = 0, \frac{1}{3}$) stand for matter and radiation which is not discussed here. Although the cosmological constant and the special equation of state ($\rho = -p$) both result in the same rate of expansion but the former cannot be used for inflation since it has to end. The key observation is that scalar fields can mimic the equation of state thus represent excellent models for inflation

$$S = \int d^4x\sqrt{-g}\left[\frac{1}{2}R + \mathcal{L}_\phi\right], \qquad \sqrt{-g} = \sqrt{-\det(g_{\mu\nu})} = a^3, \tag{6.16}$$

where

$$\mathcal{L}_\phi = -\frac{1}{2}g^{\mu\nu}\partial_\mu\phi\partial_\nu\phi - V(\phi), \tag{6.17}$$

and substituting the FLRW metric the scalar Lagrangian writes as

$$\mathcal{L}_\phi = \frac{1}{2}\dot{\phi}^2 - \frac{1}{2}\frac{1}{a^2}(\nabla\phi)^2 - V(\phi). \tag{6.18}$$

From the Euler-Lagrange equations one finds the equation of motion

$$\partial_\mu\left(\frac{\partial(\sqrt{-g}\mathcal{L}_\phi)}{\partial(\partial_\mu\phi)}\right) - \frac{\partial(\sqrt{-g}\mathcal{L}_\phi)}{\partial\phi} = 0 \;\Rightarrow\; \ddot{\phi} + 3H\dot{\phi} - \frac{1}{a^2}\nabla^2\phi + V'(\phi) = 0. \tag{6.19}$$

The stress energy tensor and its components of the scalar field are the following

$$\begin{aligned} T_{\mu\nu} &= \frac{2}{\sqrt{-g}}\frac{\delta(\sqrt{-g}\mathcal{L}_\phi)}{\delta g^{\mu\nu}} = \partial_\mu\phi\partial_\nu\phi + g_{\mu\nu}\mathcal{L}_\phi, \\ T_{00} &= \rho = \frac{1}{2}\dot{\phi}^2 + \frac{1}{2}\frac{1}{a^2}(\nabla\phi)^2 + V, \\ T_{ii} &= a^2 p = a^2\left(\frac{1}{2}\dot{\phi}^2 - \frac{1}{6}\frac{1}{a^2}(\nabla\phi)^2 - V\right). \end{aligned} \tag{6.20}$$

Let us discuss the requirements for inflation. The first observation is that over inflation the field can be considered to be homogeneous ($\nabla\phi/a = 0$). Then the relation between the density and pressure reads

$$\omega = \frac{p}{\rho} = \frac{\frac{1}{2}\dot{\phi}^2 - V}{\frac{1}{2}\dot{\phi}^2 + V} \quad \text{if} \quad \frac{1}{2}\dot{\phi}^2 \ll V \implies \omega = -1, \tag{6.21}$$

and as a consequence

$$H^2 = \frac{8\pi G}{3}\rho = \frac{8\pi G}{3}\left(\frac{1}{2}\dot{\phi}^2 + V\right) \approx \frac{8\pi G}{3}V \approx \text{const.} \tag{6.22}$$

There is another condition that is imposed in the "slow-roll" mechanism (see Eq. (10.6) of [51] or [49]) which assures a prolonged inflation

$$\ddot{\phi} \ll 3H\dot{\phi}. \tag{6.23}$$

It is clear that if the change in $\dot{\phi}$ is small then the first condition holds for a sufficiently large time interval. From the equation of motion (6.19) for a homogeneous field one gets the relation

$$3H\dot{\phi} + V' \approx 0. \tag{6.24}$$

Now rewrite these conditions for the potentials. From Eq. (6.21) one finds

$$\frac{1}{2}\frac{\dot{\phi}^2}{V} \overset{(6.24)}{=} \frac{1}{2}\frac{V'^2}{9H^2V} \overset{(6.22)}{=} \frac{1}{2}\frac{1}{3}\frac{1}{8\pi G}\frac{V'^2}{V^2} \equiv \frac{\epsilon}{3} \ll 1. \tag{6.25}$$

The first condition therefore writes as

$$\epsilon \ll 1, \qquad \epsilon \equiv \frac{1}{2}\frac{1}{8\pi G}\frac{V'^2}{V^2}. \tag{6.26}$$

Using ϵ one can get a simple equation for $\dot{H}$. From Eq. (6.22) it follows

$$2H\dot{H} = \frac{8\pi G}{3}V'\dot{\phi} \overset{(6.24)}{=} -\frac{8\pi G}{3}\frac{V'^2}{3H}, \tag{6.27}$$

$$\dot{H} = -\frac{8\pi G}{6}\frac{V'^2}{3H^2} \overset{(6.22)}{=} \frac{-V'^2}{6V} \overset{(6.22)}{=} \frac{-V'^2}{6V}\frac{3H^2}{8\pi GV} = -\epsilon H^2. \tag{6.28}$$

Thus the condition $\epsilon \ll 1$ also means $\dot{H} \ll H^2$, i.e., the Hubble constant changing slowly. Differentiating (6.24) gives

$$\begin{aligned} \ddot{\phi} &= -\frac{V''\dot{\phi}}{3H} + \frac{V'\dot{H}}{3H^2} \overset{(6.28)}{=} -\frac{V''\dot{\phi}}{3H} - \frac{V'}{3}\epsilon, \\ \frac{\ddot{\phi}}{3H\dot{\phi}} &\overset{(6.24)}{=} -\frac{1}{3}\left(\frac{V''}{3H^2} - \epsilon\right) \overset{(6.22)}{=} -\frac{1}{3}\left(\frac{1}{8\pi G}\frac{V''}{V} - \epsilon\right) \equiv -\frac{1}{3}(\eta - \epsilon) \ll 1, \end{aligned} \tag{6.29}$$

where the second condition writes as

$$\eta \ll 1, \qquad \eta \equiv \frac{1}{8\pi G}\frac{V''}{V}. \tag{6.30}$$

Thus, if $\epsilon(\phi_f) \approx 1$ or $\eta(\phi_f) \approx 1$ then the inflation ends. Further constraints coming from experimental data can be drawn by using the formal solution of the Friedmann equation and the so-called e-fold number which has to be in the range $N = 50 - 60$,

$$a(t) = \exp\left\{\int_{t_0}^{t} dt' H(t')\right\}, \tag{6.31}$$

$$\begin{aligned} N \quad &= \quad \ln\frac{a(t_f)}{a(t_i)} = \int_{t_i}^{t_f} dt' H(t') \approx H\int_{\phi_i}^{\phi_f}\frac{d\phi}{\dot\phi} \overset{(6.24)}{=} -3H^2\int_{\phi_i}^{\phi_f} d\phi \frac{1}{V'}, \\ &\overset{(6.22)}{=} -8\pi G\int_{\phi_i}^{\phi_f} d\phi \frac{V}{V'}. \end{aligned} \tag{6.32}$$

One more constraint is given by the energy scale of inflation, i.e., by the equation

$$V(\phi_i) \equiv \frac{r}{0.01}(10^{16}\,\mathrm{GeV})^4\,, \tag{6.33}$$

which fixes an overall factor for the potential [50].

Various types of inflationary potentials can be considered and the goal is always to determine the above quantities, such as ϵ, η, ϕ_i, ϕ_f and the required number for the e-fold parameter. How can one measure some of these in order to be able to select between competing scenarios? The answer is related to the temperature fluctuations of the cosmic microwave background radiation (CMBR). These fluctuations are the relic of the physical properties of the Universe at the inflation period after which the Universe has to be reheated and the quantum fluctuations (of the scalar field and of the metric) should be the seeds for structure formation. Fluctuations can be described by the power spectrum $P_g(k)$ which has the following definition for a generic quantity $g(x,t)$

$$g(x,t) = \int \frac{d^3k}{(2\pi)^{3/2}} e^{ikx} g_k(t), \qquad \left\langle g^*_{k_1}, g_{k_2}\right\rangle = \delta^{(3)}(k_1 - k_2)\frac{2\pi^2}{k^3}P_g(k). \tag{6.34}$$

Then one can define the so-called spectral index n_s for scalar and the ratio r of tensor and scalar fluctuations

$$n_s - 1 \approx \frac{V'}{V}\frac{d\ln P_R}{d\phi}, \qquad n_s - 1 \approx 2\eta - 6\epsilon, \qquad r \equiv \frac{P_T}{P_R}, \qquad r \approx 16\epsilon, \tag{6.35}$$

where P_R is the scalar and P_T is the tensor power spectrum. The spectral index (n_s) and the ratio (r) can be related to each other (being independent of N) and can be determined by experimental data. While the discussed slow-roll mechanism can be considered as a classical process, quantum fluctuations are necessary to explain the fluctuations of the CMBR and how to relate the theoretical predictions of an inflationary model to observations.

In the second part of my thesis I am going to discuss inflationary models and constrain them using the available experimental data.

Part II

Findings

Chapter 7

Optimization

The FRG equation involves a function called the regulator that can be chosen arbitrarily as long as it satisfies a few conditions. The physical results derived by the exact FRG method must not depend on the choice of the regulator, however in most cases approximations are required to obtain solutions which gives rise to scheme-dependence (see Sect. 4.2). In this chapter the goal is to study this scheme-dependence in various models and determine the optimal regulator that produces the most accurate results. The CSS regulator recovers all major type of regulators in its appropriate limits, thus it provides a useful tool to achieve this goal.

7.1 Optimization based on the principle of minimal sensitivity

One of the most used optimization methods is based on the PMS [29]. As the name suggest it attempts to choose the optimal parameters of the regulator in such a way to make the physical quantities as insensitive as possible to any changes in the parameters. If one treats a physical quantity as a function of the parameters of a regulator then the optimal parameters are those where the derivative of the regulator function is zero. Therefore one has to look for an extremum, i.e., a minimum or a maximum in the parameter space. This procedure can be utilized in any order of the gradient expansion, however its disadvantage is that it operates under the implicit assumption that the insensitivity produces the optimal parameters rather than some non-optimal values in parameter space. Thus, here the method is also tested by reproducing a number of known results, reassuring that the results of the PMS method are consistent with the globally optimal values for all regulator functions discussed in this section.

Another disadvantage of the method is that regulators that have different functional form cannot be compared to each other. However the parameter space of the CSS regulator contains all major type of regulators discussed so far in the literature, since it recovers all of them in its appropriate limits. This property allows the

comparison of various regulator functions by using the PMS optimization method. Furthermore, it has a compact support (non-zero only in a finite interval of the momentum), smooth, infinitely differentiable function, thus it can be applied at any order of the derivative expansion.

In the next sections I am going to study the regulator-dependence of the functional RG in the framework of the bosonized QED_2 [44] equivalent to the MSG model (see Sect. 5.2.2) and in the $O(N = 1)$ symmetric scalar field theory [26], within the leading order of the derivative expansion, i.e., in LPA. I am going to optimize the parameters of the CSS regulator with both normalization in LPA using the PMS optimization method, while comparing the result to the one obtained by the Litim–Pawlowski procedure.

7.1.1 Results obtained by the RG study of QED_2

Orientation

Consider first the RG study of the bosonized QED_2 described by the action (5.20), where the subscript denotes that the model is considered in $d = 2$. Two approximations of the FRG approach are used, the LPA and the single-mode Fourier approximation. In this case the dimensionless effective potential ($\tilde{V}_k = k^{-2}V_k$) of the model has a mass term and only a single cosine,

$$\tilde{V}_k = \tfrac{1}{2}\,\tilde{M}_k^2\,\varphi^2 + \tilde{u}_k\,\cos(\beta\varphi)\,, \tag{7.1}$$

with $\beta^2 = 4\pi$, fixed by the bosonisation, and the tilde superscript as usual denotes dimensionless variables, $\tilde{M}_k^2 = k^{-2}M_k^2$ and $\tilde{u}_k = k^{-2}u_k$. From (4.35) the dimensionless FRG equation for this potential in LPA writes as

$$(2 + k\partial_k)\tilde{V}_k(\varphi) = -\int_0^\infty \frac{\mathrm{d}y}{4\pi}\,\frac{dr}{dy}\,\frac{y^2}{(1+r)y + \tilde{V}_k''(\varphi)}. \tag{7.2}$$

No further approximations have been used solving this equation, all calculations presented here were obtained by the numerical integration of the above equation for the single-frequency MSG model.

The phase diagram of the MSG model presented in Fig. 5.3 is not an exception, it was obtained using equation (7.2) substituting the first normalization of the CSS regulator (4.51) with the parameter values $b = 1$, $h = 1$ and $c = 0.001 \approx 0$. The second normalization of the CSS regulator (4.53) gives almost identical results, since both normalizations converge to the same optimized form of the Litim regulator in the $c \to 0$ limit.

As discussed in Sect. 5.2.2, Fig. 5.3 shows two phases. The symmetry broken phase is represented by full lines, where the Z_2 symmetry of the MSG model is broken spontaneously. In this phase the RG trajectories merge into a single line in the IR limit and the slope of this so called master trajectory defines the critical ratio. Therefore in the IR limit of the symmetry broken phase the $\tilde{u}_k$ becomes a linear function of $\tilde{M}_k^2$,

$$\tilde{u}_k = a\;\tilde{M}_k^2 + b. \tag{7.3}$$

Both the dimensionless and the dimensionful ratio of these couplings tend to the same constant value, i.e., to the slope, $[\tilde{u}_{k\to 0}/\tilde{M}^2_{k\to 0}] = [u_{k\to 0}/M^2_{k\to 0}] = a$, since in the IR limit $\tilde{u}_k$ and $\tilde{M}^2_k$ are increasing, thus b can be neglected. The slope is also independent of the initial conditions. This is not true in the symmetric phase where $\tilde{u}_k$ is still a linear function of $\tilde{M}^2_k$ in the IR limit, but the slope depends on the initial conditions. The numerical calculations obtained in this work strongly suggest that the slope is scheme-independent and takes the value $a = 1/(4\pi)$, within the single Fourier-mode approximation.

However the convergence of the ratio of the couplings to this value depends on the regulator. For example Fig. 7.1 was obtained using the CSS regulator close to the power-law limit (4.52b) ($h \to 0$, $c \to 0$), that has poor convergence properties for $b = 1$. Therefore the RG trajectories stop at a finite scale $k_{\rm f}$, when spinodal instability occurs. This means that the ratio $\chi_c = [u_{k\to k_{\rm f}}/M^2_{k\to k_{\rm f}}]$ is scheme-dependent, and can be used to test the convergence properties of different regulators, and select the optimal one in the framework of the PMS optimization.

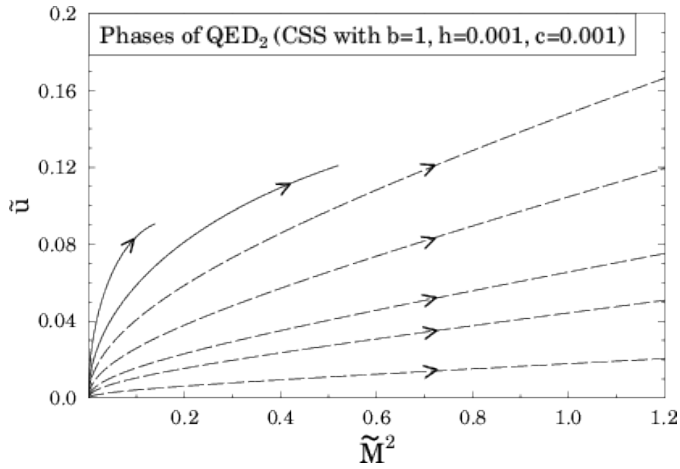

Figure 7.1: Phase diagram of the QED$_2$ model equivalent to the MSG model in $d = 2$ with $\beta^2 = 4\pi$ obtained by the CSS regulator (4.51) with the parameters $b = 1$, $h = 0.001$ and $c = 0.001$, approximating the power-law limit. RG trajectories of the symmetry broken phase (solid lines) stop at a finite scale $k_{\rm f}$.

QED$_2$ and CSS regulator with linear norm

First consier the CSS regulator with the "linear norm" (4.51) and find its optimal parameters (b, h, c). Fig. 7.2 shows how the critical ratio $\chi_c = [u/M^2]_c = \tilde{u}_{k\to k_f}/\tilde{M}^2_{k\to k_f} = u_{k\to k_f}/M^2_{k\to k_f}$ depends on the parameters b, h and c of the CSS regulator with the linear normalization. The lower value means that the regulator has better convergence. Applying the PMS method suggests that the optimal

values can be found at an extremum of a physical quantity as a function of the parameter space. In the case of the bosonised QED_2 this means that the minimum of the critical ratio $[u/M^2]_c$ gives minimal sensitivity on the change of the parameters. This can be seen in Fig. 7.2, that each subplot with a fixed b has a plateau around the minimum, that defines the optimal parameters for that fixed b value. If $b = 1$, then this minimum as a function of the remaining parameters falls into the Litim limit ($c \to 0$, $h = 1$), otherwise for different $b \neq 1$ the optimized value is a different limit $c \to 0$ but $h \neq 1$. Fig. 7.3 shows these optimal minima of the critical ratio as a function of the parameter b for every subgraph of Fig. 7.4. The minimum of these minima, i.e., the global minimum is at $b = 1$ and therefore also at $c \to 0$ and $h = 1$ leading to the Litim optimized limit of the CSS regulator. Thus the PMS optimization method produces the optimized parameters $b = 1$, $c \to 0$ and $h = 1$, approximating the Litim limit of the CSS regulator that gives the smallest critical ratio, closest to the analytic one.

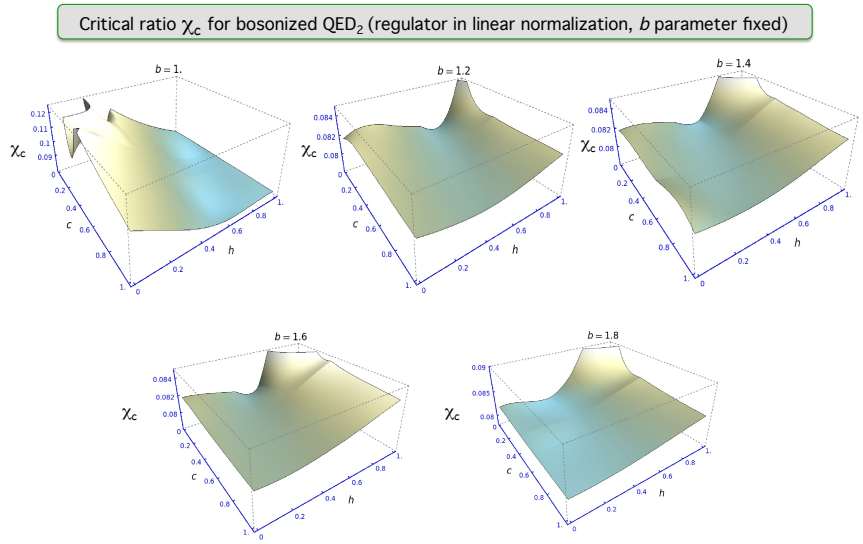

Figure 7.2: The critical ratio χ_c, defined by Eq. (5.24), of the bosonized QED_2, as a function of the parameters of the CSS regulator with the linear normalization (4.51). Smaller ratios correspond to better regulators. The parameters $b = 1$, $c = 0.001$ and $h = 1$ ("back corner" of the first subplot) produce the optimal result indicating the Litim limit of the CSS to be the optimal regulator.

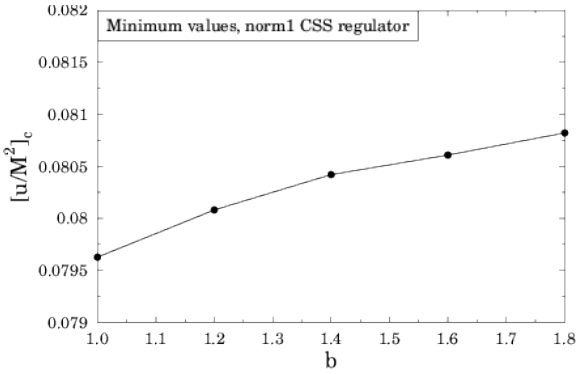

Figure 7.3: Minimum values of the critical ratio with respect to the parameters c and h as a function of the remaining parameter b for every subgraph of Fig. 7.4 obtained using the linear norm of the CSS regulator. The global minimum is at $b = 1$ and therefore also at $c \to 0$, $h = 1$ leading to the Litim limit of the CSS regulator.

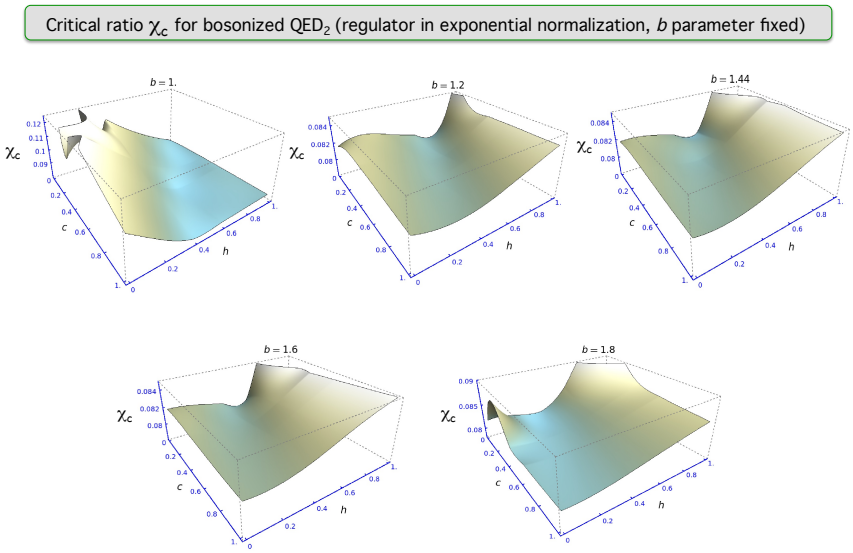

Figure 7.4: The critical ratio χ_c, defined by Eq. (5.24), of the bosonized QED_2, as a function of the parameters of the CSS regulator with the exponential normalization (4.53) instead of the linear norm shown in Fig. 7.2 similarly. Smaller ratios correspond to better regulators. Again, the parameters $b = 1$, $c = 0.001$ and $h = 1$ ("back corner" of the first subplot) produce the optimal result indicating the Litim limit of the CSS to be the optimal regulator.

QED_2 and CSS regulator with exponential norm

The calculations discussed in the previous subsection can be repeated for the exponential norm of the CSS regulator (4.53) instead of the linear one. The goal is the same, to use the PMS method and find the optimal set of parameters b, h and c, that give minimal sensitivity on the choice of these parameters. Similarly to Fig. 7.2, Fig. 7.4 shows the critical ratios of the bosonised QED_2 obtained using the CSS regulator but with the exponential norm as a function of the parameters b, h and c. Again, the lower values correspond to better regulators. Fig. 7.5 shows the local optimums of the each subgraph of Fig. 7.4 as a function of the parameter b, analog to Fig. 7.3, demonstrating that the optimum value is $b = 1$. Comparably to the previous calculations the critical ratio closest to the analytic result is obtained with the parameters $b = 1$, $c = 0.001$ and $h = 1$ favoring again the Litim limit of the CSS regulator. Therefore the PMS strategy applied in the framework of the bosonised QED_2 gives the same parameters independent of the normalization strongly indicating that the optimal regulator is indeed the Litim limit of the CSS in LPA.

In order to have a more reliable result, in the following section the PMS optimization method is performed for the CSS regulator in the framework of the $O(N = 1)$ symmetric scalar field theory in $d = 3$ dimensions.

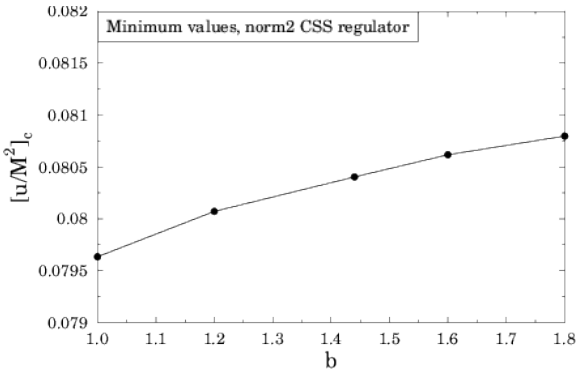

Figure 7.5: Minimum values of the critical ratio with respect to the parameters c and h as a function of the remaining parameter b for every subgraph of Fig. 7.4 obtained using the exponential norm of the CSS regulator. The global minimum is at $b = 1$ and therefore also at $c \to 0$, $h = 1$ leading to the Litim limit of the CSS regulator.

7.1.2 Three-dimensional $O(1)$ model

Orientation and previous studies

The $O(1)$ model in $d = 3$ is a well studied textbook example for the optimization of regulators. A typical physical quantity that can be easily calculated is the critical exponent ν of the WF fixed point that describes the critical behavior of the correlation length. To investigate this model in the FRG approach drastic approximations are considered. Similar to the bosonized QED_2, the $O(1)$ model is studied here in LPA, and using a drastic truncation in the Taylor series of the potential considering only the dimensionless ansatz

$$\tilde{V} = \frac{1}{2}\,\tilde{g}_1\,\tilde{\varphi}^2 + \frac{1}{4!}\,\tilde{g}_2\,\tilde{\varphi}^4, \tag{7.4}$$

with only two dimensionless couplings $\tilde{g}_1$ and $\tilde{g}_2$. Substituting this potential into Eq. (4.35) yields the RG equations for the couplings [34],

$$\begin{aligned} \dot{\tilde{g}}_1 &= -2\tilde{g}_1 + \tilde{g}_2\,\bar{\Phi}^2_{3/2}(\tilde{g}_1), \\ \dot{\tilde{g}}_2 &= -\tilde{g}_2 + 6\,\tilde{g}_2^2\,\bar{\Phi}^3_{3/2}(\tilde{g}_1), \end{aligned} \tag{7.5}$$

where the treshold function is defined as

$$\bar{\Phi}^p_n(\omega) = \frac{1}{(4\pi)^n\,\Gamma(n)} \int_0^\infty \mathrm{d}y \frac{y^{n+1}\,r'}{(y(1+r)+\omega)^p}\,. \tag{7.6}$$

These flow equations depend on the choice of the regulator, thus the ν critical exponent calculated at the WF fixed point from the inverse of the largest negative eigenvalue of the stability matrix is also regulator-dependent.

In the literature the RG flow equations has been calculated for all major type of regulators [24–26, 53]. The most accurate critical exponent is produced by the Litim regulator. It is obtained to be around $\nu \approx 0.54277$ by using the RG equations for two couplings in LPA [34]. This value is smaller than the value accepted to be exact $\nu \approx 0.63$. In order to obtain an exact result one has to solve the exact FRG equations, i.e., take into account higher order terms both in the derivative expansion and in the Taylor expansion of the potential. In this case, the regulator-dependence should vanish. The general observation in the literature is that better agreement can be achieved by better approximations. The ν critical exponent was also determined using four couplings in LPA with the Litim regulator yielding a value closer to the exact one [34].

In Ref. [34] the linear normalization of the CSS regulator has already been investigated using two and four couplings, where the optimization of the parameters of the CSS has confirmed that the optimal regulator is the Litim one, supporting the results of Sect. 7.1.1. Since the Litim regulator has the best convergence properties among the major types of regulators [24–26, 53], it is expected that the Litim limit of the CSS regulator provides the best results for a larger number of couplings as well. However the exponential norm of the CSS regulator has not yet been optimized in the framework of the $O(1)$ field theory, therefore a detailed analysis is performed in the following subsection.

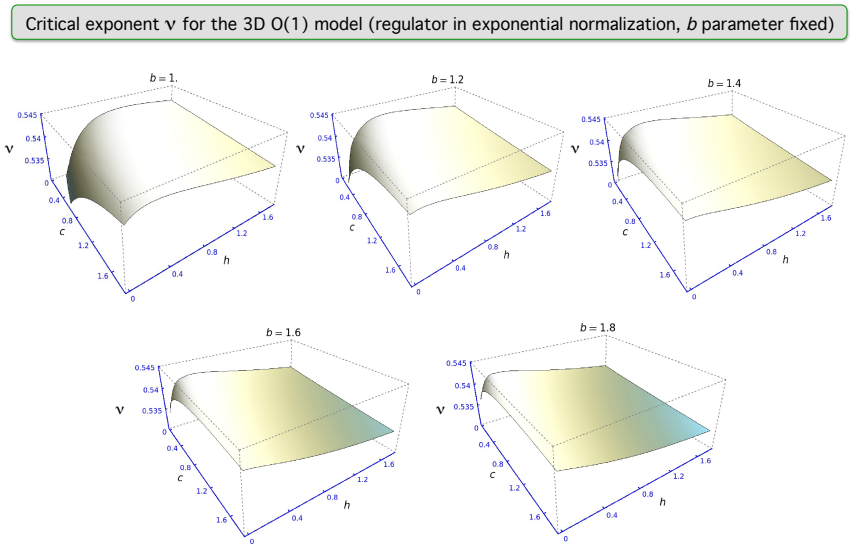

Figure 7.6: The critical exponent ν of the three-dimensional truncated $O(1)$ model (7.4) as a function of the parameters of the CSS regulator with exponential norm (4.53). Higher exponents correspond to better regulators, therefore the optimal parameters are at the Litim limit ($b = 1$, $c = 0.001$ and $h = 1$).

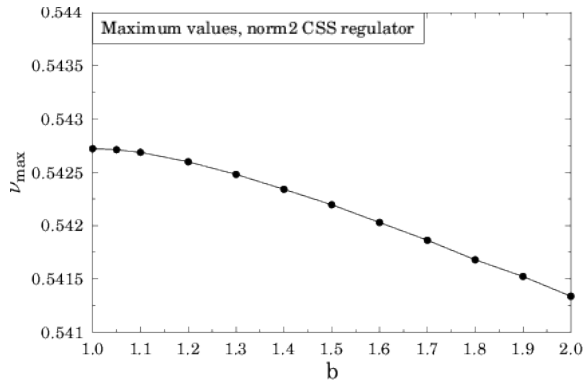

Figure 7.7: Maximum values of the critical exponent ν as a function of the parameter b obtained with the exponential norm of the CSS regulator. The global maximum is at $b = 1$ leading to the Litim limit of the CSS as the optimal result.

Three-dimensional $O(1)$ model and CSS regulator with exponential norm

In this subsection the RG study of the $O(1)$ model is performed using the exponential normalization of the CSS regulator (4.53). The goal is the same again, to look

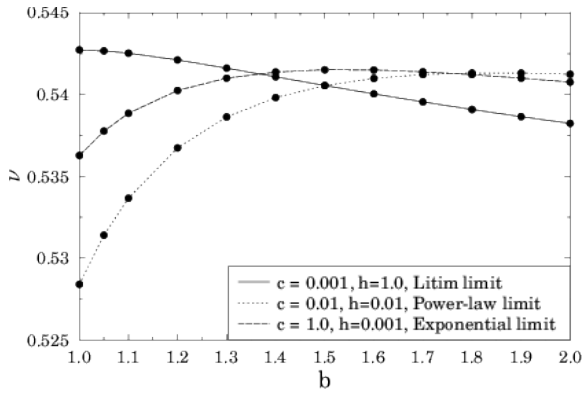

Figure 7.8: The critical exponent ν as a function of b obtained by various limits of the CSS regulator with exponential norm (4.53).

for the optimal set of parameters b, h and c, using the PMS strategy. Unlike in the case of QED_2, here, the maximum value of the critical exponent ν of the WF fixed point provides the optimized parameters. Fig. 7.6 shows this critical exponent of the $O(1)$ model as a function of the parameters b, h and c of the CSS regulator with exponential norm.

Applying the PMS method, one finds plateaus in each subplot of Fig. 7.6 around the maximums, where the optimized parameters are the least sensitive to small perturbations. Calculating the ν_{max} as the maximal critical exponent with respect to c and h for a fixed b, and then plotting it as a function of the parameter b yields Fig. 7.7. The global maximum can be also read off from Fig. 7.7 obtaining again $b = 1$, $c = 0.001$ and $h = 1$ as the optimal parameters. Therefore recalling previous studies one can conclude that the PMS strategy produces the Litim limit $c \to 0$, and $h = 1$ for both normalizations of the CSS as the optimized regulator in LPA.

Considering the CSS regulator with fixed c and h parameters gives a useful perspective too. Fig. 7.8 shows the critical exponent as a function of the remaining parameter b of the CSS with exponential norm for its various limits (4.54), i.e., the Litim, the power-law, and the exponential limit. The optimal result for the Litim limit of the CSS is $b = 1$, which is the favored value in the literature. The PMS strategy gives $b \approx 2$ for the power-law limit of the CSS, which is the optimal choice based on the Litim–Pawlowski field amplitude expansion too. In the exponential limit one finds $b \approx 1.5$ in agreement with the amplitude expansion where the optimum is $b = 1.44$. Reproducing these known results [24] ensures the consistency of the above calculations based on the PMS method. Fig. 7.8 also shows that among the limits of the CSS regulator the Litim limit with $b = 1$ provides the optimal result in accordance with Fig. 7.7. This again demonstrates that the Litim limit is the most favorable choice.

7.2 Optimization based on spontaneous symmetry breaking

Symmetries and symmetry breakings play a crucial role in physics, especially in the phase transitions of quantum field theories. For example spontaneous symmetry breaking (SSB) in the standard model gives rise for the mass generation due to the Brout-Englert-Higgs mechanism. However, in $d = 0 + 1$ dimension, there is an equivalence between quantum mechanics and quantum field theory, thus as a consequence of quantum tunneling a symmetry cannot be broken spontaneously [15,40]. Therefore, the spontaneously broken phase must vanish in one-dimensional quantum field theories.

In the following sections the goal is to introduce a new optimization strategy for the RG regulators that can be used beyond LPA and it is based on a physical requirement, that the symmetry broken phase should vanish for the exact RG flow in $d = 1$. This method also allows the comparison of different regulators at any order of the gradient expansion. The optimization is performed in the framework of the SG model [42] (see also Sect. 5.2.1). The SG model has an advantage over other models, since its RG equations beyond LPA are simpler. It does not require field-dependent wave-function renormalization, unlike for example the $O(N)$ models where the field-dependence of the wave-function renormalization must be included. First I discuss a test of the optimization method performed in [55], then the parameters of the CSS regulator are optimized (which is my contribution to the multi-author paper [2]).

7.2.1 SG model for dimensions $1 \leq d \leq 2$

Consider first the RG study of the SG model [41]. In LPA it has the action given by Eq. (5.12), but beyond LPA the effective action must include the wave-function renormalization. By rescaling the field variable $\tilde{\varphi} = \beta\varphi$ and using the single Fourier mode approximation the effective action takes the form

$$\Gamma_k = \int d^d x \left[\frac{1}{2} z_k (\partial_\mu \tilde{\varphi})^2 + u_k \cos(\tilde{\varphi}) \right], \tag{7.7}$$

where u_k is the dimensionful Fourier amplitude, while z_k is the field-independent wave-function renormalization merged with the frequency β. It can be also interpreted as the inverse of the scale-dependent frequency $z_k = 1/\beta_k^2$ and has the dimension k^{d-2}. This ansatz is an appropriate approximation, since the RG study of SG type models [41, 44, 46] is accurate without a field-dependent wave-function

renormalization. From (4.32) the RG equations can be derived for the couplings

$$k\partial_k u_k = \int_p \frac{k\partial_k R_k}{k^{2-d}u_k}\left(\frac{P-\sqrt{P^2-(k^{2-d}u_k)^2}}{\sqrt{P^2-(k^{2-d}u_k)^2}}\right), \tag{7.8}$$

$$k\partial_k z_k = \int_p \frac{k\partial_k R_k}{2}\left[\frac{-(k^{2-d}u_k)^2 P(\partial_{p^2}P+\frac{2}{d}p^2\partial^2_{p^2}P)}{[P^2-(k^{2-d}u_k)^2]^{5/2}} + \frac{(k^{2-d}u_k)^2 p^2(\partial_{p^2}P)^2(4P^2+(k^{2-d}u_k)^2)}{d\,[P^2-(k^{2-d}u_k)^2]^{7/2}}\right], \tag{7.9}$$

where $P = z_k k^{2-d}p^2 + R_k$ and the integral denotes $\int_p = \int dp\, p^{d-1}\Omega_d/(2\pi)^d$ with the d-dimensional solid angle Ω_d. In the following context it is useful to introduce the normalized dimensionless parameters $\bar{z}_k \equiv (8\pi)\tilde{z}_k$ and $\bar{u}_k \equiv \tilde{u}_k k^2/\bar{k}$ where $\tilde{z}_k = k^{2-d}z_k$ and $\tilde{u}_k = k^{-d}u_k$ are the conventional dimensionless couplings and $\bar{k} = \min_{p^2} P$.

In $d = 2$ dimensions (as discussed in Sect. 5.2.1) the SG model has two phases and a topological phase transition with a scheme-independent critical value separating the phases $1/\bar{z}_\star = 1$ [43]. In $d = 1$ dimension the approximated RG flow incorrectly indicates a Wilson-Fisher saddle point $\bar{u}_\star$, $1/\bar{z}_\star$ and two phases that can be seen for example in Fig. 7.9 which was obtained using the power-law regulator (4.46).

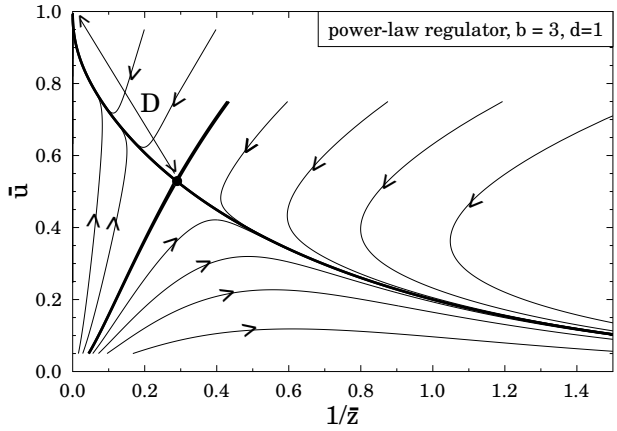

Figure 7.9: Phase diagram of the SG model in $d = 1$ dimension obtained by the numerical integration of Eqs. (7.8), and (7.9) where the power-law regulator (4.46) was substituted with $a = 1$ and $b = 3$ [2, 55]. The distance between the nontrivial IR and WF fixed point, D is defined by (7.10).

Similarly, in fractal dimensions, $1 < d < 2$ a WF saddle point appears in the RG flow, too. However, in $d = 1$ dimension the spontaneously broken phase should vanish, which means that the nontrivial IR fixed point ($1/\bar{z}_{\rm IR} \equiv 0$, $\bar{u}_{\rm IR} \equiv 1$) and

the WF saddle point should coincide. Therefore, the scheme-dependent distance between the WF saddle point and the nontrivial IR fixed point (see e.g. Fig. 7.9),

$$\begin{aligned} D &\equiv \sqrt{(\bar{u}_{\rm IR}-\bar{u}_\star)^2+(1/\bar{z}_{\rm IR}-1/\bar{z}_\star)^2} \\ &= \sqrt{(1-\bar{u}_\star)^2+1/\bar{z}_\star^2} \end{aligned} \tag{7.10}$$

can be used for the optimization of the RG equations. A smaller distance D indicates a better regulator, since all RG trajectories should converge to the other attractive IR fixed point ($\bar{u}_{k\to 0}=0$, $1/\bar{z}_{k\to 0}=\infty$) that corresponds to the symmetric phase [31, 42].

7.2.2 Optimization of the power-law regulator

In order to study the validity of this optimization strategy one can perform the optimization on the power-law regulator (4.46) [55]. The position of the saddle points calculated by the numerical integration of Eqs. (7.8) and (7.9), for dimensions $1 \le d \le 2$ are plotted in Fig. 7.10 as a function of b, the parameter of the power-law regulator. The WF fixed point of the topological phase transition of

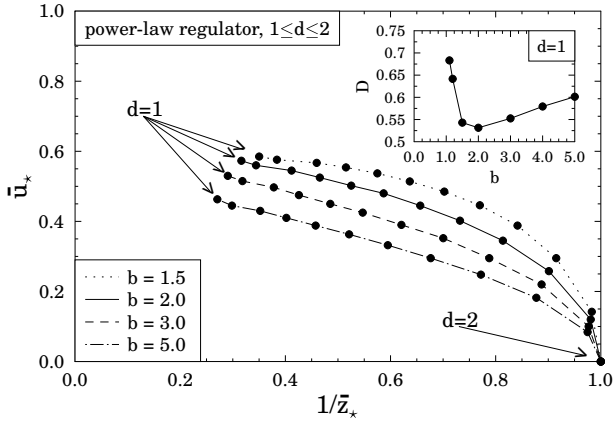

Figure 7.10: Positions of the WF saddle point of the SG model obtained using the power-law regulator (4.46) ($a=1$) in dimensions $1 \le d \le 2$ for various b [2, 55]. The inset shows the distance D defined by Eq.(7.10) as a function of the parameter b in $d=1$ dimension.

the two-dimensional SG model ($\bar{u}_\star=0$, $1/\bar{z}_\star=1$) is scheme-independent, thus the curves of Fig. 7.10 join as the dimension increases to two. However the spurious saddle point for $d=1$ and for fractal dimensions depend on the parameter of the regulator. This can be used to optimize the parameter b of the power-law regulator, since the symmetry broken phase and therefore the distance between the nontrivial IR fixed point and the saddle point (7.10) should vanish in $d=1$ dimension. The result can be read off from the inset that shows the distance D as a function of

b. The optimal parameter of the power-law regular is $b = 2$, providing the smallest distance. Therefore the procedure recovers the known result obtained by the Litim–Pawlowski optimization, validating the proposed method.

7.2.3 Optimization of the CSS regulator

In this subsection the goal is to optimize the CSS regulator (4.53) based on the minimization of the distance D (7.10) in the one-dimensional SG model. The first step is to calculate the position of the spurious WF saddle point from which the distance can be determined. For simplicity the RG equations (7.8), and (7.9) are linearized in terms of $\tilde{u}$ which is found to be usually much smaller than one. It is important to check the consistency of the method. Fig. 7.11 shows how the distance D depends on the parameter b of the CSS regulator for its different limits. The results obtained by the power-law limit (4.54b) of the CSS regulator (with parameters $c = 0.0001$ and $h = 0.0001$) is shown by the dashed line. The findings are qualitatively identical to the inset of Fig. 7.10 where the exact flow equations were used. Both curves have a minima around $b \approx 2$, in the linearized case it is at $b = 2.3$. As a reminder the Litim–Pawlowski optimization indicates $b = 2$ as the optimal parameter of the power-law regulator. The exponential limit (4.54c) of the CSS regulator (with parameters $c = 1$, $h = 0.0001$) provides another consistency check. It is represented by the dotted line in Fig. 7.11 where the minimum is situated at $b \approx 1.4$, while the optimal choice is $b = 1.44$ according to the Litim–Pawlowski method. The solid line of Fig. 7.11 corresponds to the minimum values

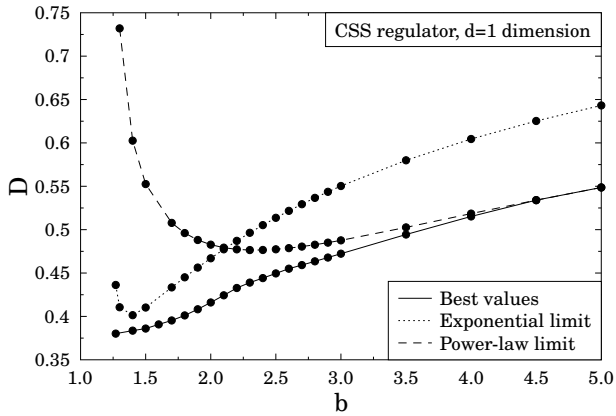

Figure 7.11: The distance D (7.10) as a function of the parameter b of the CSS regulator for its different limits (4.53). The solid line shows the best values obtained by the optimal c and h parameters as a function of the fixed b.

of D obtained by the optimal c and h parameters as a function of the fixed b. It coincides with the power-law limit for large b values and has an inflection point where the exponential and power-law limits cross each other at $b \approx 2.1$. As the solid

line shows, the minimal distance is obtained for small b where the optimal value used for c was also small but finite. This indicates that even beyond LPA the Litim limit ($b \approx 1$, $c \approx 0$) of the CSS is the optimal regulator meaning a small but nonzero value of c to preserve differentiability. Although in this limit the computations are costly due to the oscillatory behavior of the derivatives for $c \to 0$, however the derivatives always exist for a small but finite c, thus the regulator can be used at any order of the derivative expansion. This is not true for the Litim regulator itself, only for the approximate Litim limit of the CSS regulator. It is important to note that performing the PMS method, i.e., finding the global minimum of the CSS regulator gives exactly the same optimal parameters. In the previous sections based on the PMS method the Litim limit of the CSS regulator is found to be optimal with $h = 1$. Similarly, beyond LPA the optimal parameters obtained to be $c = 0.1$ and $h \approx 0.3$ for $b = 1.25$, however the optimal value for h could depend on the model and the approximations used.

7.3 Conclusion

The optimization of the regulator-dependence of the functional RG equations has been investigated focusing especially on the CSS regulator (4.49).

First, the optimization has been done in LPA based on the PMS in the framework of the two-dimensional bosonized QED_2 and the three-dimensional $O(1)$ scalar model [1]. It has been known that according to the Litim–Pawlowski field amplitude expansion the Litim regulator provides the optimal results in LPA, however the CSS regulator has not yet been subjected to a detailed study. The CSS regulator recovers all major type of regulators in its appropriate limits, thus it allows the comparison of different regulators within the framework of the PMS strategy at any order of the gradient expansion by optimizing its parameter space. This strategy, the application of the PMS optimization to the CSS regulator proved to be a very efficient way to analyze the scheme-dependece of the RG equations. Known result has been also reproduced for the exponential and power-law limit of the CSS regulator validating the method. For example, the optimal parameter of the exponential limit is obtained to be $b \approx 1.5$, while according to the field amplitude expansion it is $b = 1.44$. The CSS has been analyzed with two different normalizations, with "linear" (4.51) and "exponential" (4.53) norm. The Litim limit of the CSS (4.54a) has been found to be the optimal regulator for both normalization and for both field theory models in LPA.

In the second section of the chapter a new optimization procedure for the scheme-dependence of the RG method was also proposed and investigated [2]. It is based on the requirement that in $d = 1$ dimension the spontaneous symmetry breaking must vanish. This new strategy has been applied in the framework of the sine-Gordon model in LPA$'$. It has been validated by the fact that known results could be reproduced for the power-law and different limits of the CSS regulator. Then the CSS regulator has been optimized that indicated again that the best choice among the major type of regulators is the Litim limit of the CSS. It is

important to note that while the exact Litim limit is not differentiable, an approximate limit (with nonzero value of c) of the CSS is, and can be applied at any order of the derivative expansion. The Litim limit of the CSS is found to be optimal also by the PMS strategy in LPA for the bosonized QED_2 and for the $O(N)$ model too.

Therefore, the CSS regulator was thoroughly investigated with various optimization methods, in three different dimensions, for three different models, both in LPA and LPA$'$ and with two different normalization all indicating that the Litim limit of the CSS regulator is the optimal choice.

Chapter 8

Effects of truncations on the Mermin-Wagner theorem

FRG is a framework that requires to solve an integro-differential equation for functionals which is usually solved using approximations. These approximations can give rise to scheme-dependence and can cause the appearance of a spurious fixed point as it was discussed in the previous chapter. Therefore it is important to know the limitations of the used approximations. One way to achieve this goal is to test them against exact results like the Mermin-Wagner theorem [36–38]. The theorem states that a continuous symmetry cannot be spontaneously broken in two dimensions, which applies to classical and quantum systems as well. Therefore at finite temperature, Bose-Einstein condensation cannot form for $2d$ interacting Bose gases, and it rules out the possibility of a non-vanishing magnetization for two-dimensional magnetic systems with a continuous symmetry. However the Mermin-Wagner theorem does not apply to topological phase transitions, which can occur in two dimensions signaled by the change of correlation functions between algebraic and exponential behavior.

For the $O(N)$ models (see Sect. 5.1) the Mermin-Wagner theorem means that in two dimensions there is no SSB of the $O(N)$ symmetry if $N \geq 2$. This exact result also holds for non-translationally-invariant lattices, or more generally for graphs with non-integer, i.e., fractal dimensions [56], thus if $N \geq 2$ then SSB cannot occur for $d \leq 2$, while there is SSB for $d > 2$ [57, 58]. The $N = 1$ case, i.e., the Ising model is special, since it has a discrete symmetry, not a continuous one, like the $O(N)$ models with $N \geq 2$, thus it can have a symmetry broken phase in $d = 2$. Another interesting case is the large N-limit of $O(N)$ model that is equivalent to the spherical model when $N \to \infty$ [59], which has an exact solution [60]. In $d = 2$ for $N = 2$ the model also has the mentioned topological phase transition, which is not bounded by the Mermin-Wagner theorem.

This wide variety of the $O(N)$ model makes it an ideal framework to investigate how the appearance of SSB depends on the used approximation schemes in FRG in various dimensions. The $O(N)$ model has been widely studied by the FRG method,

notably its critical exponent was studied as a function of the dimension [58,61,62]. The regulator-dependence of the FRG and the effects of truncation was discussed in [29,53,63–65]. In low-dimension statistical mechanics models can describe single-particle quantum mechanics, hence double well potential and quantum tunneling, and quartic anharmonic oscillators were studied by FRG [40,66,67].

In this chapter my goal is to determine what level of approximation is needed to reproduce the Mermin-Wagner theorem focusing especially on how truncating the Taylor expansion of the potential affects the presence of SSB in LPA.

8.1 The truncated $O(N)$ model ($N < \infty, N_{\mathrm{CUT}} < \infty$)

Truncation around the zero field

In LPA the $O(N)$ model has the action described by Eq. (5.1) that must be $O(N)$ symmetric, and the Taylor expansion of the potential around zero is written in Eq. (5.2).

First let me demonstrate that SSB is present in the Taylor expanded $O(N)$ model with a truncation, i.e., with a finite N_{CUT} and finite N even in low dimensions. Consider one of the simplest cases, the Ising model ($N = 1$) in $d = 1$ with the most drastic truncation ($N_{\mathrm{CUT}} = 2$). In this case there are two couplings for which the dimensionless RG flow equations derived from (5.9) takes the form

$$k\partial_k g_1 = -2g_1 - \frac{1}{\pi}\frac{g_2}{(1+g_1)^2}, \tag{8.1}$$

$$k\partial_k g_2 = -3g_2 + \frac{6}{\pi}\frac{g_2^2}{(1+g_1)^3}, \tag{8.2}$$

where the Litim regulator was used (and the tilde notation is neglected). Similar equations can be derived for general d, N and N_{CUT}, see for example Eq. (5.10) for the $d = 2$ case. Fig. 8.1 shows the RG phase diagram obtained for the one-dimensional Ising model ($O(N = 1)$) by solving the equations (8.1). At finite temperature this model does not have any phase transition in $d = 1$ [10], however the presence of the WF fixed point in Fig. 8.1 indicates two phases. The IR fixed point (red dot in Fig. 8.1) associated with the convexity of the potential appears in all dimension [48,68,69]. In $d = 4$, the WF saddle point (green) merges with the Gaussian fixed point (black) in the origin. In this section strong numerical evidence will be presented that suggests that in dimensions $1 \leq d < 4$, similar phase diagrams can be obtained to Fig. 8.1 for any finite N and any finite N_{CUT}, using any regulator function, where the RG trajectories running to the IR fixed point correspond to the symmetry broken phase and the rest to the symmetric phase. However for $d \leq 2$ the Mermin-Wagner theorem excludes the presence of SSB, therefore the appearence of the symmetry broken phase in Fig. 8.1 is spurious.

The purple curve in Fig. 8.1 is determined by the vanishing mass beta function (VMB), i.e., by the RG equation of g_1. Substituting zero for the left hand side of Eq. (8.1) yields

$$g_2 = -2\pi g_1 (1+g_1)^2, \tag{8.3}$$

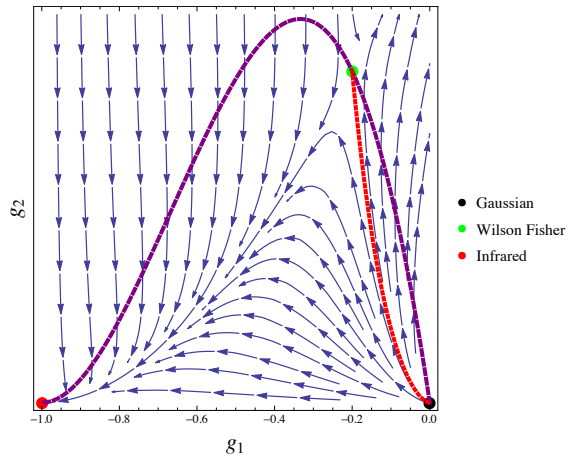

Figure 8.1: Phase diagram of the one-dimensional Ising model ($O(N = 1)$) obtained by solving the RG flow equations numerically for two dimensionless couplings ($N_{\rm CUT} = 2$) using the Litim regulator. The purple (dashed) line indicates the vanishing mass beta function while the red (dotted) line shows the separatrix separating the two phases. The IR convexity (red), the Wilson-Fisher (green) and the Gaussian (black) fixed points are also indicated.

which depends only on g_1. Increasing $N_{\rm CUT}$ does not modify this function, higher order couplings do not give contributions. Therefore the VMB curve on the g_1, g_2 plane is the same for *any* finite value of $N_{\rm CUT}$. It is important to note that all fixed points are situated on the VMB curve by definition. The VMB function also has a connection to the FRG determination of the central charge in $d = 2$ at LPA, which was discussed in [70]. The VMB and other vanishing beta functions were studied also in [71].

The position of the WF saddle point depends on the number of couplings used ($N_{\rm CUT}$), but it is always situated on the VMB curve. For different regulator functions the VMB curve is also different but qualitatively similar. This is shown in Fig. 8.2 where the WF fixed points are projected on the g_1, g_2 plane for the Litim-like regulator class. This regulator class is the $c \to 0$ and $b \to 0$ limit of the CSS regulator (4.53), keeping h as a free parameter

$$r = \left(\frac{1}{y} - h\right) \Theta(1 - hy). \tag{8.4}$$

The optimized Litim regulator has $h = 1$. While the Gaussian fixed point corresponding to the free theory is scheme-independent, the IR fixed point depends on the choice of the regulator. I have found that in $1 \leq d \leq 2$ (with d real) the qualitative picture is similar to Fig. 8.2 for general N: as $N_{\rm CUT}$ increases the WF fixed points corresponding to the different regulators converge to the respective IR fixed points.

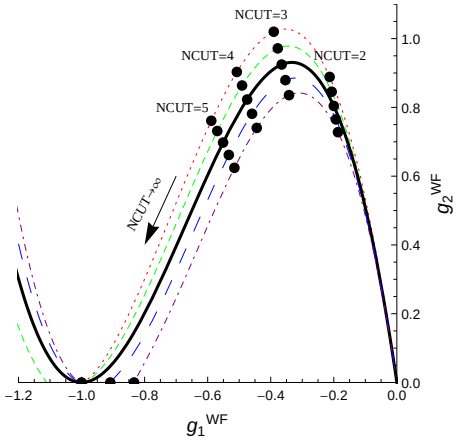

Figure 8.2: Position of the WF saddle point of the $O(N = 1)$ model situated on the VMB curves obtained with various values of $N_{\rm CUT}$ in $d = 1$. Different VMB lines are obtained using different parameter values ($0.8 < h < 1.2$) of the Litim regulator class (8.4) . The solid line corresponds to the optimized Litim regulator where $h = 1$. As $N_{\rm CUT}$ increases the WF fixed points converge to the IR fixed points which remain unchanged if $h \leq 1$.

The situation is different in $d \geq 2$ as shown for $d = 3$ in Fig. 8.3: the WF fixed points does not converge to the IR ones as for $d = 1$ for increasing $N_{\rm CUT}$, but tend to non-trivial WF saddle points. These constant, non-trivial WF fixed points are calculated using the spike plot method [72,73], where the LPA is treated exactly ($N_{\rm CUT} \to \infty$). However the position of these WF fixed points depend on the regulator. Clearly, the position of these non-trivial WF fixed points depend on the choice of the regulator. Again, plots similar to Fig. 8.3 can be obtained for general N and for dimensions $2 < d < 4$. This is illustrated in Fig. 8.4 and Fig. 8.5, where g_1 and g_2 is shown as a function of $N_{\rm CUT}$ for three different values of N in $d = 1$ and $d = 3$ dimensions.

In summary, I have analyzed the truncated $O(N)$ model with finite $N_{\rm CUT}$ and finite N that showed the presence of SSB and a WF fixed point (different from the Gaussian) for dimensions $1 \leq d < 4$ (where d is real). The results indicates that in the $N_{\rm CUT} \to \infty$ limit the symmetry broken phase disappears for $d \leq 2$, but persists for $d > 2$. This must be verified without truncating the potential, i.e., treating the LPA equation exactly, which will be referred to as "non-truncated" $O(N)$ model. Before the non-truncated $O(N)$ model, the truncation around the minimum of the potential and then the spherical model ($N \to \infty$) is discussed.

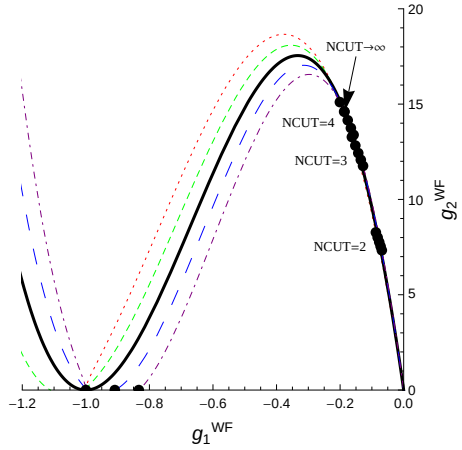

Figure 8.3: Position of the WF saddle point of the $O(N = 1)$ model situated on the VMB curves obtained with various values of $N_{\rm CUT}$ in $d = 3$. Different VMB lines are obtained using different parameter values ($0.8 < h < 1.2$) of the Litim regulator class (8.4) as in Fig. 8.2. The solid line corresponds to the optimized Litim regulator where $h = 1$. As $N_{\rm CUT}$ increases the WF fixed points converge to the WF fixed point obtained using the spike plot method (shown for the Litim regulator) [72, 73].

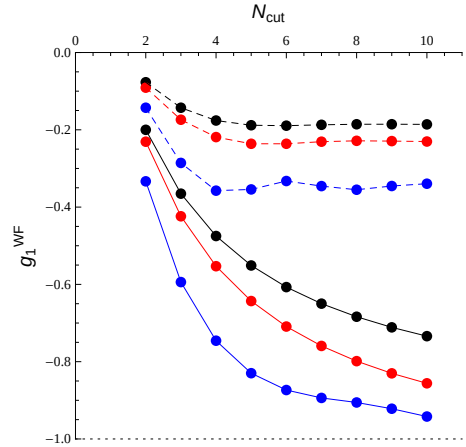

Figure 8.4: The dependence of the g_1 coordinate of the WF fixed point of the $O(N)$ model on $N_{\rm CUT}$ in $d = 1$ (solid lines) in $d = 3$ (dashed lines) and from top to bottom for $N = 1$ (black), $N = 2$ (red) and $N = 10$ (blue).

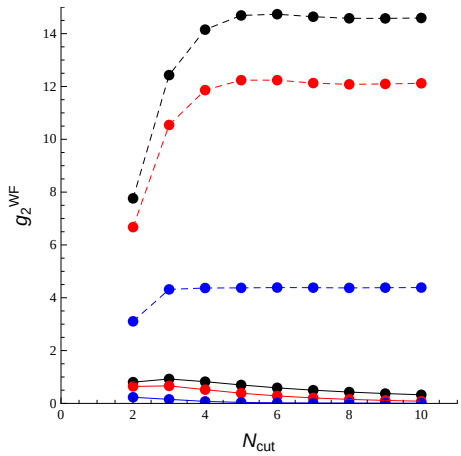

Figure 8.5: The dependence of the g_2 coordinate of the WF fixed point of the $O(N)$ model on N_{CUT} in $d = 1$ (solid lines) in $d = 3$ (dashed lines) and from top to bottom for $N = 1$ (black), $N = 2$ (red) and $N = 10$ (blue).

Truncation around the minimum

Now consider the Taylor expansion of the effective potential around the minimum by a slight modification of Eq. (5.3),

$$u_k(\rho) = \sum_{i=2}^{N_{\mathrm{CUT,m}}} \frac{\lambda_{k,i}}{i!}(\rho - \rho_0)^i. \tag{8.5}$$

First, examine the most drastic truncation by choosing $N_{\mathrm{CUT,m}} = 2$. In this case there is only one running coupling $\lambda_{k,2} \equiv \lambda$ and the running minimum ρ_0. These quantities can be related to the couplings g_1 and g_2 defined by the expansion around zero. These relations give the correct result for the WF fixed point, but not for the Gaussian one, which is $g_1 = g_2 = 0$, however the fixed point equations for ρ_0 and λ do not have a solution for a vanishing ρ_0. In general dimension and for general N the RG flow equations obtained from (5.9) take the form [74]

$$k\partial_k\rho_0 = (d-2)\rho_0 + A_d\left(1 - N - \frac{3}{(1+2\rho_0\lambda)^2}\right), \tag{8.6}$$

$$k\partial_k\lambda = \lambda\left(4 - d - 2A_d\left(N - 1 + \frac{18\lambda}{(1+2\rho_0\lambda)^3}\right)\right). \tag{8.7}$$

Substituting zero for the left hand side yields the fixed point solutions for ρ_0 and λ, for example, the WF fixed point solution for the Ising model ($N = 1$) is given by

$$\rho_0 = \frac{4(2d-5)^2 A_d}{3(d-2)^3}, \qquad \lambda = \frac{3(4-d)(d-2)^3}{16(2d-5)^3 A_d}. \tag{8.8}$$

As Eq. (8.8) shows, the minimum is well defined (positive) as long as $d > 2$, which is true for any value of N. If $d > 4$, then the solution for λ is negative, and again, this holds for general N. Another important observations is that for $N = 1$ the coupling λ is diverging at $d = 2.5$ and becomes negative for $d < 2.5$, which is an unphysical solution, since there is SSB for $N = 1$ in $d = 2$. However this is only valid for $N = 1$, for other N values, λ is not diverging in any $d > 2$, it only has a maximum, and does not change sign. In Fig. 8.6 the minimum value ρ_0 and the

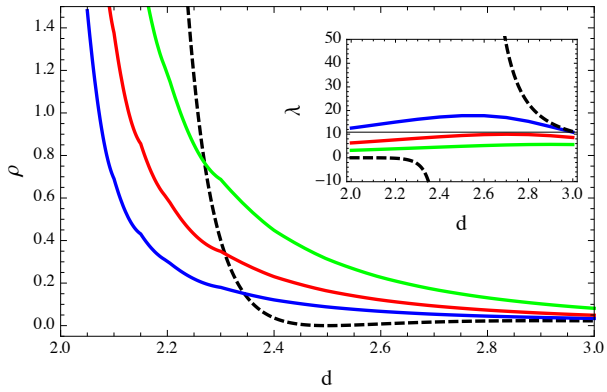

Figure 8.6: Running minimum (main plot) and the λ coupling (inset) as a function of the dimension d at the WF fixed point of the Ising model ($N = 1$, black dashed lines), the XY model ($N = 2$, blue), the Heisenberg model ($N = 3$, red) and the $O(N = 5)$ model (green solid lines), using a truncation around the minimum with $N_{\rm CUT,m} = 2$. The coupling λ is finite and positive for $N > 1$ in $d > 2$, however for $N = 1$ it is diverging at $d = 2.5$ and then turning negative at $d < 2.5$.

coupling λ are plotted for various N values as a function of the dimension at the WF fixed point. The running minimum diverges for any N at $d = 2$ in agreement with the Mermin-Wagner theorem. The inset shows that the coupling λ is finite and positive for $N > 1$ in $d > 2$, however for $N = 1$ it is diverging at $d = 2.5$ and then turning negative at $d < 2.5$. This contradicts the known exact solution of the Ising model in $d = 2$. Therefore the results imply that this truncation while gives the correct behavior for the SSB it does not give a reliable lower critical dimension for the Ising model and cannot reproduce the Gaussian fixed point, giving only a partial description of the theory space. Increasing the value of $N_{\rm CUT,m}$ is not expected to change these qualitative observations.

8.2 The spherical model without truncations ($N = \infty$, $N_{\mathrm{CUT}} = \infty$)

In the large N limit of the $O(N)$ model, i.e., in the case of the spherical model, the terms in (5.9) which are in the order of $1/N$ can be neglected. One can rescale the RG equation by an irrelevant parameter $(A_d N)$, and introduce the new variables $\rho \to \rho/(A_d N)$ and $u \to u/(A_d N)$. This rescaling does not affect the first derivative of the potential $u' \to \frac{\partial u/(A_d N)}{\partial \rho/(A_d N)} = u'$. First dividing Eq. (5.9) by $A_d N$ and then performing the rescaling, one finds

$$k\partial_k u = (d-2)\rho u' - du + \frac{1}{1+u'} - \frac{1}{N}\frac{1}{1+u'} + \frac{1}{N}\frac{1}{1+u'+2\rho u''}. \tag{8.9}$$

In the $N \to \infty$ limit only the following terms remain

$$k\partial_k u = (d-2)\rho u' - du + \frac{1}{1+u'}. \tag{8.10}$$

This RG equation describes the evolution of the effective potential for the spherical model in arbitrary dimension. Useful information can be extracted from the derivative of Eq. (8.10) with respect to ρ, which writes as

$$k\partial_k u' = (d-2)u' + (d-2)\rho u'' - du' - \frac{u''}{(1+u')^2}. \tag{8.11}$$

A physically plausible theory has a potential that is bounded from below, therefore it is reasonable to assume that it has a global minimum at some $\rho = \rho_0$. At this ρ_0 point, the derivatives of the potential have the expressions $u'(\rho_0) = 0$ and $u''(\rho_0) \equiv \lambda$ for the fixed point, thus one finds the equation

$$0 = (d-2)\rho_0\lambda - \lambda \tag{8.12}$$

that has the solution

$$\rho_0 = \frac{1}{d-2}\,. \tag{8.13}$$

If $\rho_0 > 0$ the potential has a minimum and there is SSB. This condition is satisfied in Eq. (8.13) if $d > 2$. For $d < 2$ the equation gives negative ρ_0, while in $d = 2$ it is undefined, which indicates the absence of SSB in both cases. These results can be considered exact, since in the large N limit the LPA approximation becomes exact as $N \to \infty$ [15,75]. This is also in agreement with the solution of Eq. (8.11) using the method of characteristics.

8.3 The XY ($N = 2$), sinh- and sn-Gordon model

The $N = 2$ case of the $O(N)$ model is also worth discussing, since in $d = 2$ it has a topological phase transition. This model is also known as the XY model,

and in $d = 2$ it can be mapped onto a Coulomb Gas and then to the SG model. As demonstrated analytically in Sect. 5.2.1, the FRG method can easily show the topological phase transition of the two-dimensional SG model within LPA. However it is more difficult to see this feature directly on the $O(N = 2)$ model, since one has to take into account the RG running of the anomalous dimension and go beyond LPA [18].

The SG model can be also considered with imaginary frequencies $\beta \to i\beta$ yielding the sinh-Gordon (ShG) model which has some interesting properties showing similarities to both the Ising and the SG model [10]. In two dimensions it has the potential,

$$V_{\mathrm{ShG}}(\varphi) = u_k \cos(i\beta\varphi) = u_k \cosh(\beta\varphi)\,. \tag{8.14}$$

Applying the FRG method to the ShG model proceeding with a derivation similar to the one applied to the SG model results the following flow for the dimensionless Fourier amplitude

$$\tilde{u}_k = \tilde{u}_\Lambda \left(\frac{k}{\Lambda}\right)^{-\frac{\beta^2}{4\pi}-2}, \tag{8.15}$$

where, in contrast to the SG model (5.19), there is no sign change at $\beta^2 = 8\pi$, therefore this model does not have a topological phase transition. This can be also concluded by observing the Taylor expansion of the potential, which consists only positive terms. Thus, the expanded potential is similar to the potential of the Ising model with the difference that the initial conditions of the couplings must be all positive. This is a strong constraint, which eliminates the possibility for the trajectories to converge to the IR convexity fixed point corresponding to SSB, see Fig. 5.1. Consequently the ShG model has only a single phase, namely the symmetric one. Fig. 8.7 illustrates these results showing the phase diagram of the SG model extended to imaginary frequencies obtained by the FRG method beyond LPA using the mass-cutoff, i.e., power-law regulator [4].

There are also models interpolating between the SG and the ShG models. One example is called the sn-Gordon (SnG) model with a potential

$$V_{\mathrm{SnG}}(\varphi) = A_k \,\mathrm{cd}(\beta\varphi, m)\,\mathrm{nd}(\beta\varphi, m)\,, \tag{8.16}$$

where $\mathrm{cd}(\beta\varphi, m)$ and $\mathrm{nd}(\beta\varphi, m)$ are Jacobi functions, A_k is the scale-dependent amplitude and m is the interpolating parameter. Using the identities of the Jacobi functions the potential can be expressed in the form

$$V_{\mathrm{SnG}}(\varphi) = \sum_{n=1}^{\infty} \tilde{u}_n(k)\cos(n\,b\,\varphi), \qquad b = \frac{\beta}{{}_2F_1\left(\frac{1}{2},\frac{1}{2},1,m\right)}\,. \tag{8.17}$$

This shows, that phase diagram of the SnG model is similar to the SG model with the only difference in the frequency. If $m = 0$, then $b = \beta$ and the SG model is recovered while in the $m \to 1$ limit the ShG model is reproduced. However the latter limit is non-analytic. Fig. 8.8 shows how the increase of of the interpolating parameter m changes the phase structure of the SnG model.

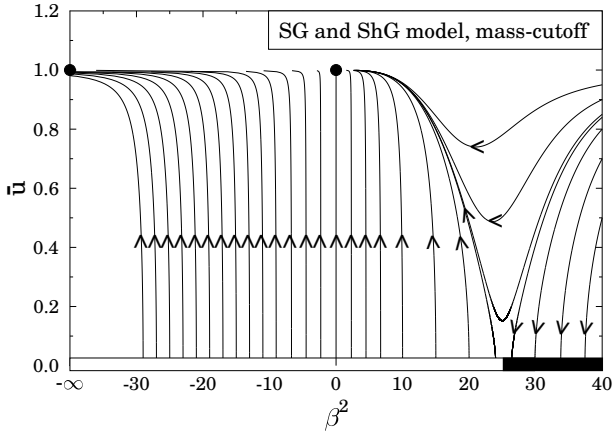

Figure 8.7: The merged phase diagram of the SG (positive β^2) and the ShG model (negative β^2). The black points correspond to the IR fixed points.

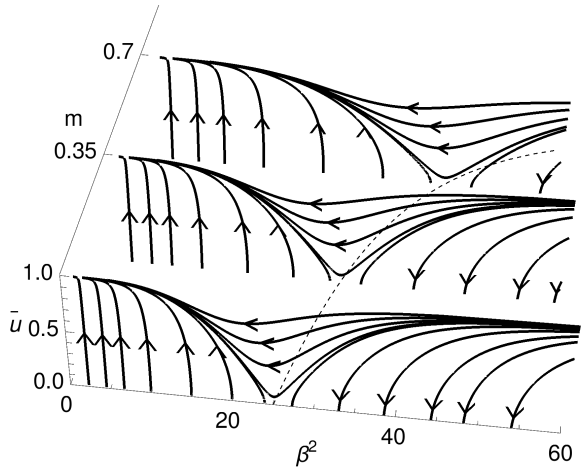

Figure 8.8: Phase diagram of the SnG model for the interpolating parameters $m = 0, 0.35, 0.7$. The dashed line corresponds to the critical frequency $\beta_c^2(m)$ of the topological phase transition.

8.4 The $O(N)$ model without truncations ($N < \infty$, $N_{\rm CUT} = \infty$)

In this section the $O(N)$ model is finally discussed with a finite N and keeping the potential non-truncated in LPA.

Consider first the Ising model ($N = 1$) with the following strategy: compute the WF saddle points for finite $N_{\rm CUT}$ values, and then observe how the $N_{\rm CUT} \to \infty$ limit behaves. In dimensions close to $d = 2$ this calculation is unfortunately ambiguous, since it is difficult to approximate the $N_{\rm CUT} \to \infty$ limit and extract the exact WF fixed point position in LPA. However the spike plot method is able to determine the WF fixed point of the non-truncated $O(N)$ model.

The results are shown in Fig. 8.9 where the position of WF fixed points are plotted on the VMB curves as a function of $N_{\rm CUT}$ for several dimensions between $d = 1$ and $d = 3$ using the Litim regulator for the Ising model. For each case the exact WF saddle points obtained by the spike plot method are also shown by the symbol X. Similar results are found for general N. As Fig. 8.9 indicates, the g_2 coordinate of the WF fixed point tends to zero for $d \leq 2$ while converges to a finite value for $d > 2$ in the $N_{\rm CUT} \to \infty$ limit. This result holds for general N in LPA, which implies that when LPA is applied for $N \geq 2$ and treated exactly without truncations, it is enough to reproduce the Mermin-Wagner theorem. In $d = 2$ the spike plot method yields that no WF fixed point and thus no SSB is present for any N. This is the correct conclusion for $N \geq 2$, however not for $N = 1$. To obtain the valid result for the two-dimensional Ising model, at least LPA$'$ is required. While the position of the WF fixed point is not universal, its occurance determines whether SSB is present or not. One might expect that calculating a universal quantity, such as a critical exponent of the WF fixed point would confirm the obtained results. Namely, for $N = 1$ the critical exponent would likely converge to a certain value in $d = 3$, but not in $d = 2$.

Besides the strong numerical evidence given by the excellent agreement between the spike plot analysis and the limit of increasing $N_{\rm CUT}$ values, where the non-truncated LPA has been sufficient to reproduce the Mermin-Wagner theorem, in the following, two analytical arguments are also presented to confirm these results.

To analytically investigate the appearance of SSB for the unexpanded potential ($N_{\rm CUT} = \infty$) of the $O(N)$ model with a finite N in LPA, consider substituting $k\partial_k u = 0$ in Eq. (5.9) to obtain the fixed point equation

$$du - (d-2)\rho u' = \frac{A_d(N-1)}{1+u'} + \frac{A_d}{1+u'+2\rho u''}. \tag{8.18}$$

The left hand side of this equation is linear in the effective potential, while the right hand side have non-linear terms in its derivatives, therefore one can use the notation

$$LP \equiv du(\rho) - (d-2)\rho u'(\rho), \tag{8.19}$$

$$NLP \equiv \frac{A_d(N-1)}{1+u'(\rho)} + \frac{A_d}{1+u'(\rho)+2\rho u''(\rho)}, \tag{8.20}$$

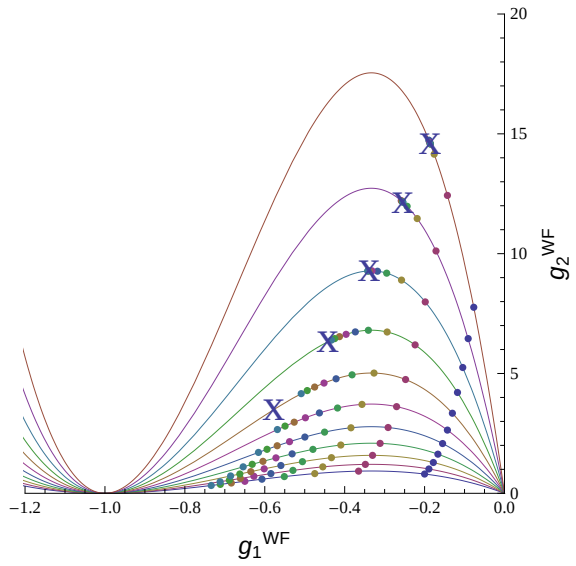

Figure 8.9: The position of the WF fixed points on the respective VMB curves for increasing values of N_{CUT} of the expanded $O(N=1)$ model in dimension between $1 \leq d \leq 3$ with the values $d = 3, 2.8, 2.6, 2.4, 2.2, 2, 1.8, 1.6, 1.4, 1.2, 1$ from top to bottom. The WF points are obtained using the truncation $N_{\mathrm{CUT}} = 2, \cdots, 10$ from right to left for each dimension. The symbol X denotes the position of the exact WF fixed point computed with the spike plot method [72, 73].

where LP means linear and NLP means non-linear part. Assuming analyticity for the potential [76] for all finite values of the field implies that the potential can only be a constant or divergent in the large field limit ($\rho \gg 1$). In the first case NLP must be a constant at infinity, and thus the potential is also just a constant for all ρ. In the second case NLP either vanish or converge to a constant (eventually to zero) at infinity, hence at large field the fixed point potential has to satisfy the condition

$$LP = C, \tag{8.21}$$

where C is a constant that is finite (or zero) and has to be treated consistently. Then the large field solution for the potential writes as

$$u(\rho) = \frac{C}{d} + a\rho^{\frac{d}{d-2}}, \tag{8.22}$$

where a is the constant of integration. Differentiating the above equation yields $u'(\rho) = a\frac{d}{d-2}\,\rho^{\frac{2}{d-2}}$, which is zero for $d < 2$ and divergent for $d > 2$ as $\rho \to \infty$. In the former case C is zero, while in the latter the assumption that u' is bounded is violated. In either case the large field limit is described by the expression

$$u(\rho) = a\rho^{\frac{d}{d-2}}. \tag{8.23}$$

Thus the general fixed point solution for the effective potential can be divided into two parts,

$$u(\rho) = f(\rho) + a\rho^{\frac{d}{d-2}}, \tag{8.24}$$

where the function $f(\rho)$ is defined to satisfy the condition $\lim_{\rho\to\infty} f(\rho) = 0$. From the effective potential the Gibbs free energy $F(m)$ can be calculated by changing the variables to dimensional ones [75], finding

$$F(m) = k^d u(k^{2-d}m^2) = k^d f(k^{2-d}m^2) + am^{\frac{2d}{d-2}}, \tag{8.25}$$

where m is the dimensional field, which can be associated with the average magnetic moment in the case of a spin system. Finally the $k \to 0$ limit of Eq. (8.25) gives the free energy, where three different cases can be distinguished.

$d > 2$

If $d > 2$, then in Eq. (8.25) the factor k^{2-d} is diverging in the argument of the function $f(\rho)$. However $f(\rho)$ tends to zero in the infinite field limit, therefore the Gibbs free energy of the $O(N)$ model for $d > 2$ in LPA writes as

$$am^{\frac{2d}{d-2}}, \tag{8.26}$$

where a is a positive constant that can be fixed by the method discussed in [76].

$d < 2$

When $d < 2$ the factor k^{2-d} is vanishing in the argument of $f(\rho)$. The effective potential given by Eq. (8.24) should be defined for all finite values of ρ, hence to compensate the divergence of the term $\rho^{\frac{d}{d-2}}$, which has a negative exponent in this case, the $f(\rho)$ function must be also divergent in zero. Consequently in the zero limit $f(\rho)$ can be written as

$$\lim_{\rho\to 0} f(\rho) = w(\rho) - a\rho^{\frac{d}{d-2}}, \tag{8.27}$$

where $w(\rho)$ is finite for vanishing arguments. Substituting this expression into Eq. (8.25) yields

$$k^d w(k^{2-d}m^2), \tag{8.28}$$

which converges to zero as $k \to 0$.

To conclude, the analysis of the $O(N)$ model in LPA showed that for $d > 2$ the fixed point free energy is either given by Eq. (8.26) or it can be zero, indicating that two phases are present [76]. When $d < 2$ the critical free energy is always zero, thus SSB does not occur. An alternative derivation reporting the same result in LPA can be found in [77].

$d = 2$

The above analysis cannot be applied to the $d = 2$ case, however the numerical investigation of Eq. (8.18) in LPA shows that the large field behavior of $u(\rho)$ is oscillatory, indicating the absence of SSB. For $N \geq 2$ this is in agreement with the Mermin-Wagner theorem, however the $N = 1$ case also has an oscillatory solution, which incorrectly predicts the absence of SSB.

In order to describe the critical behavior of the two-dimensional Ising model a better approximation is needed which goes beyond LPA. In [58] the LPA$'$ calculations show a vanishing anomalous dimension in the $d \to 2$ limit for $N \geq 2$ but a non-vanishing one for $N = 1$ providing the correct picture in the FRG framework. Of course this does not exclude the possibility of the Berezinskii Kosterlitz-Thouless phase transition [78, 79] that occurs for $N = 2$ and can be captured also by FRG [58, 80, 81].

8.5 Conclusion

In this chapter I have studied the presence of SSB in the FRG framework and whether the LPA is sufficient to retrieve the Mermin-Wagner theorem [3].

First the solutions of the Taylor expanded $O(N)$ models were investigated in LPA with finite N and finite N_{CUT} using various regulators. In this case SSB always appears even in dimensions (in $d \leq 2$ for $N \geq 2$) where it should not. This is indicated by the WF fixed points which are situated on the curves defined by the vanishing mass beta functions. In $d \leq 2$ as the number of couplings (N_{CUT}) increases the WF fixed points converge to the pertinent infrared convexity fixed point, while in $d > 2$ they tend to the respective exact LPA WF point calculated by the spike plot method. The Taylor expansion of the potential around the minimum ρ_0 was also investigated, which showed that even with the most drastic truncation ($N_{\mathrm{CUT,m}} = 2$) it is able to reproduce the expected result for the Mermin-Wagner theorem. This is shown by the diverging behavior of ρ_0 when $d \to 2$. However for the Ising model ($N = 1$) the coupling λ is diverging at $d = 2.5$ and then turning negative for smaller dimensions, which is clearly wrong, since it is well known that SSB occurs in $d = 2$ for the Ising model. In the large N limit a simple analytic expression is obtained for the spherical model in LPA, retrieving the correct result.

The XY model ($N = 2$) and the corresponding SG model was discussed where a topological phase transition is present in $d = 2$, since these type of phase transitions are not excluded by the Mermin-Wagner theorem. Extensions of the SG model, namely the sinh- and sn-Gordon model were also investigated observing a change in the critical frequency and finding a non-analytic limit of the SnG model [4].

Finally the exact LPA equations were studied considering analytic arguments based on the Gibbs free energy of the system given by the dimensional effective potential. In $d > 2$ the dimensional field associated with the average magnetic moment of a spin system can be zero, or non zero, indicating two phases and the presence of SSB, while in $d < 2$ the field can only be zero signaling no SSB. This

analysis cannot be directly applied in $d = 2$, however numerical calculations exclude the possibility of SSB, which is again, an incorrect result.

Thus, SSB always appears in the truncated $O(N)$ models, even when it should not, however the Taylor expanded potential around the minimum and the local potential approximation when treated exactly, without truncations, is sufficient to reproduce the Mermin-Wagner theorem for the $O(N \geq 2)$ models in all dimensions. The only exception when the exactly treated LPA gives an incorrect qualitative picture is for the two-dimensional Ising model, where it incorrectly predicts the absence of SSB.

Chapter 9

Higgs-inflation

Inflationary cosmology is one of the most studied theories that describes the exponential inflation of the early Universe. It is developed to explain the isotropy of the CMBR, the origin of the large-scale structure of the cosmos, the horizon and the flatness problem, and the absence of magnetic monopoles [52]. A hypothetical scalar field called inflaton is thought to be responsible for inflation as the vacuum expectation value of the field slowly rolls down from a metastable false vacuum to the real vacuum [82, 83], see Chapt. 6 for a more detailed description of the mechanism. However, the particle physics origin for inflation, and whether it is a reliable approach is still a matter of discussion [84, 85].

Another topic of intense debate is whether it is possible to identify the inflaton with the Higgs field. Indeed, the Standard Model (SM) of particle physics can be extrapolated up to very high energies and possibly the same scalar field can describe both inflationary and Higgs physics. However various issues, such as the exit from the inflationary phase or the stability of the Higgs potential, need to be addressed in these Higgs-inflationary scenarios. Reflecting to the latter issue in Ref. [86] it is argued that even if the SM vacuum is not completely stable the traditional Higgs inflation is viable within a minimalistic framework. The stability question was also studied for example in Refs. [87–89] highlighting the importance of RG running. An unstable potential can also indicate unknown new physics, which is discussed in Refs. [90, 91].

However there are still several unanswered questions regarding Higgs-inflation, which require further investigations. One question is how to construct a single scalar field that works both at electroweak and cosmological energy scales. A single model must simultaneously explain the thermal fluctuations of the CMBR and the measurements at the electroweak scale. Another problem is related to the *ad hoc* choice between the inflationary models. There is a plethora of scalar fields proposed in the literature [92], which are not excluded by the data extracted from the CMBR and work well describing the inflation, thus to naively choose one of them seems *ad hoc*. The assumption that the Higgs field is identical to the inflaton may provide an answer to this issue, since the requirement for a scalar model to

be viable both for Higgs and inflationary physics gives extra constraints and can drastically reduce the number of viable candidates. RG is a method designed to relate parameters of a model at different energy scales, therefore it is expected to provide a tool to connect the scale of inflation and the electroweak scale, and thus reduce the number of admissible inflationary models.

In the following sections a new viable inflationary model the MSG model is proposed and it is demonstrated that it works well describing the physics of inflation. Then by using an RG approach, the relation between the parameters of the model at the cosmological and the electroweak scale is discussed.

9.1 Inflationary potentials

Before proposing a new model it is important to understand the qualitative structure of inflationary potentials. One of the simplest examples is the quadratic large-field inflationary (LFI) potential ϕ^2, which has only a single minimum. More minima can be added by increasing the number of higher-order terms with the form ϕ^{2n}. Thus the question to ask is how much one should deviate from the simple quadratic potential. The relevance of the "ϕ^2 or not-ϕ^2" issue was discussed in Ref. [93]. Also a very "not-ϕ^2" potential with infinitely many minima was considered with the form $V_{\rm NI}(\phi) = u\,[1-\cos(\beta\phi)]$. This model is known as the Natural Inflation (NI) in cosmology, but in condensed matter physics and in field theory it is the well-known SG model, and it has a single phase in $d=4$ [42]. It has been a widely studied inflationary potential [42, 94–103], since as a periodic scalar field it can incorporate the axion physics too [42]. The measurements of the PLANCK mission [104–106] showed that the NI model has a better agreement with the data on the thermal fluctuations of the CMBR (namely the scalar tilt n_s and the tensor-to-scalar ratio r given in (6.35)) than the simple LFI model.

In this chapter a new scalar theory is proposed for inflation which has an overall ϕ^2 shape shifted by a constant and dressed with a periodic cosine to have many minima. This proposal can be rightfully called as the massive Natural Inflation, or as it is known in statistical field theory, the MSG model, see Sect. 5.2.2. Here, three MSG variants are considered which differ only by the constant term and by the sign of the periodic term

$$V_{\rm MSG_1}(\phi) = \frac{1}{2}m^2\phi^2 + u\,[1-\cos(\beta\phi)]\,, \tag{9.1}$$

$$V_{\rm MSG_2}(\phi) = \frac{1}{2}m^2\phi^2 + u\,[\cos(\beta\phi)-1]\,, \tag{9.2}$$

$$V_{\rm MSG_3}(\phi) = \frac{1}{2}m^2\phi^2 + u\,[\cos(\beta\phi)-1] - V_0\,, \tag{9.3}$$

where m is an explicit mass, u is the Fourier amplitude and β is the frequency. Besides the additional mass term, the first variant has the same form as the Natural Inflation, however in the second variant the sign of u is changed, while the third version also has an additional constant V_0 which is chosen in a way to keep the

global minimum of the potential at zero ($V_{\min} = V_{\mathrm{MSG}_3}(\phi_{\min}) = 0$). By tuning the m^2/u ratio, i.e., the ratio between the parabolic and periodic term, the number of local minima and the energy separation between them can also be tuned from the limit of infinite degenerate minima to only one non-degenerate minimum.

These properties make the MSG model a great candidate for inflationary physics and a possible extension of the Standard Model Higgs potential.

9.2 Cosmological scale

Scalar fields are an essential part of the Standard Model of particle physics and they also find a natural role to play in inflationary cosmology, since they can mimic the equation of state and the energy tensor required for the exponential expansion of the early Universe, see Chapt. 6. Various inflationary models have been proposed in the literature, one of the simplest among them is the single-field slow-roll models with minimal kinetic terms [92]. A reliable inflationary potential is also simple, and has a small number of adjustable parameters, which is a condition that a good candidate should satisfy. The go to example is the LFI model, which has only a quadratic mass term, $V = \frac{1}{2}\, m^2\phi^2$.

Another condition for a good inflaton potential is that it should be able to predict the cosmological observations, such as the thermal fluctuations of the CMBR measured by the PLANCK mission [104–106]. Therefore the slow-roll analysis must be performed for the MSG model to see whether it is a viable iflationary model at the cosmological scale.

First, one has to compute the quantities (see Chapt. 6 or Ref. [49]),

$$\epsilon \equiv \frac{1}{2} m_p^2 \left(\frac{V'}{V}\right)^2, \qquad \eta \equiv m_p^2 \frac{V''}{V}, \tag{9.4}$$

where $m_p^2 = 1/(8\pi G)$ is the Planck mass, and as usual $c = \hbar = 1$. The gravitational constant G and consequently the Planck mass m_p is assumed to be a constant. In Quantum Einstein Gravity these would be running parameters, however here their running is neglected. If $\epsilon \ll 1$ and $\eta \ll 1$, then the inflation is in progress, but it stops if either of these parameters reach a value in the order of one. To have a large enough expansion, the E-fold number N, defined by

$$N \equiv -\frac{1}{m_p^2} \int_{\phi_i}^{\phi_f} \mathrm{d}\phi\, \frac{V}{V'} \tag{9.5}$$

must also reach a value between $50 < N < 60$ during inflation, while the expectation value of the inflaton field slowly rolls down from its initial value ϕ_i, to its final one ϕ_f. Another constraint is given by the energy scale on which the inflation occurred [50]. For the potential this is written as

$$V(\phi_i) \equiv \frac{r}{0.01} (10^{16}\,\mathrm{GeV})^4. \tag{9.6}$$

For r values in the range of $r \approx 0.01$ this means that the scale of inflation is at the Grand Unified Theory (GUT) energy scale (10^{16} GeV).

The Planck mass appears in most of the equations, thus it is convenient to introduce dimensionless variables accordingly. In $d = 4$ dimensions the dimensionless potential and the parameters of the MSG model are obtained by the following formulas

$$\hat{V} = V/m_p^4, \quad \hat{\phi} = \phi/m_p, \quad \hat{u} = u/m_p^4\,,$$
$$\hat{m} = m/m_p, \quad \hat{\beta} = m_p\beta\,. \tag{9.7}$$

Here the hat notation is used for the dimensionless quantities, while the tilde is reserved when the dimension is taken away by the relevant running energy scale (see Eq. (9.22)) instead of the Planck mass. Since the field independent constant term is fixed for all three variants of the MSG model, and the overall factor is also fixed by the normalization using Eq. (9.6), the only free parameters are the frequency β and the ratio u/m^2. By performing the standard slow-roll analysis these two remaining parameters can be constrained.

The next step is to calculate the scalar tilt n_s and the tensor-to-scalar ratio r, by using the relations $n_s \approx 2\eta - 6\epsilon + 1$ and $r \approx 16\epsilon$ [49]. The inflation stops if either $\epsilon(\phi_{f,\epsilon}) = 1$ or $\eta(\phi_{f,\eta}) = 1$, thus the final value of the expectation value is given by $\phi_f \equiv \max(\phi_{f,\epsilon}, \phi_{f,\eta})$. Substituting ϕ_f into Eq. (9.5) the initial value of the expectation value ϕ_i can be also computed using the required range of the E-fold number $50 < N < 60$. Finally the quantities $n_s(\phi_i)$ and $r(\phi_i)$ can be calculated and compared to the measured data. The results clearly depend on the chosen potential. For the quadratic LFI model this procedure yields $n_s - 1 \approx -2/N$ and $r \approx 8/N$ giving the relation $n_s - 1 + r/4 = 0$, which however does not show a good agreement with the measurements of the PLANCK mission [104–106].

I have performed the described slow-roll analysis for all three variants of the MSG potential and compared the results to the measured fluctuations of the CMBR, namely to the measured scalar tilt n_s and the tensor-to-scalar ratio r. The result is shown in Fig. 9.1, where the best acceptance parameter regions are plotted for the three different MSG variants. It shows that there is an overlap between the variants in the small $\hat{\beta}$ range, but the results depend on the particular form of the potential. In the large $\hat{\beta}$ limit, the acceptance regions become a straight line for each considered MSG model. This line depends on the sign of the periodic term, since it is a significant change in the shape of the potential. However the numerical calculations verify that the acceptance regions of the second and third variant coincide, thus the change in the constant term do not modify the slow-roll results. This remark is true in the $\hat{\beta} \gtrsim 1.5$ region for all N values between $50 < N < 60$. From the $\hat{u}/\hat{m}^2$ ratios read from the figure, the parameters u and m^2 can be calculated using the normalization described in Eq. (9.6). For example, by choosing the middle of the acceptance region of the first MSG variant (9.1) from Fig. 9.1, one obtains

$$m \approx 1.42 \times 10^{13}\,\mathrm{GeV}\,, \quad \mathrm{u} \approx 2.4 \times 10^{64}\,\mathrm{GeV}^4\,, \quad \beta \approx 1.25 \times 10^{-19}\,\mathrm{GeV}^{-1}\,. \tag{9.8}$$

Finally the most important result which will be necessary for scaling down the model to the electroweak scale is the fact that the ratio $\hat{u}\hat{\beta}^2/\hat{m}^2$ is always larger than one in the acceptance regions. This ratio remain unchanged in the large $\hat{\beta}$ limit, and has the property

$$\hat{u}\hat{\beta}^2/\hat{m}^2 = u\beta^2/m^2 > 1\,. \tag{9.9}$$

More details about the slow-roll analysis of the MSG model are discussed in the next chapter in Sect. 10.3.

These results were obtained preserving the sinusoidal functional form of the MSG potential, however by truncating its Taylor expansion and keeping the terms up to the quartic power, one can find good agreement with the measured n_s and r quantities of the CMBR. This would require a large explicit mass, which however cannot be scaled down to the known Higgs mass at the electroweak energy scale unlike in the case of the MSG model. This point will be discussed in the next sections.

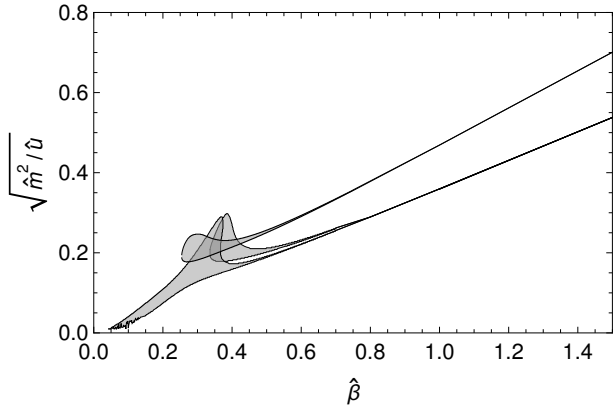

Figure 9.1: Comparison of the slow-roll results for the MSG model (9.1)-(9.3) to the Planck data [104–106] on the fluctuations of the CMBR, namely on the scalar tilt n_s and the tensor-to-scalar ratio r. The best agreement is given by the parameters located inside the gray regions. For large $\hat{\beta}$ values these regions become a straight line.

9.3 Electroweak scale

Many attempts have been made in the literature to identify the inflaton with the Higgs field. [107–117]. In the SM of particle physics the Higgs field is an $SU(2)$ complex scalar doublet which consists four real components and can spontaneously break the $SU(2)_L \times U(1)_Y$ symmetry of the electroweak sector. It has the La-

grangian

$$\mathcal{L} = (D_\mu \phi)^\star (D^\mu \phi) - V(\phi) - \frac{1}{2}\,\mathrm{Tr}\,(F_{\mu\nu} F^{\mu\nu}) \tag{9.10}$$

where

$$D_\mu = \partial_\mu + igTW_\mu + ig' y_j B_\mu, \tag{9.11}$$

and the potential is

$$V = \mu^2 \phi^\star \phi + \lambda (\phi^\star \phi)^2 \,. \tag{9.12}$$

If $\mu^2 > 0$, then the vacuum expectation value is at zero, while for $\mu^2 < 0$ it is at $\sqrt{\phi^\star \phi} = \sqrt{-\mu^2/(2\lambda)} = v/\sqrt{2}$ where the value $v = 246$ GeV has been determined from low-energy experiments. After spontaneous symmetry breaking, due to the Brout-Englert-Higgs mechanism [118, 119], from the four degrees of freedom of the Higgs doublet three are absorbed by the weak gauge bosons, which become massive as a consequence. The remaining degree of freedom is a single scalar field h. The excitation of h is the Higgs boson that was discovered by the Large Hadron Collider at CERN [120,121]. In this phase the field is usually parametrized around its minimum and the unitary phase of the field is omitted by an appropriate choice of the gauge. Thus, the Higgs sector of the SM can be written as

$$\begin{aligned}\mathcal{L} = \frac{1}{2}\partial_\mu h \partial^\mu h - \frac{1}{2} M_h^2 h^2 - \frac{M_h^2}{2v} h^3 - \frac{M_h^2}{8v^2} h^4 \\ + \left(M_W^2 W_\mu^+ W^{-\,\mu} + \frac{1}{2} M_Z^2 Z_\mu Z^\mu \right) \left(1 + 2\frac{h}{v} + \frac{h^2}{v^2} \right),\end{aligned} \tag{9.13}$$

where the Higgs mass $M_h = \sqrt{-2\mu^2} = \sqrt{2\lambda v^2}$ has a measured value of $M_h = 125.6\,\mathrm{GeV}$ implying $\lambda = 0.13$. This value is close to the one predicted assuming the validity of the SM supplemented by asymptotically safe gravity between the Fermi and Planck scales [122].

An identification must be made between the Higgs field (scalar singlet) and the inflaton field that has been used in the literature. However, this requires the reparametrized form of the Higgs Lagrangian where there is no $SU(2)$ doublet anymore. This reparametrization is straightforward in the broken phase nevertheless it might be applicable in the symmetric case too, because the Higgs mechanism is based on SSB where only the ground state breaks the symmetry not the explicit form of the Lagrangian. In my thesis I rely on the standard choice typically used in the corresponding literature [111–117], namely the identification of the Higgs singlet with the inflaton field.

In order to find a link between the Higgs and inflationary physics, one has to extrapolate the SM up to very high energies. For this reason the action, i.e., the spacetime integral of the Lagrangian is defined with the Ricci scalar R which is either multiplied by a function of a scalar field, called the Jordan frame, or not multiplied by the field, which is called the Einstein frame [123]. Various transformations exist between the frames, but usually the Einstein frame is used for

the slow-roll study. In the case of minimal coupling to gravity the action in the Einstein frame takes the form

$$S = \int d^4x\sqrt{-g}\left[\frac{m_p^2 R}{2} - \tfrac{1}{2}g^{\mu\nu}\,\partial_\mu\phi\,\partial_\nu\phi - V(\phi)\right],$$
$$V(\phi) \equiv \frac{\lambda}{4}\left(\phi^2 - v^2\right)^2 = \frac{M_h^2}{8v^2}\left(\phi^2 - v^2\right)^2, \tag{9.14}$$

where $g^{\mu\nu}$ is the metric tensor, $\sqrt{-g} \equiv \sqrt{-\det g}$, the scalar field is denoted by $\phi \equiv h$ and V is the standard quartic-type double-well potential of (9.13),

$$V(\phi) = \frac{\lambda}{4}v^4 - \frac{1}{2}\lambda v^2\phi^2 + \frac{\lambda}{4}\phi^4\,. \tag{9.15}$$

with the shift $h \to h + v$ in the field. The non-minimal inflation scenario is not discussed here.

Another way to approach Higgs inflation is to extend the SM Higgs potential with minimal coupling to gravity and assume that it develops at least a second minimum from which the inflation began [107–110]. However in this scenario the inflationary phase may become eternal. A possible solution is to add more fields, but then the simplistic nature would be lost.

Another problem with Higgs-inflation comes from fact that the measured Higgs mass is close to the lower limit that still ensures the stability of the absolute vacuum in the SM [124]. Fortunately, even if the SM vacuum is not completely stable, the conventional Higgs-inflation is still a viable scenario in a minimalistic framework [86]. Also many polynomial Higgs potentials have been investigated using the functional renormalization group method that had no stability problem [88, 89].

The Higgs potential given by (9.15) can be recovered by the Taylor expansion of the MSG model up to the quartic terms. This is not true for the first variant (9.1) since it cannot reproduce the required double-well shape, thus it is not considered in further calculations in this chapter. For the other two variants (9.2) and (9.3) the potential can be written as

$$V_{\mathrm{MSG}} \approx V_0 + \frac{1}{2}(m^2 - u\beta^2)\phi^2 + \frac{1}{24}u\beta^4\phi^4 + \mathcal{O}(\phi^6)\,, \tag{9.16}$$

therefore the parameters can be related

$$\lambda v^2 \equiv (u\beta^2 - m^2), \quad \lambda \equiv \frac{1}{6}u\beta^4. \tag{9.17}$$

From equations $M_h = \sqrt{2\lambda v^2}$ and $v = \sqrt{M_h^2/(2\lambda)}$ the Higgs mass and the VeV takes the form

$$M_h \equiv m\sqrt{2\left(\frac{u\beta^2}{m^2} - 1\right)}, \quad v \equiv \frac{1}{\beta}\sqrt{\frac{6(u\beta^2/m^2 - 1)}{u\beta^2/m^2}}. \tag{9.18}$$

with the known low-energy/IR values

$$M_{h,\mathrm{IR}} = 125\ \mathrm{GeV}, \quad v_{\mathrm{IR}} = 245\ \mathrm{GeV}\,, \tag{9.19}$$

at the electroweak scale $k_{\rm IR} \sim 250$GeV. Taking into account the higher order terms in the Taylor expansion only slightly modifies these relations and has no effect on the main results presented in the next section.

These quantities can be determined also at the cosmological scale where the slow-roll study gives a large Higgs mass. For example for the parameters shown in Eq. (9.8) the obtained Higgs mass is

$$M_{h,\rm UV} \approx 1.9 \times 10^{13}\text{GeV}\,, \tag{9.20}$$

only a few orders-of-magnitude below the high-energy (UV) scale of inflation $k_{\rm UV} \sim 10^{15}$GeV, which also depends on the choice of $\hat{\beta}$. This large mass and also the VeV must be scaled down by orders of magnitude to the elextroweak scale where they have the measured values given by Eq. (9.19). FRG is a powerful method that provides a tool to obtain the RG running of these parameters and relate them at distant scales. In the next section the RG study of the MSG model is performed to describe the post-inflation period.

9.4 Renormalization group scaling

In order to scale down a Higgs-inflation model from the cosmological to the electroweak scale within the FRG framework, one has to incorporate all fields including the fermion and gauge fields as well. However, the MSG model, besides the mass term and a trivial constant, has a periodic self-interaction, which allows to perform its RG study in a simple way. The reason can be understood by observing the structure of the RG equation given by Eq. (4.32) where the flow of the action is given by its Hessian (second derivative). Even if the scalar field is coupled to fermion or gauge fields with terms not higher than quadratic, the Hessian of the scalar sector remains periodic. Thus, it can be a reliable approximation to study only the RG evolution of the MSG potential while neglecting other fields.

The MSG model was extensively studied in $d = 2$ dimensions by functional RG [43–45], however in the case of Higgs-inflation $d = 4$ dimensions are required. Here the LPA of the functional RG is used (4.35), with the optimized Litim regulator (4.47), therefore the following RG equation is obtained for the dimensionless scaling potential

$$\left(d - \frac{d-2}{2}\tilde{\phi}\partial_{\tilde{\phi}} + k\partial_k\right)\tilde{V}_k = \frac{2\alpha_d}{d}\,\frac{1}{1+\partial_{\tilde{\phi}}^2\tilde{V}_k}\,, \tag{9.21}$$

where $\alpha_d = \Omega_d/(2(2\pi)^d)$, $\Omega_d = 2\pi^{d/2}/\Gamma(d/2)$ is the d-dimensional solid angle, and k is the running momentum scale. As usual, the tilde denotes dimensionless variables where their dimension is taken away by multiplying with the appropriate power of k,

$$\tilde{\beta} = k^{(d-2)/2}\,\beta\,, \qquad \tilde{m} = m/k\,, \qquad \tilde{u} = k^{-d}\,u\,, \qquad \tilde{\phi} = k^{-(d-2)/2}\,\phi\,. \tag{9.22}$$

Substituting the MSG potentials into Eq. (9.21) yields an expression which can be separated to periodic and non-periodic parts. This is true since the higher order

self-interaction terms originate only from the periodic part, hence it can be written as a separate equation. The right-hand side is periodic, thus the non-periodic part reads as

$$\tilde{m}^2\tilde{\phi}^2 + k\partial_k\left(\frac{1}{2}\tilde{m}^2\tilde{\phi}^2\right) - \tilde{u}\tilde{\phi}\sin\left(\tilde{\beta}\tilde{\phi}\right)\frac{d-2}{2}\tilde{\beta} + \tilde{u}\tilde{\phi}\sin\left(\tilde{\beta}\tilde{\phi}\right)(k\partial_k\tilde{\beta}) = 0. \quad (9.23)$$

By investigating the purely trigonometric and polynomial terms one can see that these terms also split into two separate equations, providing the flow equations for $\tilde{\beta}$ and $\tilde{m}$,

$$k\partial_k\tilde{\beta}_k = \frac{d-2}{2}\tilde{\beta}_k \quad \rightarrow \quad \tilde{\beta}_k = \beta\, k^{(d-2)/2}\,, \quad (9.24a)$$

$$k\partial_k\tilde{m}_k^2 = -2\tilde{m}_k^2 \quad \rightarrow \quad \tilde{m}_k^2 = m^2\, k^{-2}\,. \quad (9.24b)$$

These solutions obtained in LPA indicate that the dimensionless quantities $(\tilde{m}, \tilde{\beta})$ have a trivial scaling according to their corresponding dimension, thus the dimensionful parameters (m, β) remain unchanged during the RG running. The scaling of $\tilde{\beta}$ in (9.24a) can be also considered as the trivial RG running of the wave-function renormalization after rescaling the field as $\beta\varphi \to \tilde{\varphi}$. For the remaining parameter $\tilde{u}$, the flow equation is given by the periodic part

$$-\cos\left(\tilde{\beta}\tilde{\phi}\right)(d + k\partial_k)\tilde{u} = \frac{2\alpha_d}{d}\,\frac{1}{1 + \tilde{m}^2 + \tilde{u}\tilde{\beta}^2\cos\left(\tilde{\beta}\tilde{\phi}\right)}. \quad (9.25)$$

Similar equations can be derived for different regulators. However, the properties of the master trajectory is related to spinodal instability, i.e., to the equation $1 + \partial_{\tilde{\phi}}^2\tilde{V}_k = 0$, which is the same for all regulators in LPA. This suggests that the presented results do not depend on the regulator. The right-hand side of (9.25) contains all Fourier modes, but the characteristic behavior can be read off using the single-mode approximation taking into account only the single cosine terms of the Fourier expansion of (9.25). This provides the RG flow equation for the Fourier amplitude $\tilde{u}$ which writes as

$$(d + k\partial_k)\tilde{u}_k = -\frac{4\alpha_d}{d}\frac{1}{\tilde{\beta}_k^2\tilde{u}_k}\left(1 - \sqrt{\frac{\left(1+\tilde{m}_k^2\right)^2}{\left(1+\tilde{m}_k^2\right)^2 - \tilde{\beta}_k^4\tilde{u}_k^2}}\right). \quad (9.26)$$

One can obtain the scale dependence of the couplings and the phase diagram by simultaneously solving these partial differential equations. In this case, using the Litim regulator, spinodal instability occurs at a large enough scale so that the phase diagram can be determined. An important observation is that the RG method gives the same flow for all variants of the MSG model given in Eqs. (10.3)-(9.3), since the obtained RG equations do not change under the $\tilde{u} \to -\tilde{u}$ transformation, and the field-independent terms are eliminated by the derivatives in the Hessian.

The result of this computation is shown in Fig. 9.2. The four-dimensional MSG model has two phases controlled by the dimensionless ratio $\tilde{u}_k\tilde{\beta}_k^2/\tilde{m}_k^2$. In the (Z_2)

symmetric phase (blue lines of Fig. 9.2) this quantity depends on the initial conditions however it is always smaller than one, $\lim_{k\to 0} |\tilde{u}_k \tilde{\beta}_k^2/\tilde{m}_k^2| < 1$. In the SSB phase (green lines of Fig. 9.2) this ratio is larger than one and converges to one in the IR limit regardless of the initial conditions. The two phases are separated

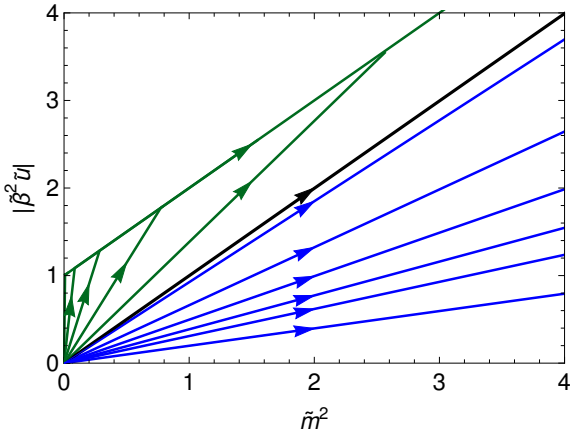

Figure 9.2: Phase diagram of the MSG model in $d = 4$ showing the flow of its parameters. The model has two phases separated by the black line with a unit slope. The blue trajectories correspond to the symmetric phase, while the trajectories of the symmetry broken phase are indicated by the green lines.

by the black line with a unit slope. The trajectories corresponding to the SSB phase merge into a single master trajectory which has also a unit slope and can be described by the equation

$$\bar{u}_k \tilde{\beta}_k^2 = 1 + \tilde{m}_k^2 \,. \tag{9.27}$$

Rearranging the above formula yields the following scaling

$$\frac{\bar{u}_k \tilde{\beta}_k^2}{\tilde{m}_k^2} - 1 = \frac{1}{\tilde{m}_k^2} = \frac{k^2}{m_{\mathrm{UV}}^2}. \tag{9.28}$$

This equation describes the running on the master trajectory which, apart from the initial part of the running, determines the scaling in the SSB phase.

Using Eq. (9.28) one can also calculate the scaling of the Higgs mass and VeV from their UV values to their IR ones (9.19). This is indeed true, since at the cosmological scale the UV initial conditions suggest that the Higgs-inflation field is in the SSB phase as a result of the ratio (9.9) being larger than one. Thus, from Eq. (9.18) the running Higgs mass writes as

$$M_h(k) = m_{\mathrm{UV}} \sqrt{2\left(\frac{\tilde{u}_k \tilde{\beta}_k^2}{\tilde{m}_k^2} - 1\right)}. \tag{9.29}$$

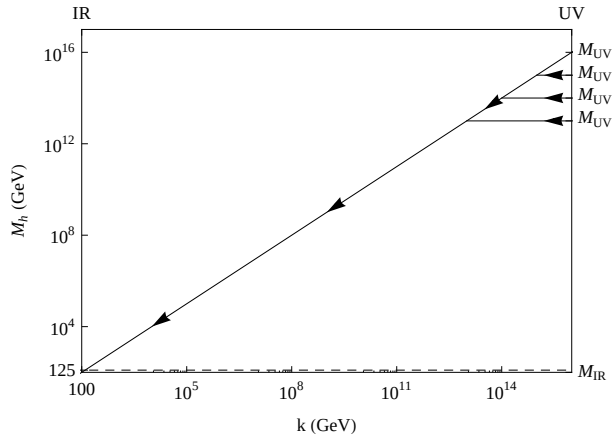

Figure 9.3: Scaling of the Higgs mass of the MSG model from the cosmological (UV) to the electroweak (IR) scale. The flow shows UV insensitivity as all trajectories merge into a single line reproducing the correct order of magnitude for the measured Higgs mass at the electroweak scale.

and substituting Eq. (9.28) yields the scaling

$$M_h(k) = m_{\rm UV}\sqrt{2}\sqrt{\frac{k^2}{m_{\rm UV}^2}} = \sqrt{2}\,\cancel{m_{\rm UV}}\frac{k}{\cancel{m_{\rm UV}}} = \sqrt{2}k, \tag{9.30}$$

where it is emphasized that the UV mass cancels. The UV independence is again, a consequence of the constant unit slope of the master trajectory. This property holds even if the initial UV condition does not fall on the master trajectory, since in the IR limit all SSB trajectories merge into it. One obtains a similar scaling for the VeV,

$$v(k) = \frac{1}{\beta_{\rm UV}}\sqrt{\frac{6(\tilde{u}_k\tilde{\beta}_k^2/\tilde{m}_k^2 - 1)}{\tilde{u}_k\tilde{\beta}_k^2/\tilde{m}_k^2}} \approx \frac{\sqrt{6}k}{m_{\rm UV}\beta_{\rm UV}}\,. \tag{9.31}$$

The electroweak (IR) scale is at $k_{\rm IR} = 250$ GeV, thus these formulas reproduce the correct order of magnitude for the measured IR values (9.19). While the IR Higgs mass is independent of the initial UV conditions, to recover the measured VeV at the electroweak scale one has to choose appropriate UV values for $m_{\rm UV}$ and $\beta_{\rm UV}$ requiring fine-tuning. These parameters can be determined from the slow-roll analysis together with a normalization condition such as $V(\phi_i) \approx k_{\rm GUT}^4$. The result is a point on the "tail" of the acceptance region in Fig. 9.1 with a large frequency $\hat{\beta} \approx 300$. However the standard normalization is given by Eq. (9.6), where the r quantity makes this determination problematic.

Fig. 9.3 shows the RG evolution of the Higgs mass from the cosmological (UV) scale to the electroweak (IR) scale which is independent of the initial UV param-

eters. It is important to note that in the perturbative RG framework the (dimensionful) SM Higgs mass has a weak running [16]. This is in agreement with the presented observations, since in the MSG model the dimensionful explicit mass m has no running at all, while the Higgs mass is an effective mass to which the periodic term also contributes. For this effective Higgs mass the non-perturbative functional RG method demonstrated a linear dependence on the running scale.

9.5 Conclusion

I have proposed the MSG model as a Higgs-inflationary potential and analyzed its properties both at cosmological and electroweak scales [5]. The MSG model has the advantage of having a rather simple functional form with only a small number of parameters. It has concave regions and many non-degenerate minima with tunable energy differences which improves its viability as a Higgs-inflationary candidate.

I have performed the slow-roll analysis of the model and determined that it works well at the cosmological level. It reproduces the data on the fluctuations of the CMBR, namely the scalar tilt and tensor-to-scalar ratio measured by the PLANCK and BICEP2 experiments, hence it provides a good agreement with observations. This has been used to constrain the parameter region of the MSG model serving as a high-energy (UV) initial condition.

The use of the MSG model represents the first step towards a possible consistent UV extension of the SM Higgs field, since at low energies (IR) it can reproduce the double-well SM Higgs potential. However in order to complete this task, i.e., the UV completion, one has to incorporate all the gauge and matter fields, and in addition the running of the gravitational and the cosmological constant. This very general framework is required to study whether a Landau singularity appears or not and/or the theory remains UV safe. This is of course a demanding task which is out of the scope of the present work.

Finally I have extended the RG study of the MSG model to $d = 4$ dimensions to describe its evolution in the post-inflation period and to connect the distant energy scales. The MSG potential contains a periodic term providing an ideal framework to compute its RG running in a straightforward way. I have obtained the phase diagram which showed that the UV parameters determined by the slow-roll analysis give the ratio $|\tilde{u}_k \tilde{\beta}_k^2 / \tilde{m}_k^2|$ in the spontaneously symmetry broken phase. Within the used approximations the measured value of the Higgs mass at the electroweak (IR) scale have been recovered by the correct order of magnitude. This result is insensitive of the UV initial parameters as long as they stay in the broken phase.

In conclusion, the proposed MSG model proved to be an excellent candidate for a Higgs-inflationary theory, since it provides a remarkable agreement with cosmological observations. By performing its RG analysis I have found that it can simultaneously describe the physics both at cosmological and electroweak scales and it recovers the Higgs mass by the correct order of magnitude at the electroweak scale in the post-inflation period independently of the high-energy (UV) initial conditions.

Chapter 10

Renormalization group induced inflation

The theory of inflation which describes the rapid expansion of the early Universe has advanced significantly, however there are still important questions that need to be answered. The original formulation of inflation [52] caused by the hypothetical inflaton field requires a relatively stable false vacuum, from which the system moves to the true vacuum (see Fig. 10.1). This induces the inflation and bubble nucleations are formed where the inflaton field reaches its low-energy vacuum state causing the bubbles to expand nearly at the speed of light. Several issues can be explained by this original inflationary scenario however it also suffers from numerous problems.

One problem is related to the fact that the Universe should undergo a reheating process after inflation, but this mechanism is not well defined in this context. Over the inflation period the exponential expansion of the observable Universe must continue long enough to dilute the magnetic monopoles, but as a consequence the bubbles become rare and they do not merge. This generates further problems, since the collision between bubble walls become so rare that they cannot generate the needed radiation. Another problem is the eternal nature of the decay process which is never complete.

A modification of the original idea provides a possible solution for these problems [82, 83]. In this new scenario the expectation value of the inflaton field starts from an excited metastable position and then slowly rolls down to the true minimum (see Chapt. 6 for more details). After inflation the oscillations of the field can produce the reheating (see Fig. 10.1). The inflation ends when the energy hill of the potential becomes steep or when the expectation value of the field gets close to the minimum solving the problem of having a "graceful exit". Yet, it does not address the question why the inflation starts with a particular initial condition. For chaotic (large-field) inflation models [125] large field fluctuations occur naturally, but then they also dominate the classical evolution of the field and can make the field move up the potential leading again to an eternal inflation. However for small-field infla-

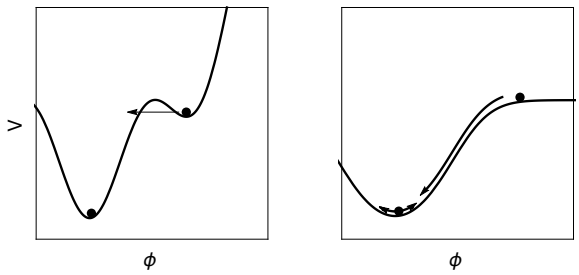

Figure 10.1: The original inflationary scenario starting from a false vacuum (left) and the slow-roll scenario (right) where the oscillations of the field can cause the reheating of the Universe.

tion the initial conditions are even more problematic, since the interactions should homogenize the Universe on a scale larger than the horizon. Several other theories, like the cyclic Universe [84, 85], have been proposed to solve these problems. The particular form of the potential is also unknown, thus it is important to find principles to constrain its shape.

To address these problems in this chapter the goal is to propose a new inflationary mechanism based on the proper treatment of quantum fluctuations in the pre-inflationary period that can result in the RG evolution of the potential. After the description of the proposed analysis, its validity is also shown for the MSG model as a working example.

10.1 Proposed inflationary scenario

The RG technique has already been successfully applied to the post-inflation period for Higgs-inflationary models, see for example the previous chapter, or the overview in Ref. [87]. Here the discussion is centered around the RG scaling of the potential in the pre-inflationary period as a mechanism to induce inflation which connects the original (Ref. [52]) and the modern (Ref. [82,83]) scenarios and gives a possible solution for the initial condition problem.

Although the slow-roll process during inflation is considered to be classical, in the pre-inflationary period quantum fluctuations can have a strong effect, thus the RG approach is widely applied in cosmology [126]. According to Ref. [126] the running momentum scale k of the RG method can be identified with the inverse of the cosmological time ($k \sim 1/t$) which is a relation used in a series of papers describing the RG evolution of the Einstein equation, and the physics of the FLRW cosmology and Quantum Einstein Gravity [127].

Here the proposed scenario inspired by the RG method assumes that the inflaton has a false vacuum in the pre-inflationary period in which the vacuum expectation value (VeV) of the field is trapped. Then the effective potential has an RG evolution over time due to quantum fluctuations and tends to a convex shape releasing the

trapped field leading to its slow-roll to the true vacuum initiating inflation. This RG induced inflation welcomes fluctuations even below the scale of inflation where the slow-roll is commonly considered as a classical process, however these have less relevance as the false vacuum vanishes.

The cornerstone concept of this inflationary scenario relies on the fact that any potential tends to a convex one during its RG running. It starts with a concave shape at high energies (around the Planck scale), since it has a false vacuum where the VeV is trapped, then it becomes less and less concave at lower energies (around the scale of the Grand Unified Theory (GUT)) releasing the field to induce inflation. The RG evolution between the two scales should be sufficient to provide the necessary change in the potential. The validity of this general picture is shown using explicit RG calculations in the framework of the MSG model in flat Euclidean space. An argument can be made that one should also include the effects of curved spacetime to have a reliable RG study. This has been investigated for functional RG in an FLRW metric for example in Refs. [128–130]. The results show (see Fig. 9 of Ref. [130]) that in the FLRW metric the RG flow leads to even more enhanced convexification effects compared to the flat-space approximation used here in Eq. (10.4), which only strengthens the proposed idea.

It is important to stress that the presented RG induced inflation scenario is independent of the choice of the inflationary potential. However the potential must have a concave region and at least one false vacuum. If these conditions are met, then the method can be implemented in the following three steps:

- The first step is to perform the slow-roll analysis of the chosen model constraining the parameters and the shape of its potential. This produces a potential ideal for slow-roll which means that the concave region of the false vacuum must be almost flat, therefore it can release the VeV to induce inflation.

- The second step is to determine the RG flow of the couplings, i.e., the RG evolution of the inflaton potential. For example when it does not break any symmetry of the model, the potential can be expanded into a Taylor series as

$$V = V_0 + g_1\phi + \frac{1}{2!}g_2\phi^2 + \frac{1}{3!}g_3\phi^3 + \dots, \tag{10.1}$$

  and then the specific RG flow equations for the generated couplings $g_1, g_2, g_3, ...$ can be determined. This approximation is expected to give an accurate RG running if an appropriate number of couplings are taken into account.

- In the final step the initial state of the model is determined at the Planck scale. Using the obtained RG equations one has to determine the initial potential so that after its RG evolution in the pre-inflationary period it takes the form of the slow-roll potential at the scale of inflation ($k \sim 10^{16}$ GeV).

Suitability of the ϕ^6 and MSG Models

One of the simplest models which has a Z_2 symmetry and satisfies the mentioned conditions is the ϕ^6 model with a potential

$$V_{\phi^6} = \frac{1}{2}g_2\phi^2 + \frac{1}{4!}g_4\phi^4 + \frac{1}{6!}g_6\phi^6\,, \tag{10.2}$$

with the signature $g_2 > 0$, $g_4 < 0$, $g_6 > 0$, thus it has two false vacua. According to the proposed scenario, at very high energies in the pre-inflationary period the VeV is trapped in one of these false vacua which flattens out and vanishes in the low-energy limit allowing the VeV to slowly roll down to the true minimum. The couplings of the model over inflation can be obtained by the slow-roll analysis using the PLANCK data [104–106]. However the ϕ^6 scalar model is nonrenormalizable, therefore it cannot be considered as a possible UV completion of an inflationary potential. This problem is solved by the MSG model which represents the simplest (non-perturbatively) renormalizable UV completion of the ϕ^6 model.

Another reason to consider the MSG model is based on the PLANCK results. Although the periodic natural inflation potential [93–95] has certain disagreement with the PLANCK measurements it still provides a better fit than the simple quadratic mass term called large field inflation (LFI). Combining the two into the MSG model might give an even better agreement, like in the case of the combination of a linear and a periodic function [131], which is however not bounded from below.

The MSG model also has the advantage of being bounded from below, it is Z_2 symmetric, serves as a non-perturbatively renormalizable UV extension and most importantly it has many non-degenerate minima separated by an adjustable energy difference ideal for the RG induced inflation from a false vacuum. The MSG potential has the form

$$V_{\rm MSG}(\phi) = \frac{1}{2}m^2\phi^2 + u\left[1 - \cos(\beta\phi)\right]. \tag{10.3}$$

with the Euclidean action considered in flat space

$$S = \int d^4x \left[\frac{1}{2}(\partial_\mu\phi)^2 + V_{\rm MSG}(\phi)\right]. \tag{10.4}$$

It is important to clarify that a flat action can be identified with the full FLRW action given by Eq. (6.16) by ignoring the curvature term. Substituting the FLRW metric into Eq. (6.16) yields the kinetic term

$$g^{\mu\nu}\partial_\mu\phi\partial_\nu\phi = -\left(\frac{\partial\phi}{\partial t}\right)^2 + \frac{1}{a(t)^2}\left(\frac{\partial\phi}{\partial\vec{r}}\right)^2. \tag{10.5}$$

After stretching the spatial coordinates by the scale factor

$$\vec{r}' = a(t)\vec{r}, \qquad \phi(t,\vec{r}) = \phi'(t,\vec{r}') \tag{10.6}$$

the primed variables can be re-identified with the unprimed ones. The factor $\sqrt{-\det g} = a^3$ cancels with the Jacobian of this transformation leading to the Euclidean action defined in Eq. (10.4) after a Wick rotation. This Wick rotation can be problematic, however in the present work the FRG method is applied only for a single scalar field where the usage of an Euclidean action is a standard approach. It is important to note that, in the calculations reported below, this rescaling (10.6) does not affect the connection between the running momentum k of the RG method and some parameter related to the inverse of the cosmological time.

In the following sections the main attention is given to the MSG model in the form of Eq. (10.3), however it is important to emphasize here that the reported conclusions are more general and should hold for any field that fulfills the mentioned criteria. For example other MSG variants with different constant terms can be considered as in Eqs. (9.2) and (9.3) without changing the results significantly.

10.2 Pre-inflationary period and RG running

In this section the goal is to show how the RG induced inflation works in the specific case of the MSG model. One of the best frameworks to achieve this goal is the functional RG method, since it is based on a non-perturbative, exact equation (4.32). To apply the functional RG technique to cosmology, it is necessary to identify the running momentum scale of the method (k) with a running quantity in cosmology as it has been done in a series of papers [126] where the RG scale is identified with the inverse of the cosmological time ($k \sim 1/t$). Including time-dependence in a quantum field theory is a complicated task which can be done by introducing a closed-time-path (or Schwinger–Keldysh) formalism [132,133] leading to an open system that generally requires an external heat bath. In cosmology a time-dependent background can be considered with an external bath of particles which also gives a solution to the so-called overshoot problem [134]. However this approach and the assumption that time-dependence necessarily follows from the RG scaling is not used here which does not exclude the possibility to connect the RG momentum scale with the inverse of the cosmological time.

The functional RG study of the MSG model in $d = 4$ has already been discussed in the previous chapter, see Sect. 9.4. Before summarizing the results and applying for the pre-inflationary period, it is important to note that while the functional RG equation for the field-dependent terms do not require a modification, additional subtraction terms are might needed to obtain the correct evolution of the field-independent constant term $V_k(0)$. The reason emerges from the fact that the functional RG equation is constructed in such a way that imposes certain conditions to the regulator (4.9) making the determination of field-independent constant term ambiguous which can result in an unphysical divergence. A carefully chosen subtraction scheme may solve this problem like in the case of the one-dimensional anharmonic oscillator [135]. However none of the presented conclusions depend on the evolution of this constant term.

The functional RG analysis in the local potential approximation showed that

the dimensionful parameters of the MSG model, the explicit mass m and the frequency β remain unchanged during the RG running (9.24). Thus only the Fourier amplitude u changes during the RG evolution of the potential while the running momentum scale k is decreasing from a high-energy value Λ around the Planck scale to a low-energy one around the scale of inflation k_i.

To see how, it is helpful to rewrite the obtained flow equation (9.26) for the Fourier amplitude in a dimensionful form that writes as

$$k\partial_k u_k = -\frac{4\alpha_d}{d}\frac{k^{d+2}}{\beta^2 u_k}\left(1-\sqrt{\frac{\left(k^2+m^2\right)^2}{\left(k^2+m^2\right)^2-\beta^4 u_k^2}}\right). \tag{10.7}$$

Assuming that $\beta^2 u_k/(k^2+m^2) \ll 1$ and linearizing around the Gaussian fixed point yields

$$\begin{aligned} k\partial_k u_k &= -\frac{4\alpha_d}{d}\frac{k^{d+2}}{\beta^2 u_k}\left(1-\sqrt{\frac{1}{1-\beta^4 u_k^2/(k^2+m^2)^2}}\right) \\ &\approx \frac{2\alpha_d}{d}\frac{k^{d+2}}{\beta^2 u_k}\,\frac{\beta^4 u_k^2}{(k^2+m^2)^2}\,. \end{aligned} \tag{10.8}$$

If the mass can be neglected compared to the momentum scale $m^2 \ll k^2$, then the above equation can be can be further simplified and written as

$$k\partial_k u_k \approx \frac{2\alpha_d}{d}k^{d-2}\beta^2 u_k\,, \tag{10.9}$$

which is identical to the linearized RG equation obtained for the *massless* sine-Gordon model. This is an UV approximated flow equation for the MSG model, however it is not a trivial scaling, since the couplings on the right-hand side depend on the scale k, in contrast to the independent mode approximation in perturbation theory where they do not. Recalling that β does not run in this approximation, the above equation has the following solution in $d=4$ dimensions ($\alpha_{d=4}=1/16\pi^2$)

$$u_k = u_\Lambda \exp\left[\frac{\beta^2}{64\pi^2}(k^2-\Lambda^2)\right], \tag{10.10}$$

where u_Λ is the high-energy initial value of u_k at the UV scale Λ. In the pre-inflationary framework the natural choice is the Planck scale $\Lambda = \Lambda_p = 2.4\times 10^{18}$ GeV. It should be noted that in this context the applied procedure is different than the usual RG analysis, since here the astronomical measurements provide values at lower energies at the scale of inflation k_i, and not at the UV, i.e., at the Planck scale. Thus the parameters of the MSG model, namely the constant dimensionful mass m, the frequency β, and the running Fourier amplitude u_k are also fixed at the the scale of inflation k_i, around the GUT scale, $k_i \sim k_{\rm GUT} = 2\times 10^{16}$ GeV. This is performed by matching the parameters at the scale of inflation k_i with the initial conditions of the slow-roll analysis, which will be denoted here as

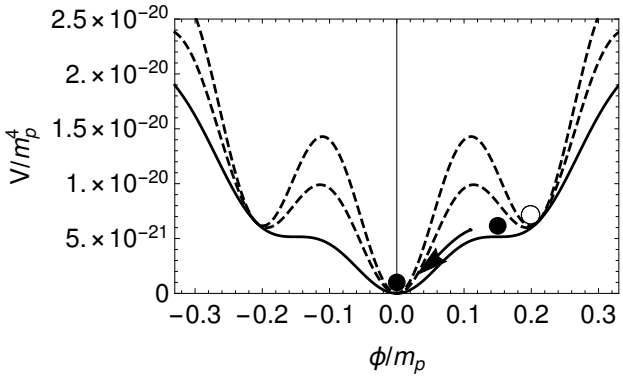

Figure 10.2: RG scaling of the MSG potential (10.3) in the pre-inflationary period. The solid line corresponds to the potential obtained from the slow-roll analysis at the scale of inflation ($k_i = 2.0 \times 10^{13}$ GeV) where $\hat{\beta} = 30$ is chosen from the acceptance region shown in Fig. 10.4 resulting the normalized parameters $\hat{m} = 5.4\times10^{-10}$, $\hat{u} = 1.5\times10^{-21}$, $\hat{\beta} = 30$. The dashed lines stand for the pre-inflationary UV values obtained from the RG analysis using Eq. (10.10). The black disk shows the VeV rolling down to induce inflation.

$$u_{k_i} = u_0, \quad \beta = \beta_0, \quad m = m_0. \tag{10.11}$$

After these parameters are determined, the UV value u_Λ can be calculated using Eq. (9.24) or if the mass is much smaller than the running momentum scale then using the approximate solution given by Eq. (10.10). This also determines the RG scaling of the potential. One can immediately observe that u_k is decreasing during the RG running in agreement with the general statement that the potential must tend to a convex shape in the low energy limit, see Eq. (3.15).

In comparsion the quadratic LFI model is a free theory and therefore it does not have an RG evolution, its single parameter the dimensionful mass stays constant. This is also true for the explicit mass of the MSG potential, however the periodic self-interaction term has a non-trivial RG running resulting in the RG evolution of the potential. Therefore in the case of the MSG model the RG-induced inflationary mechanism can be described as follows. In the pre-inflationary period at very high energies the vacuum expectation value (VeV) of the field is trapped in one of the second minima of the MSG potential, see Fig. 10.2. Then the RG running makes the potential flatter and more convex and eventually the local minima disappear at the scale of inflation releasing the VeV. At this point the parameters of the potential can be matched with the results of slow-roll analysis. As the VeV is released it starts to roll down to the global minimum inducing the desired inflation.

10.3 Inflationary period and slow-roll

The inflationary period begins after the RG scaling forces the false vacua to vanish and the VeV starts to slowly roll down the remaining energy hill at the scale of inflation. Over this period the potential is assumed to remain unchanged, since the slow-roll process is considered to be classical. To discuss this period it is convenient to use the reduced Planck units and set $c \equiv \hbar \equiv 1$, and $m_p^2 = 1/(8\pi G)$. Therefore in this context the dimensionless couplings of the MSG model are

$$\hat{u} = \frac{u_0}{m_p^4}, \qquad \hat{\beta} = \beta_0\, m_p, \qquad \hat{m} = \frac{m_0}{m_p}\,, \tag{10.12}$$

where the dimensionful parameters denoted as u_0, β_0 and m_0 are defined at the scale of inflation k_i similar or below the GUT scale $k_{\rm GUT} = 2 \times 10^{16}$GeV and not around the Planck scale $m_p = 2.4 \times 10^{18}$ GeV. Thus, the ratio between these energy scales are at least

$$\frac{k_{\rm GUT}}{m_p} \approx \frac{1}{120}\,. \tag{10.13}$$

Here, the slow-roll analysis (described in Sect. 9.2) is performed only for one variant of the MSG model (10.3), but similar results are found for different variants.

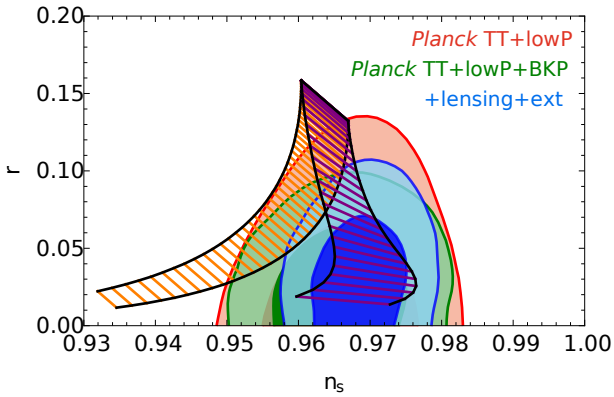

Figure 10.3: Theoretical predictions of the natural inflation (orange line segments on the left) and the MSG model (purple line segments in the middle) for the scalar tilt n_s and tensor-to-scalar ratio r using various frequencies $\hat{\beta}$ and a fixed ratio $\hat{u}/\hat{m}^2 = 1/(0.22)^2$ for the MSG model. For each $\hat{\beta}$ parameter there is a corresponding line segment where the e-fold number varies in the range $50 < N < 60$. The two model has the same prediction for $\hat{\beta} = 0$, which line segment is also equivalent to the prediction of the simple quadratic ϕ^2 inflationary potential. The results are compared to the measurements made by the PLANCK mission [104–106], where the combined data from BICEP2/Keck Array and Planck Collaborations are indicated by the colored areas. The darker regions correspond to 95% CL while the lighter regions to 68% CL adopting the notation from Refs. [104–106].

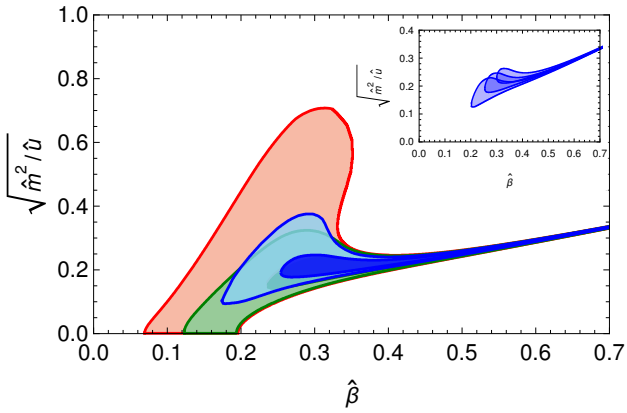

Figure 10.4: Acceptance levels of the parameter space of the MSG model (10.3) indicated by colored regions using the conventions of Fig. 10.3 for the e-fold number $N = 55$. The dark blue regions correspond to the best agreement with the Planck data which is shown in the inset for the e-fold numbers $N = 50, 55, 60$.

A comparison can be made between the results obtained for the MSG and the sine-Gordon, i.e., the natural inflation model as shown in Fig. 10.3 which clearly indicates that the MSG model has a better agreement with the measured scalar tilt n_s and tensor-to-scalar ratio r. Predictions with different parameter values fall into regions with different levels of acceptance corresponding to different colors. This is plotted in Fig. 10.4 for the parameter space of the MSG model where the regions are colored according to their level of acceptance.

As Fig. 10.4 shows, the slow-roll analysis only fixes the ratio $\hat{u}/\hat{m}^2$ and the frequency $\hat{\beta}$ leaving out a free overall factor. However the normalization of the potential can be fixed too at the starting point of the slow-roll ϕ_i, which originates from the disappearing false vacuum. The MSG potential (10.3) can be written as

$$V_{\mathrm{MSG}}(\phi) \quad = u \left(\frac{1}{2} \frac{m^2}{u} \phi^2 + [1 - \cos(\beta\phi)] \right) , \tag{10.14}$$

making it evident that after the slow-roll study one has to also fix the value of $u = u_{k_i}$ at the scale of inflation substituting $\phi = \phi_i$. This can be done by using the condition for the absolute value of the potential [50] given by

$$V(\phi_i) \equiv \frac{r}{0.01} (10^{16}\,\mathrm{GeV})^4 , \tag{10.15}$$

where the tensor-to-scalar ratio r depends on the parameters determined by the slow-roll. If the obtained value is in the range of $r \approx 0.1$, then the energy scale of the potential is around the GUT scale $k_{\mathrm{GUT}} = 2 \times 10^{16}$GeV. From the above

formula the scale of inflation can be determined as

$$V(\phi_i) \equiv k_i^4\,, \qquad k_i = \left(\frac{r}{0.01}\right)^{\frac{1}{4}} 10^{16}\ \text{GeV}, \tag{10.16}$$

which also depends on the tensor-to-scalar ratio. For example, as it can be seen in Fig. 10.4, the parameters $\hat{u}/\hat{m}^2 = 1/(0.22)^2$ and $\hat{\beta} \approx 0.3$ provide one of the best levels of acceptance, yielding $r \approx 0.05$ and consequently putting the scale of inflation around $k_i = 1.5 \times 10^{16}\,\text{GeV}$ close to the GUT scale.

Thus, the parameters of the MSG model can be chosen to give an excellent agreement with the astrophysical observations which fixes these parameters at the scale of inflation using the slow-roll analysis. It is useful to discuss the obtained results by separating the parameter space of the MSG model into two regions.

Fit to experimental data for small β

Taking a closer look at the acceptance regions of the MSG model plotted in Fig. 10.4 reveals an interesting feature. For frequencies smaller than $\hat{\beta} < 1.5$ these regions are relatively large areas, but for larger frequencies the acceptance region becomes nearly a straight line along which the parameters satisfy the relation

$$\frac{\hat{u}\hat{\beta}^2}{\hat{m}^2} = \frac{u_0\beta_0^2}{m_0^2} \approx \frac{0.3^2}{0.22^2} > 1\,. \tag{10.17}$$

For small $\hat{\beta}$ values the parameters that provide the best fit are situated in the dark blue "blob" at the starting point of the line. Reading off the parameter values of this location leads to the values around $\hat{\beta} \approx 0.3$ and $\hat{u}/\hat{m}^2 = 1/(0.22)^2$, thus the relation (10.17) also holds for the best fits in the small $\hat{\beta}$ region. Using the normalization given by Eq. (10.15) with the results of the slow-roll analysis fixes all three parameters of the MSG model yielding the numerical values

$$\hat{m}^{\text{small}} \approx 5.92 \times 10^{-6} \Rightarrow m_0^{\text{small}} \approx 1.42 \times 10^{13}\,\text{GeV}\,, \tag{10.18a}$$

$$\hat{u}^{\text{small}} \approx 7.24 \times 10^{-10} \Rightarrow u_0^{\text{small}} \approx 2.4 \times 10^{64}\,\text{GeV}^4\,, \tag{10.18b}$$

$$\hat{\beta}^{\text{small}} \approx 0.3 \quad \Rightarrow \quad \beta_0^{\text{small}} \approx 1.25 \times 10^{-19}\,\text{GeV}^{-1}\,. \tag{10.18c}$$

These are also the parameters chosen in Fig. 10.3, for which the scale of inflation is obtained to be around the same order-of-magnitude as the GUT scale, namely $k_i = 1.5 \times 10^{16}$ GeV, as mentioned above.

It must be pointed out that the dimensionful explicit mass calculated by the slow-roll (10.18a) is small compared to the obtained scale of inflation, therefore the approximate RG equation (10.10) can be used to determine the RG flow of the potential and to scale it up to higher energies. Over the RG evolution from the Planck (m_p) to the GUT scale (k_{GUT}) the dimensionful β remain unchanged, thus the quantity $\beta\, k = \beta_0\, k$ takes values between

$$\hat{\beta}\,\frac{k_{\text{GUT}}}{m_p} < (\beta_0\, k) < \hat{\beta}\,. \tag{10.19}$$

In the proposed RG-induced inflationary scenario the false vacuum must disappear during the RG flow of the potential between the Planck and GUT scale, therefore it must undergo a significant change. To measure this change one can substitute the ratio of the scales (10.13) into Eq. (10.10) obtaining

$$\chi = \frac{u_{m_p}}{u_{k_{\mathrm{GUT}}}} = \exp\left[\frac{1}{64\pi^2}\left(\hat{\beta}^2 - \frac{\hat{\beta}^2}{120^2}\right)\right] . \tag{10.20}$$

In the acceptance region where

$$\hat{\beta} \gtrsim 30\,, \qquad \chi \gtrsim 4.2\,, \tag{10.21}$$

the change in the coupling u is more than four-fold, as indicated by the ratio χ. For smaller $\hat{\beta}$ values this ratio is too small. In this case an option is to consider an RG flow from super-Planckian scales, which would be problematic. This makes the large $\hat{\beta}$ region more favorable which is discussed in the following subsection.

Fit to experimental data for large β

For large $\hat{\beta}$ values the accepted region is found to be a straight line for all the considered MSG variants (10.3), (9.2), (9.3) as indicated by Fig. 10.4 and Fig. 9.1. Furthermore, the choice of the constant term does not affect the results in this region, since the obtained lines coincides for variants where the periodic term has the same sign.

The tensor-to-scalar ratio and consequently the scale of inflation depends on the chosen parameter values. If one chooses a small $\hat{\beta}$ from the best acceptance region then the inflation takes place at the GUT scale, however for large $\hat{\beta}$ values along the acceptance line, it occurs at smaller scales. For example, the scale of inflation is found to be $k_i \approx 2 \times 10^{13}\,\mathrm{GeV}$ for $\hat{\beta} = 30$. In this case the obtained normalized parameters are

$$\hat{m}^{\mathrm{large}} \approx 5.4 \times 10^{-10} \Rightarrow m_0^{\mathrm{large}} \approx 1.3 \times 10^{9}\,\mathrm{GeV}\,, \tag{10.22a}$$

$$\hat{u}^{\mathrm{large}} \approx 1.5 \times 10^{-21} \Rightarrow u_0^{\mathrm{large}} \approx 5.0 \times 10^{52}\,\mathrm{GeV}^4\,, \tag{10.22b}$$

$$\hat{\beta}^{\mathrm{large}} \approx 30 \Rightarrow \beta_0^{\mathrm{large}} \approx 1.25 \times 10^{-17}\,\mathrm{GeV}^{-1}\,. \tag{10.22c}$$

for which the RG evolution produces a sufficient change in the only running coupling $u(k = m_p)/u(k_i) \approx 4.2$. Fig. 10.5 shows the RG scaling of the MSG potential where at the scale of inflation the above parameters are reproduced similarly to Fig. 10.2.

An important observation to make is related to how large $\hat{\beta}$ values can be choosen. For the VeV to be "securely" trapped in the false vacuum so that the initial quantum fluctuations cannot push it over the energy barrier, the barrier must be high enough and consequently the RG running must produce a significant change in the potential. As mentioned, this means that the large frequencies $\hat{\beta} \gtrsim 30$ are favored from the acceptance region, because then the ratio of the Fourier amplitude at the Planck scale and at the scale of inflation is sufficiently large $\chi \gtrsim 4.2$. However

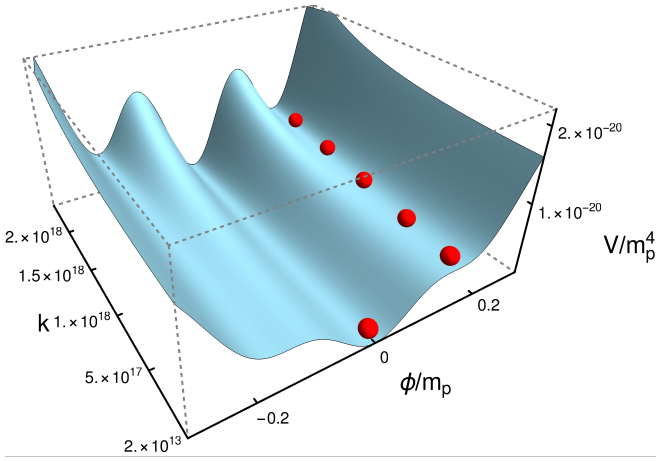

Figure 10.5: RG running of the MSG potential in the pre-inflationary period from the Planck scale to the scale of inflation $k_i = 2 \times 10^{13}$ GeV, where the parameters of the potential are fixed by the slow-roll analysis with the choice $\hat{\beta} = 30$. The VeV is indicated by the red ball which is initially trapped in a false vacuum at large scales, however after the RG evolution the false vacuum vanishes releasing the VeV to slowly roll down to the true vacuum at the scale of inflation.

the scale of inflation decreases towards larger frequencies, and around $\hat{\beta} \sim 300$ it is below the GUT scale by more than four orders of magnitude, which can be problematic. This is an important point, since for large $\hat{\beta}$ parameters the acceptance region is a single line, therefore after choosing a $\hat{\beta}$ value, the slow-roll analysis together with the normalization condition (10.15) fixes all the parameters of the MSG model.

10.4 Conclusion

I have proposed a new inflationary scenario based on the RG evolution and convexification of the inflaton potential due to the quantum fluctuations in the pre-inflationary period [6]. According to the proposed mechanism the vacuum-expectation value (VeV) of the inflaton field is initially trapped in a false vacuum at very high energies around the Planck scale, then as a consequence of the RG scaling towards the scale of inflation the potential tends to a more convex shape. The false vacuum disappears as the potential flattens out releasing the VeV to slowly roll down to the ground state inducing inflation. This scenario can be viable for a large number of inflationary models which have concave regions and at least one false vacuum.

The MSG model is a good candidate for the described mechanism, since it has many non-degenerate minima separated by a tunable amount of energy interpo-

lating between a model with infinite degenerate minima (sine-Gordon model) and one with a single minimum. I have demonstrated by the slow-roll analysis that the model also shows an excellent agreement with cosmological observations on the scalar tilt and tensor-to-scalar ratio made by the Planck mission. I have explicitly showed the flattening of the MSG potential due to its RG evolution using the functional RG method in local potential approximation. This produces a sufficient change in the potential over the pre-inflationary period to make the local minima disappear releasing the VeV of the field to initiate the inflation. Although a complete demonstration would involve all the fields from the Standard Model of particle physics considering a particular unified theory, however the inclusion of other fields do not change the general statement that the effective potential must be convex in the low-energy (IR) limit.

There are many inflationary models in the literature. One type of them are the hybrid inflationary models which are almost excluded by the Planck measurements because contrary to the data they predict $n_s > 1$ [136, 137]. Chaotic, large-field inflationary scenarios are better candidates, but they need large quantum fluctuations to excite the inflaton field to the required values, thus the initial position of the VeV rely on random fluctuations leading to the so-called initial condition problem. This is even more problematic for small-field inflationary models. However the presented mechanism has, in this sense, a unique value for the initial VeV determined by the position of the false vacuum which explains why the slow-roll starts from a particular value and solves the initial condition problem. It also supports a particle physics origin, since the problematic large quantum fluctuations are no longer needed at the scale of inflation.

Therefore I have proposed a valid inflationary scenario which suggests that the inflation was induced by the RG running of the potential in the pre-inflationary period which also solves the initial condition problem. It is based on the convexification of the effective potential in the low-energy (IR) limit. The vacuum expectation value of the inflaton field is assumed to be trapped in a false vacuum at high energies around the Planck scale then it is released as the potential flattens out inducing inflation. I have showed the validity of the mechanism for the massive sine-Gordon model, which has an excellent agreement with cosmological measurements fixing its parameters at the scale of inflation. I have calculated the RG evolution of the model using the functional RG method demonstrating the disappearance of its second minima due to the RG running from the Planck scale towards the scale of inflation.

Summary

In my thesis I have worked within the framework of the functional renormalization group (FRG). It is an exact method to obtain the phase diagram of various models and to describe their phase transitions and critical behavior by integrating out the modes of fluctuations successively.

The FRG equation is an integro-differential equation that constitutes functionals, thus there are only a few special cases when exact solutions can be indicated, which means that approximations are required. When approximations are used the results could depend on the so called regulator function. The question arises, which regulator function gives the most accurate predictions for physical quantities such as critical exponents at a certain level of approximation? To answer this question I have studied the compactly supported smooth (CSS) regulator using the optimization method called the principle of minimal sensitivity. I have applied this principle in the framework of the $O(N)$ and the massive sine-Gordon (MSG) model in local potential approximation (LPA). The parameters of the CSS regulator has been also optimized based on the requirement of the absence of spontaneous symmetry breaking (SSB) in the one-dimensional sine-Gordon model beyond LPA.

T1: The CSS regulator was thoroughly investigated with various optimization methods, in three different dimensions, for three different models, both in LPA and LPA$'$ and with two different normalization all indicating that the Litim limit of the CSS regulator is the optimal choice. [1, 2]

Approximate results may also suggest unphysical properties of a system, like the presence of a fixed point indicating a spurious phase transition. Thus, it is crucial to know what is a sufficient approximation that produces reliable results when different models are investigated. Therefore I examined the reliability of the FRG method on $O(N)$ models paying special attention to its truncated Taylor expanded potential and the local potential approximation discussing what is sufficient to recover the Mermin-Wagner theorem.

T2: SSB always appears in the truncated $O(N)$ models, even when it should not, however the Taylor expanded potential around the minimum and the LPA when treated exactly, without truncations, is sufficient to reproduce the Mermin-Wagner theorem for the $O(N \geq 2)$ models in all dimensions. The only exception when the exactly treated LPA gives an incorrect qualitative picture is for the two-

dimensional Ising model ($N = 1$), where it incorrectly predicts the absence of SSB. [3, 4]

FRG can also find its applications in cosmology if the time evolution of the Universe can be identified with a renormalization group (RG) scaling. A consequence of this connection is the possibility to first, constrain the parameters of a candidate Higgs-inflationary model at the scale of inflation by astrophysical observations, then using the RG method to calculate its RG running down to the electroweak scale, where it should recover the measured parameters of the Standard model Higgs potential. I have investigated this scenario proposing the MSG model as a Higgs-inflationary scalar field.

T3: The proposed MSG model proved to be an excellent candidate for a Higgs-inflationary theory, since it provides a remarkable agreement with cosmological observations. By performing its RG analysis I have found that it can simultaneously describe the physics both at cosmological and electroweak scales and it recovers the Higgs mass by the correct order of magnitude at the electroweak scale in the post-inflation period independently of the high-energy (UV) initial conditions. [5]

Furthermore, the RG approach could be applied not only in the post-inflationary, but also in the pre-inflationary period up to very high energies around the Planck scale.

T4: I have proposed a new inflationary scenario which suggests that the inflation was induced by the RG running of the potential in the pre-inflationary period which could also solve the initial condition problem. It is based on the convexification of the effective potential in the low-energy (IR) limit. The vacuum expectation value of the inflaton field is assumed to be trapped in a false vacuum at high energies around the Planck scale then it is released as the potential flattens out inducing inflation. I have showed the validity of the mechanism for the MSG model, which has an excellent agreement with cosmological measurements fixing its parameters at the scale of inflation. I have calculated the RG evolution of the model using the functional RG method demonstrating the disappearance of its second minima due to the RG running from the Planck scale towards the scale of inflation. [6]

Összegzés

Tézisemben a funkcionális renormálási csoport (FRG) módszer keretében végeztem kutatást. Ez egy egzakt metódus, amely lehetővé teszi különböző modellek fázisdiagramjának meghatározását, fázisátalakulásuk és kritikus viselkedésük leírását a rendszer különböző módusú fluktuációinak eliminálásával.

Az FRG egyenlet egy funkcionálokra vonatkozó integrált tartalmazó differenciálegyenlet, így csak néhány speciális esetben lehetséges egzaktul megoldani, ami azt jelenti, hogy közelítések szükségesek. Közelítések használatakor azonban az eredmények függést mutathatnak az úgynevezett regulátor függvénytől. Így felmerül a kérdés, melyik regulátor függvény biztosítja a fizikai mennyiségek, mint például a kritikus exponensek legpontosabb jóslatait. A kérdés megválaszolásához a minimális érzékenység elvét alkalmaztam a kompakt tartójú, sima (CSS) regulátor optimalizáláshoz az $O(N)$ és a tömeges sine-Gordon modell (MSG) keretében lokális potenciál közelítésben (LPA). A CSS regulátor paramétereit optimalizáltam egy másik módszerrel is, kihasználva a spontán szimmetriasértés (SSB) hiányának megkövetelését az egy-dimenziós sine-Gordon modellben.

T1: Alapos vizsgálatnak vetettem alá a CSS regulátort különböző optimalizálási módszerekkel, három különböző dimenzióban, három modellre, LPA-ban és LPA$'$-ban, két különböző normálással, amely azt mutatta, hogy a CSS regulátor Litim limesze az optimális választás. [1, 2]

A közelítő eredmények hamis jóslatokat is adhatnak, például egy nem-fizikai fixpontot jelezve, ami egy nem létező fázisátmenet jelenlétére utal. Emiatt elengedhetetlenül fontos tudni, hogy melyek azok a közelítések, amik elegendően pontosak ahhoz, hogy megbízható eredményeket szolgáltassanak különböző modellek vizsgálatakor. Ezen célból tanulmányoztam az FRG módszer megbízhatóságát az $O(N)$ modellek esetében különös figyelmet szentelve a csonkolt Taylor sorfejtett potenciál és a lokális pontenciál közelítésre, megvizsgálva, hogy ezek elengedőek-e, hogy a Mermin-Wagner tételt helyesen visszaadják.

T2: SSB mindig megjelenik a csonkolt $O(N)$ modellben, olyan esetben is, amikor ez nem megengedett. Azonban a minimum körül Taylor sorfejtett potenciált és az egzakt (nem csonkolt) LPA-t használva, az eredmények helyesen visszaadják a Mermin-Wagner tételt az $O(N \geq 2)$ modellekre, minden dimenzióban. A kétdimenziós Ising modell ($N = 1$) az egyedüli kivétel, amikor az egzaktul kezelt LPA

hibás kvalitatív képet ad, tévesen az SSB hiányát jelezve. [3, 4]

Az FRG módszer a kozmológiában is alkalmazható, ha az Univerzum időbeli fejlődését azonosítani lehet egy renormálási csoport (RG) skálázással. Ez a kapcsolat azt eredményezheti, hogy miután egy lehetséges Higgs-inflációs modell paraméterei rögzítésre kerülnek az infláció energiaskáláján, figyelembe véve asztrofizikai megfigyeléseket, azután az RG módszer használatával kiszámolható az RG futása az elektrogyenge skáláig, ahol a Standard modell Higgs potenciál paramétereit kell visszaadnia. Az MSG modellt, mint Higgs inflációs skalármezőt javasolva tanulmányoztam ezt a forgatókönyvet.

T3: A javasolt MSG modell egy kitűnő Higgs-inflációs elméletnek bizonyult, hiszen figyelemreméltó egyezést mutat a kozmológiai megfigyelésekkel. Az RG analízisét végrehatjva azt találtam, hogy a modell képes egyszerre leírni a kozmológiai és elektrogyenge skálán történő méréseket, valamint nagyságrendileg visszaadja a Higgs részecske tömegét az infláció utáni elektrogyenge skálán, a nagyenergiás (UV) kezdőértékektől függetlenül. [5]

Mindez azt sugallja, hogy az RG megközelítés nem csak az infláció utáni szakaszra, hanem az infláció előtti időszakra is alkalmazható lehet a nagyobb energiák felé, egészen akár a Planck skáláig.

T4: Egy új inflációs mechanizmust javasoltam, amely szerint az inflációt a potenciál RG futása indukálja az Univerzum korai szakaszában, ami megoldhatja a kezdeti feltétel problémáját. A mechanizmus az effektív potenciál konvexifikációjára alapszik az alacsony energiás (IR) határesetben. A kezdeti feltételezés, hogy a Planck skála körüli nagy energiákon az inflaton vákuum várható értéke beragadt egy hamis vákuumba, majd ahogyan a potenciál ellaposodik elegendi a várható értéket, elindítva az inflációt. Megmutattam ezen forgatókönyv alkalmazhatóságát az MSG modellre, amely kiváló egyezést mutat a kozmológiai mérésekkel, rögzítve a modell paramétereit az infláció skáláján. Meghatároztam az MSG potenciál RG evolúcióját a funkcionális RG módszer használatával, megmutatva a lokális minimumok eltűnését a Planck skálától az inflációs skáláig történő RG futás következtében. [6]

Acknowledgments

First of all I would like to thank my supervisor Dr. István Nándori, who helped my research since the first year of my bachelor studies. I am glad that I could always count on his advice while he has became one of my best friends over the years. Without him this thesis would not have been possible.
I would like to thank to the members of the very welcoming MTA-DE Particle Physics Research Group that provided an excellent community to discuss new ideas in physics creating a wonderful atmosphere.
I acknowledge the fruitful collaboration with my co-authors, spending time with them is always a pleasure especially in Trieste discussing over a great meal.
I am very glad to my family who have constantly supported and encouraged me to achieve my goals.
I am grateful to my friends who always made my days happier and gave me inspiration.
I greatly appreciate the excellent insights of my referees.
Finally I would like to thank all the administrative staff of the University of Debrecen.

Bibliography

[1] I. G. Márián, U. D. Jentschura, I. Nándori, J. Phys. G **41**, 055001 (2014).

[2] I. Nándori, I. G. Márián, V. Bacsó, Phys. Rev. D **89**, 047701 (2014).

[3] N. Defenu, P. Mati, I. G. Márián, I. Nándori, A. Trombettoni, JHEP **05**, 141 (2015).

[4] N. Defenu, V. Bacsó, I. G. Márián, I. Nándori, A. Trombettoni, J. Phys. A, **52**, 345002 (2019).

[5] I. G. Márián, N. Defenu, U. D. Jentschura, A. Trombettoni, I. Nándori, Nucl. Phys. B **945**, 114642 (2019).

[6] I. G. Márián, N. Defenu, U. D. Jentschura, A. Trombettoni, I. Nándori, JCAP **06**, 028 (2020).

[7] Zs. Iszály, K. Lovász, I. Nagy, I. G. Márián, J. Rácz, I. A. Szabó, L. Tóth, N. F. Vas, V. Vékony, I. Nándori, JMMM **466**, 452 (2018).

[8] T. G. Kovács, *Statisztikus fizika*, University Lecture Note (2018).

[9] R. K. Pathria, P.D. Beale, *Statistical Physics*, Academic Press (2011).

[10] G. Mussardo, *Statistical field theory: an introduction to exactly solved models in statistical physics* (Oxford, Oxford University Press, 2010).

[11] J. Cardy, *Scaling and Renormalization in Statistical Physics*, Cambridge Lecture Notes in Physics, pp. I-Vi (1996).

[12] K. G. Wilson, Rev. Mod. Phys. **47**, 773 (1975).

[13] L. P. Kadanoff, *Statistical physics: statics, dynamics and renormalization*, Singapore, World Scientific (2000).

[14] B. Delamotte, *An Introduction to the Nonperturbative Renormalization Group*, Lecture Notes in Physics, **852**, (2012).

[15] J. Zinn-Justin, *Quantum Field Theory and Critical Phenomena*, Oxford, Clarendon (1989).

[16] M. E. Peskin and D. V. Schroeder, *An introduction to quantum field theory* (Reading, Addison-Wesley, 1995).

[17] R. J. Rivers, *Path Integral Methods in Quantum Field Theory*, (Cambridge University Press, 1987).

[18] N. Defenu, A. Trombettoni, I. Nándori, T. Enss, Phys. Rev. B **96**, 174505 (2017).

[19] A. Codello, et al., Eur. Phys. J. C **76**, 226 (2016).

[20] N. Defenu, *Application of functional renormalization group approach to spin systems and long range models* PhD thesis, SISSA (2017).

[21] C. Wetterich, Nucl. Phys. B **352**, 529 (1991); *ibid*, Phys. Lett. B**301**, 90 (1993); J. Berges, N. Tetradis, C. Wetterich, Phys. Rept. **363**, 223 (2002).

[22] T. R. Morris, Int. J. Mod. Phys. A **9**, 2411 (1994).

[23] I. Nandori, *Lecture Note on the Functional Renormalization Group Study of Sine-Gordon Models* (in preparation).

[24] D. F. Litim, Phys. Lett. B **486**, 92 (2000); Phys. Rev. D **64**, 105007 (2001); JHEP **0111**, 059 (2001).

[25] J. M. Pawlowski, Ann. Phys. **322**, 2831 (2007).

[26] D. F. Litim, Nucl.Phys. B **631**, 128 (2002).

[27] T. R. Morris, JHEP **0507**, 027 (2005).

[28] O. J. Rosten, Phys. Rept. **511**, 177 (2012).

[29] L. Canet, B. Delamotte, D. Mouhanna and J. Vidal, Phys. Rev. D **67**, 065004 (2003); *ibid*, Phys.Rev. B **68** 064421 (2003); L. Canet, Phys.Rev. B **71** 012418 (2005).

[30] A. Jakovác, A. Patkós, Lect. Notes Phys. **912** (2016).

[31] I. Nándori, JHEP **1304**, 150 (2013).

[32] F. J. Wegner, A. Houghton, Phys. Rev. A. **8**, 401 (1973).

[33] J. Polchinski, Nucl. Phys B **231**, 269 (1984).

[34] S. Nagy, B. Fazekas, L. Juhász, and K. Sailer Phys. Rev. D **88**, 116010 (2013).

[35] G. Parisi and J. J. Ruiz-Lorenzo, Phys. Rev. B **55**, 6082 (1997).

[36] N. D. Mermin and H. Wagner . Phys. Rev. Lett. **17**, 1133 (1966).

[37] P. C. Hohenberg, Phys. Rev. **158**, 383 (1967).

[38] S. Coleman, Comm. Math. Phys. **264**, 259 (1973).

[39] P. Mati, Phys. Rev. D **94**, 065025 (2016).

[40] S. Nagy, K. Sailer, Annals Phys. **326**, 1839 (2011).

[41] S. R. Coleman Phys. Rev. D **11**, 2088 (1975). I. Nándori, J. Polonyi, K. Sailer, Phys. Rev. D **63**, 045022 (2001); S. Nagy, K. Sailer, J. Polonyi, J. Phys. A **39**, 8105 (2006); S. Nagy, I. Nándori, J. Polonyi, K. Sailer, Phys. Lett. B **647**, 152 (2007); V. Pangon, S. Nagy, J. Polonyi, K. Sailer, Phys. Lett. B **694**, 89 (2010); I. Nándori, U. D. Jentschura, K. Sailer, G. Soff, Phys. Rev. D **69**, 025004 (2004); S. Nagy, I. Nándori, J. Polonyi, K. Sailer, Phys. Rev. Lett. **102** 241603 (2009). J. Alexandre, D. Tanner, Phys. Rev. D **82**, 125035 (2010); V. Pangon, Int. J. Mod. Phys. A **227**, 1250014 (2012).

[42] I. Nándori, arXiv:1108.4643 [hep-th].

[43] I. Nándori, S. Nagy, K. Sailer, A. Trombettoni, Phys. Rev. D **80**, 025008 (2009); *ibid*, JHEP **1009**, 069 (2010).

[44] Nándori, Phys. Rev. D **84**, 065024 (2011).

[45] S. Nagy, I. Nandori, J. Polonyi, and K. Sailer, Phys. Rev. D **77**, 025026 (2008).

[46] S. Nagy, J. Polonyi, K. Sailer, Phys. Rev. D **70**, 105023 (2004); I. Nándori, J. Phys. A: Math. Gen. **39**, 8119 (2006); I. Nándori, Phys. Lett. B **662**, 302 (2008); S. Nagy, Phys. Rev. D **79**, 045004 (2009); J. Kovács, S. Nagy, I. Nándori, K. Sailer, JHEP **1101**, 126 (2011).

[47] T. M. Byrnes, P. Sriganesh, R. J. Bursill and C. J. Hamer, Phys. Rev. D **66**, 013002 (2002).

[48] S. Nagy, K. Sailer, Int. J. Mod. Phys. A **28**, 1350130 (2013);S. Nagy, Nucl. Phys. B **864**, 226 (2012); S. Nagy, Phys. Rev. D **86**, 085020 (2012); V. Pangon, S. Nagy, J. Polonyi, K. Sailer, Int. J. Mod. Phys. **A26**, 1327 (2011).

[49] M. Postma, NIKHEF 53 (2009).

[50] D. Baumann, *TASI Lectures on Inflation*, available as arXiv:0907.5424 [hep-th].

[51] Zs. Frei, A. Patkós, Inflációs kozmológia (2004).

[52] A. H. Guth, Phys. Rev. D **23**, 347 (1981).

[53] R. D. Ball, P. E. Haagensen, J. I. Latorre and E. Moreno, Phys. Lett. B **347**, 80 (1995); D. F. Litim, Phys. Lett. B **393**, 103 (1997); K. Aoki, K. Morikawa, W. Souma, J. Sumi and H. Terao, Prog. Theor. Phys. **99**, 451 (1998); S.B. Liao, J. Polonyi, M. Strickland, Nucl. Phys. B **567**, 493 (2000); J. I. Latorre and T. R. Morris, JHEP **0011**, 004 (2000); F. Freire and D. F. Litim, Phys. Rev.

D **64**, 045014 (2001); C. Bervillier, B. Boisseau, H. Giacomini, Nucl. Phys. B **789**, 525 (2008); C. Bervillier, B. Boisseau, H. Giacomini, Nucl. Phys. B **801**, 296 (2008); C. S. Fischer, A. Maas, J. M. Pawlowski, Ann. Phys. **324**, 2408 (2009).

[54] M. Reuter, Phys. Rev. D **57**, 971 (1998); M. Reuter, F. Saueressig, New J. Phys. **14**. 055022 (2012); D. F. Litim, Phys. Rev. Lett. **92**, 201301 (2004); M. Reuter, F. Saueressig, Phys. Rev D **65**, 065016 (2002); S. Nagy, J. Krizsan, K. sailer, JHEP **1207**, 102 (2012).

[55] V. Bacsó, *Fázisátalakulások vizsgálata Renormálási Csoport módszerrel* PhD thesis (2018).

[56] D. Cassi, Phys. Rev. Lett. **68**, 3631 (1992); *ibid.*, **76**, 2941 (1996).

[57] R. Burioni and D. Cassi, Phys. Rev. Lett. **76**, 1091 (1996).

[58] A. Codello and G. D'Odorico, Phys. Rev. Lett. **110**, 141601 (2013).

[59] H. E. Stanley, Phys. Rev. Lett. **20**, 589 (1968).

[60] G. S. Joyce, in *Phase Transitions and Critical Phenomena*, Vol. 2, C. Domb and M. S. Green eds., p. 375 (Academic Press, 1972).

[61] H. Ballhausen, J. Berges, and C. Wetterich, Phys. Lett. B **582**, 144 (2003).

[62] A. Codello, N. Defenu, and G. D'Odorico, Phys. Rev. D **91**, 105003 (2015).

[63] J.-P. Blaizot, R. Mendez-Galain, and N. Wschebor, Phys. Lett. B **632**, 571 (2006).

[64] F. Benitez, J.-P. Blaizot, H. Chate, B. Delamotte, R. Mendez-Galain, and N. Wschebor, Phys. Rev. E **80**, 030103 (2009); *ibid.* **85**, 026707 (2012).

[65] J. M. Caillol, Nucl. Phys. B **865**, 291 (2012).

[66] A. Kapoyannis and N. Tetradis, Phys. Lett. A **276**, 225 (2000).

[67] D. Zappalà, Phys. Lett. A **290**, 35 (2001).

[68] N. Tetradis and C. Wetterich, Nucl. Phys. B **383**, 197 (1992).

[69] J. Braun, H. Gies, and D. D. Scherer, Phys. Rev. D **83**, 085012 (2011).

[70] A. Codello, G. D'Odorico, and C. Pagani, JHEP **1407**, 040 (2014).

[71] P. Mati, Phys. Rev. D **91** 125038 (2015).

[72] T. R. Morris, Phys. Lett. B **334**, 355 (1994).

[73] A. Codello, J. Phys. A **45**, 465006 (2012).

[74] B. Delamotte, in *Order, disorder and criticality: advanced problems of phase transition theory*, Yu. Holovatch ed., p. 1 (Singapore, World Scientific, 2007) [arXiv:cond-mat/0702365].

[75] N. Tetradis and C. Wetterich, Nucl. Phys. B **422**, 541 (1994).

[76] T. R. Morris, Int. J. Mod. Phys. B, **12**, 1343 (1998).

[77] P. Mati, *Non-perturbative Methods inQuantum Field Theories*, PhD thesis, (2015).

[78] V. L. Berezinskii, Zh. Eksp. Teor. Fiz. **61**, 1144 (1971) [Sov. Phys. JETP **34**, 610 (1972)].

[79] J. M. Kosterlitz and D. J. Thouless, J. Phys. C **6**, 1181 (1973).

[80] M. Gräter and C. Wetterich, Phys. Rev. Lett. **75**, 378 (1995).

[81] G. v. Gersdorff and C. Wetterich, Phys. Rev. B **64**, 054513 (2001).

[82] A. Linde, Phys. Lett. B **108**, 389 (1982).

[83] A. Albrecht and P. J. Steinhardt, Phys. Rev. Lett. **48**, 1220 (1982).

[84] J. Earman and J. Mosterin, Philos. Sci. **66**, 1 (1999).

[85] P. J. Steinhardt, Sci. Am. **304**, 18 (2011).

[86] F. Bezrukov, J. Rubio, and M. Shaposhnikov, Phys. Rev. D **92**, 083512 (2015).

[87] J. Rubio, Front. Astron. Space Sci. **5**, 50 (2019).

[88] J. Borchardt, H. Gies, and R. Sondenheimer, Eur. Phys. J. C **76**, 472 (2016).

[89] A. Jakovac, I. Kaposvari, and A. Patkos, Mod. Phys. Lett. A **32**, 1750011 (2017).

[90] V. Branchina and E. Messina, Phys. Rev. Lett. **111**, 241801 (2013).

[91] V. Branchina, E. Messina, A. Platania, JHEP **1409**, 182 (2014); E. Bentivegna, V. Branchina, F. Contino, and D. Zappala, *ibid.* **1712**, 100 (2017).

[92] J. Martin, C. Ringeval, and V. Vennin, *Encyclopaedia Inflationaris*, Phys. Dark Univ. **5-6**, 75 (2014).

[93] P. Creminelli, D. Lopez Nacir, M. Simonovic, G. Trevisan, and M. Zaldarriaga, Phys. Rev. Lett. **112**, 241303 (2014).

[94] K. Freese, J. A. Frieman, and A. V. Olinto, Phys. Rev. Lett. **65**, 3233 (1990).

[95] K. Freese and W. H. Kinney, JCAP **03**, 044 (2015).

[96] C. P. Burgess, M. Cicoli, F. Quevedo, and M. Williams, JCAP **11**, 045 (2014).

[97] K. Yonekura, JCAP **10**, 054 (2014).

[98] K. Kohri, C. S. Lim, and C. M. Lin, JCAP **08** 001 (2014).

[99] T. Chiba, K. Kohri, PTEP **2014**, 093E01 (2014).

[100] L. Boyle, K. M. Smith, C. Dvorkin, and N. Turok, Phys. Rev. D **92**, 043504 (2015).

[101] I. P. Neupane, Phys. Rev. D **90**, 123502 (2014).

[102] J. B. Munoz and M. Kamionkowski, Phys. Rev. D **91**, 043521 (2015).

[103] C. Burgess and D. Roest, JCAP **06**, 012 (2015).

[104] P. A. R. Ade *et al.* [Planck], Astron. Astrophys. **594**, A13 (2016).

[105] P. A. R. Ade *et al.* [Planck], Astron. Astrophys. **594**, A20 (2016).

[106] P. A. R. Ade *et al.* [BICEP2 and Keck Array], Phys. Rev. Lett. **116**, 031302 (2016).

[107] D. L. Bennett, H. B. Nielsen, and I. Picek, Phys. Lett. B **208**, 275 (1988).

[108] C. D. Froggatt, H. B. Nielsen, Phys. Lett. B **368**, 96 (1996).

[109] C. P. Burgess, V. Di Clemente, and J. R. Espinosa, JHEP **0201**, 041 (2002).

[110] G. Isidori, V. S. Rychkov, A. Strumia, and N. Tetradis, Phys. Rev. D **77**, 025034 (2008).

[111] F. Bezrukov and M. Shaposhnikov, Phys. Lett. B **659**, 703 (2008).

[112] F. Bezrukov and M. Shaposhnikov, JHEP **0907**, 089 (2009).

[113] C. P. Burgess, H. M. Lee, and M. Trott, JHEP **0909**, 103 (2009).

[114] J. L. F. Barbon and J. R. Espinosa, Phys. Rev. D **79**, 081302 (2009).

[115] A. De Simone, M. P. Hertzberg, and F. Wilczek, Phys. Lett. B **678**, 1 (2009).

[116] R. N. Lerner and J. McDonald, Phys. Rev. D **82**, 103525 (2010).

[117] G. F. Giudice and H. M. Lee, Phys. Lett. B **694**, 294 (2011).

[118] F. Englert and R. Brout, Phys. Rev. Lett. **13**, 321 (1964).

[119] P. W. Higgs, Phys. Rev. Lett. **13** 508 (1964).

[120] ATLAS Collaboration, Phys. Lett. B **710**, 49 (2012).

[121] CMS Collaboration, Phys. Lett. B **710**, 26 (2012).

[122] M. Shaposhnikov and C. Wetterich, Phys. Lett. B **683**, 196 (2010).

[123] M. Postma, M. Volponi, Phys. Rev. D **90** 103516 (2014).

[124] G. Degrassi, S. Di Vita, J. Elias-Miró, J. R. Espinosa, G. F. Giudice, G. Isidori, and A. Strumia, JHEP **08**, 098 (2012).

[125] A. D. Linde, Phys. Lett B **129**, 177–181 (1983); Phys. Lett. B **175**, 395–400 (1986).

[126] A. Bonanno and M. Reuter, Phys. Rev. D **65**, 043508 (2002); A. Bonanno and M. Reuter, Phys. Lett. B **527**, 9–17 (2002); A. Bonanno and M. Reuter, Int. J. Mod. Phys. D **13**, 107–121 (2004); E. Bentivegna, A. Bonanno and M. Reuter, J. Cosmology Astropart. Phys. **0401**, 001 (2004); I. L. Shapiro, J. Sola, J. High Energy Phys. **2002**, 006–006 (2002); I. L. Shapiro, J. Sola, Phys. Lett. B **530**, 10–19 (2002); I. L. Shapiro, J. Sola, Phys. Lett. B **475**, 236–246 (2000); I. L. Shapiro, J. Sola, Nucl. Phys. B Proc. Suppl. **127**, 71–76 (2004); I. L. Shapiro, J. Sola, H. Stefancic, J. Cosmol. Astropart. Phys. **2005**, 012–012 (2005); I. L. Shapiro, J. Sola, Phys. Lett. B **682**, 105–113 (2009).

[127] Y.-F. Cai, Y.-C. Chang, P. Chen, D. A. Easson and T. Qiu, Phys. Rev. D **88**, 083508 (2013); G. Kofinas and V. Zarikas, Phys. Rev. D **94**, 103514 (2016); R. Moti and A. Shoja, Eur. Phys. J. C **78**, 32 (2018).

[128] A. Kaya, Phys. Rev. D **87**, 123501 (2013).

[129] J. Serreau, Phys. Lett. B **730**, 271–274 (2014); T. Prokopec and G. Rigopoulos, J. Cosmology Astropart. Phys. **1808**, 013 (2018).

[130] M. Guilleux and J. Serreau, Phys. Rev. D **92**, 084010 (2015).

[131] T. Kobayashi, O. Seto and Y. Yamaguchi, Prog. Theor. Exp. Phys. **2014**, 103E01 (2014); T. Higaki, T. Kobayashi, O. Seto and Y. Yamaguchi, J. Cosmology Astropart. Phys. **1410**, 025 (2014).

[132] L. V. Keldysh, Zh. Eksp. Teor. Fiz. **47**, 1515–1527 (1964); [Sov. Phys. JETP **20**, 1018 (1965)]; O. V. Konstantinov and V. I. Perel, Zh. Eksp. Teor. Fiz. **39**, 197 (1960); [Sov. Phys. JETP **12**, 142 (1961)]; J. Schwinger, J. Math. Phys. **2**, 407–432 (1961); L. P. Kadanoff and G. Baym, *Quantum Statistical Mechanics*, (Benjamin, New York) (1962).

[133] J. Polonyi, Phys. Rev. D **74**, 065014 (2006); S. Nagy, J. Polonyi, I. Steib, Phys. Rev. D **93**, 025008 (2016); S. Nagy, J. Polonyi, I. Steib, Phys. Rev. D **97**, 085002 (2018).

[134] R. Brustein, S. P. de Alwis and P. Martens, Phys. Rev. D **70**, 126012 (2004).

[135] H. Gies, Lect. Notes Phys. **852**, 287 (2012).

[136] D. H. Lyth, Lect. Notes Phys. **738** 81-118 (2008).

[137] D. H. Lyth and A. Riotto, Phys. Rept. **314** 1-146 (1999).